FOUR-WAVE MIXING AND LUMINESCENCE OF CONFINED EXCITONS IN MOLECULAR AGGREGATES AND NANOSTRUCTURES. MANY-BODY GREEN FUNCTION APPROACH

Vladimir CHERNYAK, Ningjun WANG, Shaul MUKAMEL

Department of Chemistry, University of Rochester, Rochester NY 14627, USA

ELSEVIER

AMSTERDAM – LAUSANNE – NEW YORK – OXFORD – SHANNON – TOKYO

ELSEVIER

Physics Reports 263 (1995) 213–309

PHYSICS REPORTS

Four-wave mixing and luminescence of confined excitons in molecular aggregates and nanostructures. Many-body Green function approach

Vladimir Chernyak, Ningjun Wang, Shaul Mukamel

Deparment of Chemistry, University of Rochester, Rochester NY 14627, USA

Received February 1995; editor: D.L. Mills

Contents

0370-1573/95/$29.00
SSDI 0370-1573(95)00015-1

Abstract

Four-wave mixing and spontaneous emission spectra of confined Frenkel excitons in molecular assemblies are calculated using a unified Green function approach. Applications to various time- and frequency-domain techniques show an interplay of coherent motion of two-exciton states and exciton transport in the third order response. Effect of exciton–phonon interactions and static disorder are studied. Many-body collective resonances which reflect level correlations and may not be attributed to specific pairs of eigenstates are predicted. A Kramers–Kronig representation of the nonlinear response in terms of a multidimensional spectral density offers a convenient computational scheme in condensed phases.

1. Introduction

The nature of electronic excitations and the optical properties of molecular assemblies constitute a fundamental theoretical problem with numerous practical implications. Much effort has been focused on molecular crystals [1–5] and on molecular aggregates, either in condensed phases [6–16] or in supersonic beams [17] where isolated ultracold clusters of a given size can be prepared. More recently, the ability to fabricate artificial nanometer-scale structures such as monolayers, superlattices, or quantum wires have opened up exciting possibilities of controlling the basic photophysical and photochemical processes in such systems [18–24]. These developments are closely related to the rapid progress in the studies of semiconductor quantum wells and quantum dots [25–28]. The basic interest in such systems is connected with the collective nature of electronic excitations, defining and understanding the key coherence sizes involved, and the unique mesoscopic interpolation between microscopic and macroscopic behavior. The function of many biological systems (e.g., the reaction center, and the light harvesting antenna) [29–31] depends on intermolecular coherences in assemblies of chromophores, and on the rates and pathways of energy transfer processes [32]. Possible device applications include light emitting diodes [33–35], which require manipulating charge transport and radiative recombination, and nonlinear optical devices which utilize the enhanced nonlinear susceptibilities of these systems [14, 19, 36].

In this article we develop a theoretical framework for calculating the electronic excitations of molecular assemblies (crystals, aggregates and superlattices), and interpreting their spectroscopic signatures. The elementary electronic excitations of molecular assemblies can be adequately described using the Frenkel exciton model [1–3]. Consequently, optical measurements are related to the dynamics of geometrically confined Frenkel excitons. The physical picture underlying the optical response is simplified considerably by the fact that the exciton bandwidth is usually much smaller than the molecular transition frequency (typical values are $500\,cm^{-1}$ and $20\,000\,cm^{-1}$, respectively) [3]. Consequently, one can adopt the Heitler–London approximation for the dipole–dipole coupling [1], and the Frenkel exciton hamiltonian then conserves the number of excitons. Since only the interaction with the radiation field can create excitons, the ground state is simply the vacuum state with no excitons, and successive interactions with the radiation field create very few excitons. We shall develop a Green function many-body theory that can address diverse phenomena such as coherent motions of one- and two-exciton states, exciton transport due to exciton scattering on phonons and static disorder, long exciton memory in elastic scattering and strong level correlations between one- and two-exciton states. We will then identify the optical techniques that can best be used to probe the various aspects of exciton dynamics.

The simplest optical measurement which probes coherent motion of optical excitons (excitons with optical wavelength) is linear absorption [37]. Considerable attention was given to characterizing the exciton states, and phenomena related to their coherent motion such as exciton annihilation [38, 39], dephasing, and cooperative radiative decay (superradiance) [11, 40–42]. Incoherent (diffusive) motion of single excitons (including short wavelength excitons) can be probed by applying time and frequency resolved fluorescence measurements [37]. An excitation (pump) pulse creates an initial exciton distribution whose subsequent evolution is determined by incoherent exciton scattering processes induced by phonons and static disorder. The time-dependent luminescence spectrum thus provides a direct probe for incoherent exciton motion.

Two-exciton states show up only in nonlinear optical measurements. Four-wave mixing measurements which can be performed in the frequency as well as in the time domain offer a multitude of techniques which can be used to study different effects. In the most general configuration, the system interacts with three incident waves with wave vectors and frequencies, and $\boldsymbol{k}_j\omega_j$, $j = 1, 2, 3$. A coherent signal is then observed in the direction determined by the wave vectors $\boldsymbol{k}_s$ and frequency ω_s. In general $\boldsymbol{k}_s = \pm\boldsymbol{k}_1 \pm \boldsymbol{k}_2 \pm \boldsymbol{k}_3$ and $\omega_s = \pm\omega_1 \pm \omega_2 \pm \omega_3$, where any combination of signs is possible, and defines a distinct technique. In practice we need consider only the following combinations:

$$\boldsymbol{k}_s = \boldsymbol{k}_1 + \boldsymbol{k}_2 + \boldsymbol{k}_3; \qquad \omega_s = \omega_1 + \omega_2 + \omega_3 . \tag{1.1}$$

$$\boldsymbol{k}_s = \boldsymbol{k}_1 - \boldsymbol{k}_2 + \boldsymbol{k}_3, \qquad \omega_s = \omega_1 - \omega_2 + \omega_3 . \tag{1.2}$$

$$\boldsymbol{k}_s = \boldsymbol{k}_1 - \boldsymbol{k}_2 - \boldsymbol{k}_3, \qquad \omega_s = \omega_1 - \omega_2 - \omega_3 . \tag{1.3}$$

All other combinations can be obtained by a simple permutation of ω_j and $\boldsymbol{k}_j$.

We will focus on a broad class of optical techniques with the choice of the direction of observation given by Eq. (1.2). Once $\boldsymbol{k}_s$ is fixed, different frequency-domain techniques correspond to various choices of $\boldsymbol{k}_j$ and ω_j: $\boldsymbol{k}_1 = \boldsymbol{k}_2 = \boldsymbol{k}_3$ and $\omega_1 = \omega_2 = \omega_3$ represents the nonlinear absorption and nonlinear reflection, $\boldsymbol{k}_1 = \boldsymbol{k}_3$ and $\omega_1 = \omega_3$ with tuning of ω_2 represents hole burning, $\boldsymbol{k}_1 \approx \boldsymbol{k}_2$ and $\omega_1 \approx \omega_2$ (often with off-resonant ω_3) correspond to degenerate four-wave mixing. The advent of femtosecond time-domain four-wave mixing techniques such as photon echo, transient grating, coherent Raman, optical Kerr and pump probe spectroscopy has opened up new possibilities for probing the dynamics of the system [37, 43–45]. In addition to the choice of the observation direction and the pulse frequencies, time-domain techniques allow a control of the pulse timing and the temporal profile of the signal. For example, in the time-domain transient grating technique pulses 1 and 2 coincide in time and come first, and pulse 3 comes after a variable delay. The signal, observed in the direction (1.2) then probes exciton transport and two-exciton coherent motion. Degenerate four-wave mixing is a closely related frequency-domain technique. When the pulse sequence is reversed (pulse 2 first followed by simultaneous 1 and 3 pulses) we have the photon echo which can probe level correlations, and eliminates inhomogeneous broadening. Hole burning is a closely related frequency-domain technique. As indicated earlier, the Heitler–London approximation for the Frenkel exciton model greatly simplifies the theoretical treatment of molecular assemblies. It then follows that the linear optical response is determined by properties of one-exciton states alone, and the third-order nonlinear optical response depends on one- as well as two-exciton states. Therefore, if one does not take into account additional (e.g., nuclear) degrees of freedom, calculating the optical response becomes a finite-body problem. It is then possible to derive exact expressions for the third-order optical response using a variety of methods: diagonalization of the Frenkel exciton Hamiltonian, equations of motion for one- and two-exciton variables, and Green function techniques [46]. Confined Frenkel-excitonic systems are sufficiently simple to allow for exact solutions; yet, they show a nontrivial behavior connected with geometric confinement, which affects the exciton states and their interactions with the transverse electromagnetic field. The situation becomes more complicated if one incorporates additional degrees of freedom. A common example is static disorder which often exists in organic materials due to their relatively weak intermolecular forces [21, 47]. This can include fluctuations of energies (diagonal disorder) or

of exciton hopping matrix elements due to topological disorder (off-diagonal disorder). Coupling to additional dynamical degrees of freedom such as phonons turns this into a genuine many-body problem which may not be solved exactly. Exciton–phonon interactions [48] and disorder lead to interesting effects which show up in coherent four-wave mixing techniques [5]. Exciton transport induced by exciton–phonon interactions can be probed in the time domain by means of the transient grating technique [5, 49, 50]. It has been shown in [51] that the frequency-domain counterpart of the transient grating technique is the degenerate four-wave mixing [52, 53].

Optical susceptibilities in the condensed phase are most commonly calculated using the local field approximation (LFA), following a procedure developed by Bloembergen and coworkers [54, 55]. The LFA neglects completely all cooperative many-body effects and it, therefore, breaks down near two-photon resonances where the nonlinear optical response is determined by the coherent motion of two-excitons. A theory that incorporates these effects explicitly for the purely excitonic system (with no additional degrees of freedom) was developed by Spano, Leegwater, and Mukamel [14, 56]. The theory is based on equations of motion which are closed by invoking a certain factorization of expectation values of products of exciton operators. Exciton–exciton scattering due to their hard core repulsion (also known as the Pauli exclusion) is included in this approach. Another generalization of the LFA was developed by Knoester and Mukamel [5] who incorporated exciton–phonon coupling and exciton transport into the equation of motion. This procedure, like the LFA works well far from two-photon resonances involving the two-exciton states, and we will refer to this approximation as LFA′. Effects of disorder in four-wave mixing such as dephasing induced resonances [5, 53, 56], are described in the local field approximation (far from two-photon resonances) by transport properties of single-exciton states. The coherent nonlinear optical response depends on transport properties of one-exciton states as well as the coherent motion of two-exciton states, affected by exciton–exciton scattering due to their hard core repulsion. We thus expect to observe some clear signatures of the interplay of one-exciton transport and two-exciton coherent motions in resonant four-wave mixing.

In ordered systems with a high oscillator strength per unit volume and weak dephasing, the excitons and photons strongly couple to form new elementary excitations: polaritons. The description of polaritons involves taking into account exciton interactions with the quantum electromagnetic field to all orders. Incorporation of polariton effects in the linear optical response is straightforward [59–63], but in nonlinear optics this leaves a much more complex issue [23, 46]. It is more convenient in this case to deal with the optical response with respect to the external field rather than the Maxwell field. Clear examples of polariton (rather than exciton) transport in nonlinear optics have been demonstrated [5, 20, 57, 58].

The microscopic theory which will be developed in this article provides a unified treatment for exciton transport and two-exciton dynamics which takes into account effects of exciton–exciton and exciton–phonon interactions, disorder, and radiative decay, and shows the limitations of the local field approximation. Both four-wave mixing and luminescence spectroscopic probes will be analyzed. In Section 2 we introduce the Hamiltonian of a nonrelativistic material system in the multipolar form, interacting with the transverse electromagnetic field, define optical signals for different kinds of measurements, and express the optical signals in terms of correlation functions of the polarization operator in a system with external sources which create the external electromagnetic field. We then introduce the optical response functions with respect to the external field which determine expansions of the polarization of the system (for coherent measurements) or bilinear

products of the polarization (for incoherent measurements) in powers of the external field. In Section 3 we calculate the coherent linear and third-order nonlinear optical response of assemblies of interacting two-level molecules with arbitrary geometry. The approach is based on deriving equations of motion for the optical polarization and other related variables. The equations are closed by a suitable factorization of higher-order expectation values; this factorization is exact for the Frenkel exciton model. In Section 4 we apply the results of Section 3 to obtain the linear and nonlinear optical response of molecular nanostructures with static disorder. The factorization applied in Section 3 is generally not possible once additional phonon degrees of freedom are included. In the following sections we, therefore, develop a more general procedure. In Section 5 we express the coherent optical response in terms of equilibrium correlation functions of the polarization operators. These correlation functions are evaluated in the joint system containing the transverse quantum electromagnetic field and the matter degrees of freedom, but excluding the external polarization. In Section 6, we start with the general expressions derived in Section 5, and obtain the Green function expressions (GFE) for the coherent optical response of molecular nanostructures with additional dynamical degrees of freedom. The key difference from the equations of motion procedure is that now we work with multitime correlation functions (as opposed to the single life expectation values used in the equations of motion). Factorization of higher multitime correlation function into lower-order ones offers a more powerful set of approximations, which are necessary in this case. The Bethe–Salpeter equation and diagrammatic techniques [64] are used in these derivations. In Section 7, we introduce a model of a periodic molecular assembly with exciton–phonon interaction, and starting with the GFE of Section 6, we calculate the optical response in terms of the one-exciton Green function, the two-exciton scattering matrix and the Green function of the Boltzmann equation for exciton transport. In Section 8, we use the GFE to discuss various many-body resonances of the nonlinear optical response, and present frequency and time domain techniques which may be used to probe these resonances. We pay special attention to situations in which the interplay of one-exciton transport and two-exciton coherent motion plays an important role and the signals cannot be described adequately within the framework of mean-field theories.

Spontaneous emission (Raman and fluorescence) spectroscopy is another technique which directly probes exciton motion. Formally this is a linear technique since the signal is proportional to the incoming field intensity. However, due to the quantum nature of the spontaneous emission it has a close resemblance to four-wave mixing, and it can be expressed using very similar correlation functions. This analogy and connection were established previously for the simple model of a single chromophore in a bath within the rotating wave approximation which holds for resonant excitation [65]. Here we generalize this treatment to include exciton effects. Spontaneous emission in molecular nanostructures depends on the transport properties of one-exciton states, which do not show up in the linear optical response, and are responsible for spectral diffusion in time-resolved luminescence [66]. Other interesting effects include long radiative-decay times connected with exciton scattering induced by disorder [67, 20], and light backscattering [68] in luminescence [23]. The comparison of spontaneous emission and coherent four-wave mixing spectroscopy in molecular nanostructures is an important problem. In Section 9 we obtain GFE for the frequency- and time-resolved luminescence signal from periodic molecular nanostructures with exciton–phonon interaction and present numerical calculations. In Section 10 we consider the coherent optical response and luminescence with both static disorder and exciton-phonon interaction.

In Section 11 we discuss resonances in the frequency domain third-order nonlinear optical response function, using the global exact eigenstates of the system. An important result that comes naturally out of the present treatment is the prediction of new collective resonances which are not related to specific pairs of eigenstates of the system. In Section 12 we introduce the Kramers–Kronig representation for the optical response, and establish the connection between level correlations which show up in the multidimensional spectral density of the system, and the collective resonances. We expect this representation to be particularly useful in molecular dynamics simulations of nonlinear spectroscopy. Details of the derivations are presented in Appendices (A)–(G).

2. The multipolar Hamiltonian and the optical signals

The dynamics of a nonrelativistic material system interacting with the transverse electromagnetic field can be described by the Hamiltonian [69]:

$$H = \hat{H}_{\mathrm{m}} + \hat{H}_{\mathrm{rad}} - \int \mathrm{d}\boldsymbol{r}\, \hat{\boldsymbol{P}}(\boldsymbol{r})\cdot\hat{\boldsymbol{D}}^{\perp}(\boldsymbol{r}) + 2\pi \int |\hat{\boldsymbol{P}}^{\perp}(\boldsymbol{r})|^2\, \mathrm{d}\boldsymbol{r}\,. \tag{2.1}$$

This multipolar Hamiltonian can be obtained from the more common minimum coupling Hamiltonian by performing a canonical (gauge) transformation, and neglecting the magnetic terms. The longitudinal part of the electric field is taken into account by incorporating the Coulomb interaction in the molecular Hamiltonian $\hat{H}_{\mathrm{m}}$. We denote an operator by a caret $\hat{Q}$, and set $\hbar = 1$. $\hat{H}_{\mathrm{rad}}$ is the free field Hamiltonian:

$$\hat{H}_{\mathrm{rad}} = \frac{1}{8\pi}\int \mathrm{d}\boldsymbol{r}\,\{D^{\perp}(\boldsymbol{r})^2 + [\nabla\times\hat{A}(\boldsymbol{r})]^2\}\,, \tag{2.2}$$

where $A(\boldsymbol{r})$ is the vector potential in the Coulomb gauge satisfying $\nabla\cdot\hat{A}(\boldsymbol{r}) = 0$, the $\hat{D}^{\perp}(\boldsymbol{r})$ operator represents the transverse part of the displacement field, with $\nabla\cdot D^{\perp}(\boldsymbol{r}) = 0$. The term $(1/4\pi)\hat{D}^{\perp}(\boldsymbol{r})$ is the momentum conjugate to $\hat{A}(\boldsymbol{r})$. Both $\hat{A}$ and $\hat{D}^{\perp}$ commute with all material operators and satisfy the commutation rules

$$[\hat{D}_i^{\perp}(\boldsymbol{r}), \hat{A}_j(\boldsymbol{r}')] = 4\pi\mathrm{i}\,\delta_{ij}^{\perp}(\boldsymbol{r}-\boldsymbol{r}')\,, \tag{2.3a}$$

where $\delta_{ij}^{\perp}(\boldsymbol{r}-\boldsymbol{r}')$ is the transverse δ function (i.e. the projection of the function $\delta_{ij}\delta(\boldsymbol{r}-\boldsymbol{r}')$ onto the subspace of transverse functions). The commutation relation (2.3a) can be written in the form

$$[\hat{D}_i^{\perp}(\boldsymbol{r}), (\nabla\times\hat{A}(\boldsymbol{r}))_j] = 4\pi\mathrm{i}\sum_m \varepsilon_{ijm}\frac{\partial}{\partial r'_m}\,\delta_{ij}^{\perp}(\boldsymbol{r}-\boldsymbol{r}')\,, \tag{2.3b}$$

where ε_{ijm} is the antisymmetric Levi–Civita tensor. The transverse electromagnetic field $\hat{E}^{\perp}(\boldsymbol{r})$ is related to the electric displacement $\hat{D}^{\perp}(\boldsymbol{r})$ by

$$\hat{E}^{\perp}(\boldsymbol{r}) \equiv \hat{D}^{\perp}(\boldsymbol{r}) - 4\pi\hat{P}^{\perp}(\boldsymbol{r})\,, \tag{2.4a}$$

where $\hat{P}^{\perp}(\boldsymbol{r})$ is the transverse part of the polarization operator $P(\boldsymbol{r})$ defined as [69]

$$\hat{P}_i(\boldsymbol{r}) \equiv \int_0^1 \mathrm{d}\xi \int \mathrm{d}\boldsymbol{r}'\, \boldsymbol{r}_i' \hat{n}(\boldsymbol{r}')\delta(\boldsymbol{r} - \xi\boldsymbol{r}') \tag{2.4b}$$

where $\hat{n}(\boldsymbol{r}')$ is the electron charge density operator. $\hat{P}^{\perp}(\boldsymbol{r})$ being a material operator, commutes with the field operators $A(\boldsymbol{r}')$ and $D^{\perp}(\boldsymbol{r}')$. It should be emphasized that when using the multipolar Hamiltonian, $E^{\perp}$ is not a pure field operator but is rather a mixed material and field operator. It, therefore, does not generally commute with either field or material operators. To obtain the Hamiltonian of the system in the presence of external sources, we substitute $\hat{P} + P_{\mathrm{ext}}$ for $\hat{P}$ in Eq. (2.1) and get[1]

$$\hat{H}_{\mathrm{T}}(t) = \hat{H} - \int \mathrm{d}\boldsymbol{r}\, P_{\mathrm{ext}}(\boldsymbol{r}, t) \cdot E^{\perp}(\boldsymbol{r}) \,. \tag{2.5}$$

Here P_{ext} is an external polarization representing degrees of freedom not included explicitly in our Hamiltonian. Its time evolution is given, and not affected by the dynamics of the system.

In this section we consider a quantum material system coupled to the quantum electromagnetic field, and relate the optical signals to correlation functions of the field and material operators. Once these relations are established, we can concentrate on developing theoretical techniques for evaluating these correlation functions. We will consider a material system with a finite size L located in the vicinity of the coordinate origin $\boldsymbol{r} = 0$. The system interacts with the transverse external field $\mathscr{E}$, and a detector which measures the energy of the transverse electromagnetic field is located at point $\boldsymbol{R}$. Usually the distance R is much larger than the size of the material system L, $L \ll R$ (far field) but the reverse situation is also of interest in, e.g., near-field measurements ([70]). In the forthcoming sections we will consider systems (monolayers and chains) of infinite size. This does not contradict the above inequality since an infinite size system is an adequate model for a system with the size L much larger than its all coherent sizes and the inequality $L \ll R$ can still hold.

The Hamiltonian $\hat{H}_{\mathrm{T}}(t)$ describes the coupled dynamics of the matter and field degrees of freedom in their joint space, in the presence of external sources. The system's evolution operator in the Heisenberg picture $\tilde{U}(t, t')$ satisfies the equation

$$\mathrm{d}\tilde{U}(t, t')/\mathrm{d}t = -\mathrm{i}\hat{H}_{\mathrm{T}}(t)\tilde{U}(t, t') \,, \tag{2.6a}$$

with $\tilde{U}(t', t') = \hat{I}$, where $\hat{I}$ is the system's unit operator. We further introduce two additional time evolution operators. The first represents the evolution of the isolated system with $P_{\mathrm{ext}} = 0$

$$\mathrm{d}\hat{U}(t, t')/\mathrm{d}t = -\mathrm{i}\hat{H}\tilde{U}(t, t') \,, \tag{2.6b}$$

the second describes the propagation of the material system alone

$$\mathrm{d}\bar{U}(t, t')/\mathrm{d}t = -\mathrm{i}\hat{H}_{\mathrm{m}}\bar{U}(t, t') \tag{2.6c}$$

with $\hat{U}(t', t') = \bar{U}(t', t') = \hat{I}$.

[1] We have omitted a term $2\pi \int \mathrm{d}\boldsymbol{r} |P_{\mathrm{ext}}(\boldsymbol{r}, t)|^2$. This is a classical function, which does not affect the evolution of the system.

In the Heisenberg picture, the time evolution of an arbitrary operator $\hat{Q}$ is controlled by the complete Hamiltonian, and is given by

$$\tilde{Q}(t) \equiv \tilde{U}^{\dagger}(t, -\infty)\hat{Q}\tilde{U}(t, -\infty) . \tag{2.7a}$$

In addition, we introduce the following two interaction picture operators:

$$\hat{Q}(t) \equiv \tilde{U}^{\dagger}(t, -\infty)\hat{Q}\hat{U}(t, -\infty) , \qquad \bar{Q}(t) \equiv \bar{U}^{\dagger}(t, -\infty)\hat{Q}\bar{U}(t, -\infty). \tag{2.7b,c}$$

$Q(t)$ evolves with the Hamiltonian $\hat{H}$ with no external sources and $\bar{Q}(t)$ evolves with the purely matter Hamiltonian $\hat{H}_{\mathrm{m}}$.

The Heisenberg equation of motion $\dot{\hat{Q}} = (\mathrm{i}/\hbar)\,[\hat{H}, \hat{Q}]$ for the field operators will yield the Maxwell equations. For a material operator $\hat{Q}$ we have [46]

$$\frac{\mathrm{d}}{\mathrm{d}t}\tilde{Q} = \mathrm{i}[H_{\mathrm{m}}, \tilde{Q}] - \frac{i}{2}\int \mathrm{d}\boldsymbol{r}\{[\tilde{P}(\boldsymbol{r}), \tilde{Q}]\cdot\tilde{E}^{\perp}(\boldsymbol{r}) + \tilde{E}^{\perp}(\boldsymbol{r})\cdot[\tilde{P}(\boldsymbol{r}), \tilde{Q}]\} . \tag{2.8}$$

It is important to note that if $E^{\perp}$ were to commute with material variables, this equation could be derived from a Hamiltonian with radiation–matter interaction $-\int \mathrm{d}\boldsymbol{r}\hat{P}(\boldsymbol{r})\cdot\hat{E}^{\perp}(\boldsymbol{r})$. This is, however, not the case, since $\hat{E}^{\perp}$ is a matter and field operator. Nevertheless, this equation comes as close as possible to a $\hat{P}\cdot\hat{E}$ form of the radiation–matter coupling. It should be emphasized that despite the dipolar appearance of the interaction, here we have not made the dipole approximations and our interaction contains all multipoles.

The energy density of the transverse field at point $\boldsymbol{r}$ and time t is proportional to $\langle\tilde{E}(\boldsymbol{r}, t)\tilde{E}(\boldsymbol{r}, t)\rangle$, i.e., the expectation value of the operator $\tilde{E}(\boldsymbol{r}, t)\tilde{E}(\boldsymbol{r}, t)$.

The signal field E_{s} generated by the polarization P is given by

$$\tilde{E}_{\mathrm{s}}(\boldsymbol{r}, t) = \int \mathrm{d}\boldsymbol{r}'\,\mathrm{d}t'\,\mathscr{G}(\boldsymbol{r} - \boldsymbol{r}'; t - t')\tilde{P}(\boldsymbol{r}', t') , \tag{2.9}$$

where $\mathscr{G}(\boldsymbol{r}, t)$ is the Green function of the Maxwell equations in vacuum

$$\mathscr{G}_{kj}(\boldsymbol{r}, t) = \int \frac{\mathrm{d}\boldsymbol{p}}{(2\pi)^3}\frac{\mathrm{d}\omega}{2\pi}\exp(\mathrm{i}\boldsymbol{p}\boldsymbol{r} - \mathrm{i}\omega t)\mathscr{G}_{kj}(\omega, \boldsymbol{p}) , \tag{2.10a}$$

$$\mathscr{G}_{kj}(\omega, \boldsymbol{p}) = 4\pi\omega^2(\delta_{kj} - p_k p_j/\boldsymbol{p}^2)/[(\omega + \mathrm{i}0)^2 - \boldsymbol{p}^2] . \tag{2.10b}$$

We will denote the expectation value of the operator $\tilde{E}_{\mathrm{s}}$ by E_{s}

$$E_{\mathrm{s}}(\boldsymbol{r}, t) \equiv \langle\tilde{E}_{\mathrm{s}}(\boldsymbol{r}, t)\rangle . \tag{2.10c}$$

We will concentrate on two types of measurements: coherent measurements which probe E_{s} directly, and time-resolved spectral measurements which carry additional information regarding correlations in the scattered field.

The simplest coherent measurement uses homodyne detection. It involves passing the scattered field through a time gate function $F(t'' - t)$ peaked at the desired time t, and then measuring the total intensity of the field. The resulting signal is

$$I_{\mathrm{hom}}(t) = \int \mathrm{d}t''\,|E_{\mathrm{s}}(\boldsymbol{R}, t'')|^2 F(t'' - t) . \tag{2.11a}$$

The homodyne signal can be also expressed in terms of the expectation value of the polarization operator

$$I_{\mathrm{hom}}(t) = \int \mathrm{d}t'' \int \mathrm{d}t_1\, \mathrm{d}t_2\, \mathrm{d}\boldsymbol{r}_1\, \mathrm{d}\boldsymbol{r}_2\, \mathscr{G}(\boldsymbol{R} - \boldsymbol{r}_1, t'' - t_1)\mathscr{G}(\boldsymbol{R} - \boldsymbol{r}_2, t'' - t_2)$$
$$\times \langle \tilde{P}(\boldsymbol{r}_1, t_1)\rangle \langle \tilde{P}(\boldsymbol{r}_2, t_2)\rangle F(t'' - t)\,. \tag{2.11b}$$

Heterodyne detection [71, 72] involves mixing the scattered field with an additional heterodyne field $\mathscr{E}_{\mathrm{h}}$ (usually a replica of one of the incoming fields) whose amplitude as well as phase can be controlled. It gives a stronger signal and can provide the amplitude as well as the phase of the scattered field. The total electric field is given by

$$\tilde{E}(\boldsymbol{r}, t) = \mathscr{E}_{\mathrm{h}}(\boldsymbol{r}, t) + \tilde{E}_{\mathrm{s}}(\boldsymbol{r}, t)\,, \tag{2.12a}$$

which yields

$$\tilde{E}^2(\boldsymbol{R}, t) = [\mathscr{E}_{\mathrm{h}}(\boldsymbol{R}, t) + \tilde{E}_{\mathrm{s}}(\boldsymbol{R}, t)]^2. \tag{2.12b}$$

Since one can perform separate measurements of $\mathscr{E}_{\mathrm{h}}^2$ and $\langle \tilde{E}_{\mathrm{s}}^2 \rangle$ (without mixing), it is possible to extract the cross-term $\mathscr{E}_{\mathrm{h}} \cdot E_{\mathrm{s}}$. Measuring the intensity of the field with a gate function $F(t'' - t)$, we obtain the following expression for the signal $I_{\mathrm{het}}(t)$:

$$I_{\mathrm{het}}(t) = 2\int \mathrm{d}t''\, \mathscr{E}_{\mathrm{h}}(\boldsymbol{R}, t'')E_{\mathrm{s}}(\boldsymbol{R}, t'')F(t'' - t)\,. \tag{2.13a}$$

Combining Eqs. (2.9) and (2.13a), the coherent signal can be also expressed in terms of the expectation value of the polarization operator $\tilde{P}$:

$$I_{\mathrm{het}}(t) = 2\int \mathrm{d}t'' \int \mathrm{d}t'\, \mathrm{d}\boldsymbol{r}\, \mathscr{G}(\boldsymbol{R} - \boldsymbol{r}', t'' - t')\mathscr{E}_{\mathrm{h}}(\boldsymbol{R}, t'')\langle \tilde{P}(\boldsymbol{r}', t')\rangle F(t'' - t)\,. \tag{2.13b}$$

From Eq. (2.13b) we see that the heterodyne signal is linear in the expectation value of the polarization operator. By varying the phase of the heterodyne field, one can obtain information about the amplitude and the phase of the scattered field. This will be demonstrated below.

In a time-resolved auto-correlation measurement [72], the scattered field is split into two beams, and following a variable relative delay τ the two beams are then mixed again. The measured electric field in this case has the form

$$\tilde{E}(\boldsymbol{r}, t) = \tilde{E}_{\mathrm{s}}(\boldsymbol{r}, t) + \tilde{E}_{\mathrm{s}}(\boldsymbol{r}, t - \tau)\,. \tag{2.14}$$

Extracting the cross-terms in the same manner as for the coherent measurement, we obtain the following expression for the signal:

$$I_{\mathrm{cor}}(t, \tau) = \int \mathrm{d}t'\, I_{\mathrm{c}}(\boldsymbol{R}t', \boldsymbol{R}t' - \tau)F(t' - t)\,, \tag{2.15a}$$

where we have used the notation

$$I_{\mathrm{c}}(\boldsymbol{r}_1 t_1, \boldsymbol{r}_2 t_2) \equiv \langle \tilde{E}_{\mathrm{s}}(\boldsymbol{r}_1, t_1)\tilde{E}_{\mathrm{s}}(\boldsymbol{r}_2, t_2)\rangle + \langle \tilde{E}_{\mathrm{s}}(\boldsymbol{r}_2, t_2)\tilde{E}_{\mathrm{s}}(\boldsymbol{r}_1, t_1)\rangle\,. \tag{2.15b}$$

Performing the Fourier transform with respect to τ in Eq. (2.15a) we obtain the cross-correlation signal as a function of time t and frequency Ω:

$$I_{\mathrm{cor}}(\Omega, t) = \int \mathrm{d}t' \mathrm{d}\tau \exp(\mathrm{i}\Omega\tau) I_{\mathrm{c}}(\boldsymbol{R}t', \boldsymbol{R}t' - \tau) F(t' - t) . \tag{2.15c}$$

The correlation function Eq. (2.15b) can be expressed in terms of a correlation function of the polarization operators $\mathscr{C}_{\mathrm{p}}$,

$$\mathscr{C}_{\mathrm{p}}(\boldsymbol{r}_1 t_1, \boldsymbol{r}_2 t_2) \equiv \tfrac{1}{2}[\langle \tilde{P}(\boldsymbol{r}_1, t_1) \tilde{P}(\boldsymbol{r}_2, t_2) \rangle + \langle \tilde{P}(\boldsymbol{r}_2, t_2) \tilde{P}(\boldsymbol{r}_1, t_1) \rangle] . \tag{2.16a}$$

Making use of Eq. (2.9) we obtain

$$I_{\mathrm{c}}(\boldsymbol{r}_1 t_1, \boldsymbol{r}_2 t_2) = 2 \int \mathrm{d}\boldsymbol{r}'_1 \, \mathrm{d}t'_1 \, \mathrm{d}\boldsymbol{r}'_2 \, \mathrm{d}t'_2 \, \mathscr{G}(\boldsymbol{r}_1 - \boldsymbol{r}'_1, t_1 - t'_1) \mathscr{G}(\boldsymbol{r}_2 - \boldsymbol{r}'_2, t_2 - t'_2) \mathscr{C}_{\mathrm{p}}(\boldsymbol{r}'_1 t'_1 \, \boldsymbol{r}'_2 t'_2) . \tag{2.16b}$$

Combining Eqs. (2.15) and (2.16) we see that the signal is linear in the correlation function (2.16a) of the polarization operator.

Finally we express the signals in terms of the material polarization for far-field measurements, i.e., when the size of the material system L is much smaller than the distance between it and a detector R ($L \ll R$). To that end we substitute the asymptotic form of the field Green function $\mathscr{G}(\boldsymbol{r}, t)$ for large r,

$$\mathscr{G}_{kj}(\boldsymbol{r}, t) = \int \frac{\mathrm{d}\omega}{2\pi} \exp(\mathrm{i}\omega r - \mathrm{i}\omega t) \frac{\omega^2}{r} \left(\delta_{kj} - \frac{r_k r_j}{r^2} \right) \tag{2.17}$$

where $r \equiv |\boldsymbol{r}|$ into Eqs. (2.9a), (2.13b) and (2.16b), and obtain

$$\tilde{E}_{sj}(\boldsymbol{r}, t) = \int \frac{\mathrm{d}\omega}{2\pi} \exp(-\mathrm{i}\omega t + \mathrm{i}\omega r) \frac{\omega^2}{r} \left(\delta_{jm} - \frac{r_j r_m}{r^2} \right) \tilde{P}_m(\boldsymbol{k}(\omega), \omega) \tag{2.18a}$$

where $P(\boldsymbol{k}, \omega)$ is the polarization in the frequency and momentum domain,

$$\tilde{P}(\boldsymbol{k}, \omega) = \int \mathrm{d}t \, \mathrm{d}^3 r \exp(\mathrm{i}\omega t - \mathrm{i}\boldsymbol{k} \cdot \boldsymbol{r}) \tilde{P}(\boldsymbol{r}, t) , \qquad \boldsymbol{k}(\omega) \equiv \omega \boldsymbol{R}/R . \tag{2.18b,c}$$

By substituting the expansion Eq. (2.18a) into the expressions for the signals [Eqs. (2.11), (2.13) and (2.15)] and eliminating some geometrical factors, we can calculate the signal for various detection modes.

By a proper choice of the gate function $F(t'' - t)$ we can control the various detection modes (homodyne, heterodyne, and autocorrelation). Setting $F(t'' - t) = \delta(t'' - t)$, we obtain the time-resolved signal.[2] Taking F to be a constant independent of time we obtain the time-integrated signal. Finally, in frequency-domain experiments the pulse envelopes change very slowly with

[2] This limit implies that the gate is very short compared with the time variation of the signal. Note, however, that it is still long compared with the optical carrier frequency.

time, and we can define the signal as the time-integrated signal divided by the duration of the measurement.

We start with the homodyne signal. The frequency-domain signal has the form

$$S_{\mathrm{hom}}(\boldsymbol{k}_s, \omega_s) = |P(\boldsymbol{k}_s, \omega_s)|^2 , \quad P(\boldsymbol{k}_s, \omega_s) \equiv \int d\boldsymbol{r}\, dt \exp(-i\boldsymbol{k}_s \cdot \boldsymbol{r} + i\omega_s t)\langle \tilde{P}(\boldsymbol{r}, t)\rangle . \tag{2.19a,b}$$

The time-resolved signal is given by

$$S_{\mathrm{hom}}(\boldsymbol{k}_s, t) = |P(\boldsymbol{k}_s, t)|^2 , \quad P(\boldsymbol{k}_s, t) \equiv \int d\boldsymbol{r} \exp(-i\boldsymbol{k}_s \cdot \boldsymbol{r})\langle \tilde{P}(\boldsymbol{r}, t)\rangle . \tag{2.19c,d}$$

Finally the time-integrated signal is

$$S^{\mathrm{I}}_{\mathrm{hom}}(\boldsymbol{k}_s) = \int dt\, S_{\mathrm{hom}}(\boldsymbol{k}_s, t) = \int dt\, |P(\boldsymbol{k}_s, t)|^2 . \tag{2.19e}$$

The corresponding heterodyne signals are

$$S_{\mathrm{het}}(\boldsymbol{k}_s, \omega_s) = \mathrm{Re}[E^*_{\mathrm{h}}(\boldsymbol{k}_s\omega_s)P(\boldsymbol{k}_s\omega_s)] , \tag{2.20a}$$

$$S_{\mathrm{het}}(\boldsymbol{k}_s, t) = \mathrm{Re}[\mathscr{E}^*_{\mathrm{h}}(\boldsymbol{k}_s, t)P_s(\boldsymbol{k}_s, t)] , \tag{2.20b}$$

$$S^{\mathrm{I}}_{\mathrm{het}}(\boldsymbol{k}_s) = \int dt\, S_{\mathrm{het}}(\boldsymbol{k}_s, t) = \int dt\, \mathrm{Re}[\mathscr{E}^*_{\mathrm{h}}(\boldsymbol{k}_s, t)P(\boldsymbol{k}_s, t)] . \tag{2.20c}$$

Here E_{h} and $\mathscr{E}_{\mathrm{h}}$ are the heterodyne field amplitudes, i.e., the heterodyne field $\mathscr{E}_{\mathrm{h}}(\boldsymbol{r}, t)$ is represented in the form

$$\mathscr{E}_{\mathrm{h}}(\boldsymbol{r}, t) = E_{\mathrm{h}}(\boldsymbol{k}_s\omega_s)\exp(-i\omega_s t + i\boldsymbol{k}_s \cdot \boldsymbol{r}) + \mathrm{c.c.} \tag{2.20d}$$

in a frequency-domain measurement and

$$\mathscr{E}_{\mathrm{h}}(\boldsymbol{r}, t) = \mathscr{E}_{\mathrm{h}}(\boldsymbol{k}_s, t)\exp(i\boldsymbol{k}_s \cdot r) + \mathrm{c.c.} \tag{2.20e}$$

in a time-domain measurement. The wave vector $\boldsymbol{k}_s$ in Eqs. (2.19) and (2.20) is related to the frequency ω_s by means of Eq. (2.18c).

In frequency-domain measurements the heterodyne field has the same frequency of the signal (see Eq. (2.20d)). In time-domain measurements the heterodyne field usually has the same carrier frequency of the signal, i.e.,

$$\mathscr{E}_{\mathrm{h}}(\boldsymbol{k}_s, t) = E_{\mathrm{h}}(\boldsymbol{k}_s, t)\exp(-i\omega_s t) , \qquad P(\boldsymbol{k}_s, t) = P_s(\boldsymbol{k}_s, t)\exp(-i\omega_s t) , \tag{2.21a,b}$$

where $E_{\mathrm{h}}(\boldsymbol{k}_s\omega_s, t)$ and $P_s(\boldsymbol{k}_s, t)$ are the slow envelopes of the heterodyne field and the polarization. By varying the phase of the heterodyne field we can obtain both $\mathrm{Re}[P_s(\boldsymbol{k}_s, t)]$ and $\mathrm{Im}[P_s(\boldsymbol{k}_s, t)]$. This will be demonstrated in the coming sections.

Finally, we consider the correlation signal

$$\begin{aligned} &S_{\mathrm{cor}}(\boldsymbol{k}_s, \Omega) = 2\mathscr{G}_{\mathrm{p}}(\Omega, \boldsymbol{k}_s) , \qquad S_{\mathrm{cor}}(\boldsymbol{k}_s, \Omega; t) = 2\mathscr{G}_{\mathrm{p}}(\Omega, \boldsymbol{k}_s; t) , \\ &S^{\mathrm{I}}_{\mathrm{cor}}(\boldsymbol{k}_s, \Omega) = 2\int dt\, \mathscr{G}_{\mathrm{p}}(\Omega, \boldsymbol{k}_s; t) , \end{aligned} \tag{2.22a, b, c}$$

where

$$\mathscr{C}_{\mathrm{p}}(\Omega, \boldsymbol{k}_{\mathrm{s}}; t) \equiv \int \mathrm{d}\boldsymbol{r}_1\, \mathrm{d}\boldsymbol{r}_2\, \mathrm{d}\tau \exp[-\mathrm{i}\boldsymbol{k}_{\mathrm{s}}\cdot(\boldsymbol{r}_1 - \boldsymbol{r}_2) + \mathrm{i}\Omega\tau]\mathscr{C}_{\mathrm{p}}(\boldsymbol{r}_1 t, \boldsymbol{r}_2 t + \tau)\,. \tag{2.22d}$$

In the frequency-domain experiment $\mathscr{C}_{\mathrm{p}}(\Omega, \boldsymbol{k}_{\mathrm{s}}; t)$ does not depend on t and we set $\mathscr{C}_{\mathrm{p}}(\Omega, \boldsymbol{k}_{\mathrm{s}}) \equiv \mathscr{C}_{\mathrm{p}}(\Omega, \boldsymbol{k}_{\mathrm{s}}; t)$ in Eq. (2.22a). Expressions for the luminescence signal in terms of the same correlation function $\mathscr{C}_{\mathrm{p}}$ will be derived in Section 9.

In summary, we have related the signal obtained from any nonrelativistic material system using various detection modes to nonequilibrium correlation functions of the polarization operator of the system driven by external sources. In particular applications these correlations functions are usually expanded in powers of the external fields $\mathscr{E}(\boldsymbol{r}, t)$.

$$\mathscr{E}(\boldsymbol{r}, t) \equiv \int \mathrm{d}\boldsymbol{r}'\, \mathrm{d}t'\, \mathscr{G}(\boldsymbol{r} - \boldsymbol{r}', t - t')P_{\mathrm{ext}}(\boldsymbol{r}', t')\,. \tag{2.23}$$

These expansions have the form

$$P(\boldsymbol{r}, t) = \sum_{n=0}^{\infty} \frac{1}{n!} \int \mathrm{d}\boldsymbol{r}_1\, \mathrm{d}t_1 \ \ldots\ \mathrm{d}\boldsymbol{r}_n\, \mathrm{d}t_n R^{(n)}(\boldsymbol{r}t; \boldsymbol{r}_1 t_1, \ldots, \boldsymbol{r}_n t_n)\mathscr{E}(\boldsymbol{r}_1, t_1) \cdots \mathscr{E}(\boldsymbol{r}_n, t_n) \tag{2.24a}$$

$$\mathscr{C}_{\mathrm{p}}(\boldsymbol{r}t, \boldsymbol{r}'t') = \sum_{n=0}^{\infty} \frac{1}{n!} \int \mathrm{d}\boldsymbol{r}_1\, \mathrm{d}t_1 \ \ldots\ \mathrm{d}\boldsymbol{r}_n\, \mathrm{d}t_n R_{\mathrm{c}}^{(n)}(\boldsymbol{r}t, \boldsymbol{r}'t'; \boldsymbol{r}_1 t_1, \ldots \boldsymbol{r}_n t_n)\mathscr{E}(\boldsymbol{r}_1, t_1) \cdots \mathscr{E}(\boldsymbol{r}_n, t_n)\,. \tag{2.24b}$$

The optical response functions $R^{(n)}$ and $R_{\mathrm{c}}^{(n)}$ define the expansions of the expectation values of the polarization operator and bilinear combination of the polarization operators, respectively, in powers of the external field.

In the following sections considering the coherent optical response we will concentrate on the third-order nonlinear optical response related to the four-wave mixing (in this context we will omit the index (3) where possible writing R instead of $R^{(3)}$). In a time-domain four-wave mixing it is common to represent the external electric field, as a sum of three waves,

$$\mathscr{E}(\boldsymbol{r}, t) = \mathscr{E}_1(t)\exp(\mathrm{i}\boldsymbol{k}_1\cdot\boldsymbol{r}) + \mathscr{E}_2(t)\exp(\mathrm{i}\boldsymbol{k}_2\cdot\boldsymbol{r}) + \mathscr{E}_3(t)\exp(\mathrm{i}\boldsymbol{k}_3\cdot r) + \mathrm{c.c.} \tag{2.25a}$$

We further introduce the Fourier transforms

$$\mathscr{E}_j(t) = \int \frac{\mathrm{d}\omega}{2\pi} \exp(-\mathrm{i}\omega t)\mathscr{E}_j(\omega) + \mathrm{c.c.} \tag{2.25b}$$

We look for the signal generated in the direction $\boldsymbol{k}_{\mathrm{s}} = \boldsymbol{k}_1 + \boldsymbol{k}_3 - \boldsymbol{k}_2$. The relevant component of the nonlinear polarization is

$$P(\boldsymbol{r}, t) = P(\boldsymbol{k}_{\mathrm{s}}, t)\exp(\mathrm{i}\boldsymbol{k}_{\mathrm{s}}\cdot\boldsymbol{r}) \tag{2.26a}$$

with

$$P(\boldsymbol{k}_{\mathrm{s}}, t) = \int \frac{\mathrm{d}\omega_1}{2\pi}\frac{\mathrm{d}\omega_2}{2\pi}\frac{\mathrm{d}\omega_3}{2\pi} R(-\omega_{\mathrm{s}} - \boldsymbol{k}_{\mathrm{s}};\ \omega_1\boldsymbol{k}_1,\ -\omega_2 - \boldsymbol{k}_2, \omega_3\boldsymbol{k}_3)$$
$$\times \exp(-\mathrm{i}(\omega_1 + \omega_3 - \omega_2)t)\mathscr{E}_1(\omega_1)\mathscr{E}_2(-\omega_2)\mathscr{E}_3(\omega_3)\,. \tag{2.26b}$$

We introduce the carrier frequencies of the pulses Ω_i, time delays τ_i' and the slowly varying envelopes $E_i(t)$ with the following relations

$$\mathscr{E}_i(t) = E_i(t - \tau_i')e^{-i\Omega_i t} \tag{2.27}$$

Taking the heterodyne field in the direction $\boldsymbol{k}_s$ and on the carrier frequency of the signal $\Omega_s = \Omega_1 - \Omega_2 + \Omega_3$ and varying its time delay we can obtain the signals $S_{het}(\boldsymbol{k}_s, t) \propto \mathrm{Re}(P_s(\boldsymbol{k}_s, t))$ or $\mathrm{Im}(P_s(\boldsymbol{k}_s, t))$ and $S^1_{het}(\boldsymbol{k}_s) \propto \int dt\, \mathrm{Re}(P_s(\boldsymbol{k}_s, t))$ or $\int dt\, \mathrm{Im}(P_s(\boldsymbol{k}_s, t))$.
In a frequency-domain measurement we set

$$\mathscr{E}_j(\omega) = E_j\delta(\omega - \omega_j) \tag{2.28}$$

and obtain

$$P(\boldsymbol{r}, t) = P(\boldsymbol{k}_s\omega_s)\exp(-i\omega_s t + i\boldsymbol{k}_s \cdot \boldsymbol{r}), \tag{2.29a}$$

with the amplitude

$$P(\boldsymbol{k}_s\omega_s) = R(-\omega_s - \boldsymbol{k}_s; \omega_1\boldsymbol{k}_1, -\omega_2 - \boldsymbol{k}_2, \omega_3\boldsymbol{k}_3)E_1E_2^*E_3. \tag{2.29b}$$

Using a heterodyne field with frequency ω_s and direction $\boldsymbol{k}_s$, and varying its phase we obtain the signal $S_{het} \propto \mathrm{Re}(P_s)$ or $S_{het} \propto \mathrm{Im}(P_s)$ and, therefore, we can measure the real and imaginary part of the nonlinear response R.

Eqs. (2.29) together with the expressions for the nonlinear response function R in the frequency domain provide a closed-form expression for the frequency-domain four-wave mixing. Eqs (2.25) and (2.26) together with the expressions for the nonlinear optical response function R in the frequency domain provide a closed-form expression for time resolved four-wave mixing. Eq. (2.26b) contains a triple Fourier transform and the expression for the signal is rather complicated. However, for impulsive (short pulse) excitation we can perform at least two frequency integrations analytically and derive more tractable expressions for the signal (see Eqs. (4.23), (8.4a), (8.7), (8.17) and (9.17b)). Since, even for short pulses the general time-domain signal contains information about the material in a rather complicated form, in the forthcoming sections we will consider specific time-domain techniques. These make it possible to extract specific information about molecular aggregates such as properties of coherent one-exciton and two-exciton motion, exciton transport in real space, and correlations between one-exciton and two-exciton states.

In Section 5 we shall express the response functions $R^{(n)}$ and $R_c^{(n)}$ in terms of equilibrium correlation functions of the free system without external sources $P_{ext} = 0$. In the following sections we evaluate the latter correlation functions for various models of molecular nanostructures.

3. Equations of motion and Green function expressions for response functions in real space

In this section we derive closed formal expressions for the optical response of a molecular assembly with arbitrary geometry. We will use these expressions in the next section where we incorporate static disorder.

Consider an assembly of interacting two-level molecules described by the Hamiltonian

$$\hat{H}_m = \sum_n \Omega_n \hat{B}_n^\dagger \hat{B}_n + \sum_{m \neq n} J_{mn}\hat{B}_m^\dagger \hat{B}_n . \tag{3.1a}$$

$\hat{B}_m(\hat{B}_m^\dagger)$ is the exciton annihilation (creation) operator of the mth two-level system, which changes its excited state to the ground state. They satisfy the commutation relations

$$[\hat{B}_m, \hat{B}_n^\dagger] = (1 - 2\hat{B}_m^\dagger \hat{B}_n)\delta_{mn}. \tag{3.1b}$$

Ω_m is the excitation energy of the mth molecule, and J_{mn} is the intermolecular coupling which is responsible for exciton hoping. We shall derive equations of motion for the optical polarization of the system driven by an external polarization P_{ext}. By expanding the expectation value of the polarization operator in powers of the external field $\mathscr{E}(\boldsymbol{r}, t)$ defined by Eq. (2.23), we obtain the polarization $P(\boldsymbol{r}, t)$ in the form of Eq. (2.24a). $R^{(1)}$ and $R^{(3)}$ were calculated in [46] (note that $R^{(2)} \equiv 0$ for a system with the Hamiltonian (3.1a)). Below we will briefly sketch the derivation.

The polarization operator $\hat{P}(\boldsymbol{r})$ for the model described by Eq. (3.1) has the form [46]:

$$\hat{P}(\boldsymbol{r}) = \sum_m \hat{P}_m(\boldsymbol{r}), \qquad \hat{P}_m(\boldsymbol{r}) = |\mu|\rho(\boldsymbol{r} - \boldsymbol{R}_m)(\hat{B}_m + \hat{B}_m^\dagger), \qquad \left|\int \rho(\boldsymbol{r})\,\mathrm{d}\boldsymbol{r}\right| = 1. \tag{3.2a,b,c}$$

In the dipole approximation we set

$$\rho(\boldsymbol{r}) = \delta(\boldsymbol{r}). \tag{3.2d}$$

Expressions for the optical response of molecular assemblies is of arbitrary geometry which take into account effects of radiative decay were obtained in [46]. In this section, for the sake of simplicity and clarity, we will neglect radiative-decay effects (we will address this problem in the forthcoming sections), which is equivalent to substituting the classical transverse external field $\mathscr{E}$ instead of the operator $\tilde{E}^\perp$ in Eq. (2.8). For the operator $\tilde{B}_n$ Eq. (2.8) then takes the form:

$$\frac{1}{i}\frac{\mathrm{d}}{\mathrm{d}t}\tilde{B}_n = -\Omega_n \tilde{B}_n - \sum_{m \neq n} J_{nm}\tilde{B}_m + 2\sum_{m \neq n} J_{nm}\tilde{B}_n^\dagger \tilde{B}_n \tilde{B}_m + \mu_n E_n(t)(1 - 2\tilde{B}_n^\dagger \tilde{B}_n). \tag{3.3a}$$

where

$$E_n(t) \equiv \int \mathrm{d}\boldsymbol{r}\,\rho(\boldsymbol{r} - \boldsymbol{R}_n)\mathscr{E}(\boldsymbol{r}, t). \tag{3.3b}$$

Making use of Eq. (3.3a) to obtain an equation of motion for the operator $\hat{B}_m\hat{B}_n$ we take the expectation value of this equation and Eq. (3.3a), and make the factorization

$$\langle \tilde{B}^\dagger(t_1)\cdots\tilde{B}^\dagger(t_n)\tilde{B}(t_1')\cdots\tilde{B}(t_m')\rangle = \langle \tilde{B}^\dagger(t_1)\cdots\tilde{B}^\dagger(t_n)\rangle\langle \tilde{B}(t_1')\cdots\tilde{B}(t_m')\rangle. \tag{3.4}$$

which is exact to third-order in the field. We finally end up with the following closed system of equations:

$$\frac{1}{i}\frac{\mathrm{d}}{\mathrm{d}t}\langle\tilde{B}_n\rangle = -\Omega_n\langle\tilde{B}_n\rangle - \sum_{m \neq n} J_{nm}\langle\tilde{B}_n\rangle + 2\sum_{m \neq n} J_{nm}\langle\tilde{B}_n^\dagger\rangle\langle\tilde{B}_n\tilde{B}_m\rangle + \mu_n E_n(t)(1 - 2\langle\tilde{B}_n^\dagger\rangle\langle\tilde{B}_n\rangle), \tag{3.5a}$$

$$\frac{1}{i}\frac{\mathrm{d}}{\mathrm{d}t}\langle\tilde{B}_n\tilde{B}_{n'}\rangle = -(\Omega_n + \Omega_{n'})\langle\tilde{B}_n\tilde{B}_{n'}\rangle - \sum_{m \neq n} J_{nm}\langle\tilde{B}_n\tilde{B}_m\rangle - \sum_{m \neq n'} J_{n'm}\langle\tilde{B}_n\tilde{B}_m\rangle + 2\delta_{nn'}\sum_{m \neq n'} J_{n'm}\langle\tilde{B}_m\tilde{B}_n\rangle + \mu_n E_n(t)\langle\tilde{B}_{n'}\rangle + \mu_{n'}E_{n'}(t)\langle\tilde{B}_n\rangle - \delta_{nn'}\mu_n E_n(t)\langle\tilde{B}_n\rangle. \tag{3.5b}$$

Solving Eq. (3.5) and making use of Eq. (3.2) we obtain exact expressions for the response functions [46]:

$$R^{(1)}(\boldsymbol{r}t;\boldsymbol{r}_1t_1)=\sum_{nm_1}\rho(\boldsymbol{r}-\boldsymbol{R}_n)\rho(\boldsymbol{r}_1-\boldsymbol{R}_{m_1})R_{nm_1}(t;t_1),$$

$$R^{(3)}(\boldsymbol{r}t;\boldsymbol{r}_1t_1,\boldsymbol{r}_2t_2,\boldsymbol{r}_3t_3)=\sum_{nm_1m_2m_3}\rho(\boldsymbol{r}-\boldsymbol{R}_n)\rho(\boldsymbol{r}_1-\boldsymbol{R}_{m_1})\rho(\boldsymbol{r}_2-\boldsymbol{R}_{m_2})\rho(\boldsymbol{r}_3-\boldsymbol{R}_{m_3}) \tag{3.6a}$$

$$\times R_{nm_1m_2m_3}(t;t_1,t_2,t_3). \tag{3.6b}$$

We will adopt the following convention for the relation between the response functions in the time and frequency domain:

$$R_{nm_1}(t;t_1)=\int\frac{\mathrm{d}\omega}{2\pi}R_{nm_1}(\omega)\mathrm{e}^{-\mathrm{i}\omega(t-t_1)}. \tag{3.7a}$$

$$R_{nm_1m_2m_3}(t;t_1,t_2,t_3)=\int\frac{\mathrm{d}\omega_s}{2\pi}\frac{\mathrm{d}\omega_1}{2\pi}\frac{\mathrm{d}\omega_2}{2\pi}\frac{\mathrm{d}\omega_3}{2\pi}2\pi\delta(\omega_1-\omega_2+\omega_3-\omega_s)$$

$$\times R_{nm_1m_2m_3}(-\omega_s;\omega_1,-\omega_2,\omega_3)$$

$$\times\exp(-\mathrm{i}\omega_st+\mathrm{i}\omega_1t_1-\mathrm{i}\omega_2t_2+\mathrm{i}\omega_3t_3), \tag{3.7b}$$

$$\omega_s=\omega_1+\omega_3-\omega_2. \tag{3.7c}$$

The linear response function in the frequency domain has the following form:

$$R_{nm_1}(\omega)=\mu^2[G_{nm_1}(\omega)+G^*_{m_1n}(-\omega)], \tag{3.8}$$

where $G_{nm}(\omega)$ is the one-exciton Green function

$$G_{nm}(\omega)=-\mathrm{i}\int_0^\infty\mathrm{d}t\,\mathrm{e}^{\mathrm{i}\omega t}\langle\bar{B}_n(t)\bar{B}^\dagger_m(0)\rangle. \tag{3.9a}$$

Here the expectation value is taken in the system without external field, and G_{nm} is given by

$$G_{nm}(\omega)=[(\omega-h)^{-1}]_{nm},\quad h_{nm}\equiv\Omega_n\delta_{nm}+J_{nm}(1-\delta_{nm}). \tag{3.9b,c}$$

For the nonlinear optical response function we obtain:

$$R_{nm_1m_2m_3}(-\omega_s;\omega_1,-\omega_2,\omega_3)=\mu^4\sum_{\substack{\text{perm}\\ m_i,\omega_i}}\sum_{n'n''}G_{nn'}(\omega_s)G^*_{n'm_2}(\omega_2)G_{n''m_3}(\omega_3)G_{n''m_1}(\omega_1)\bar{\Gamma}_{n'n''}(\omega_1+\omega_3)$$

$$+\text{c}'.\text{c}'. \tag{3.10}$$

where the sum over permutations includes 6 permutations of 3 pairs (ω_1, m_1), $(-\omega_2, m_2)$ and (ω_3, m_3), and c'.c'. means complex conjugation and changing the signs of all frequencies. $\bar{\Gamma}_{n'n''}$ is the two-exciton scattering matrix which is related to the two-exciton Green function $\bar{G}_{nmn'm'}(\omega)$,

$$\bar{G}_{nmn'm'}(\omega)\equiv\int_0^\infty\mathrm{d}t\,\mathrm{e}^{\mathrm{i}\omega t}\langle\bar{B}_n(t)\bar{B}_m(t)\bar{B}^\dagger_{n'}(0)\bar{B}^\dagger_{m'}(0)\rangle. \tag{3.11a}$$

by means of the Bethe–Salpeter equation

$$\bar{G}_{nmn'm'}(\omega) = \bar{G}^{(0)}_{nmn'm'}(\omega) + \sum_{ab} \bar{G}^{(0)}_{nmaa}(\omega)\bar{\Gamma}_{ab}(\omega)\bar{G}_{bbn'm'}(\omega) . \tag{3.11b}$$

Here $\bar{G}^{(0)}$ is the two-particle Green function of a "free boson" system whose Hamiltonian is given by Eq. (3.1a), except that the commutation relations have the form

$$[\hat{B}_m, \hat{B}^\dagger_n] = \delta_{mn} . \tag{3.12a}$$

This means that in each site we have a harmonic oscillator instead of a two-level molecule. The Hamiltonian of the "free boson" system, though having the form of Eq. (3.1a), is different from $\hat{H}_m$, since it acts in a different space of states; we shall denote it $\hat{H}_0$. We have

$$\bar{G}^{(0)}_{nmn'm'}(\omega) \equiv \int_0^\infty dt\ e^{i\omega t}[\langle \bar{B}_n(t)\bar{B}^\dagger_{n'}(0)\rangle_0 \langle \bar{B}_m(t)\bar{B}^\dagger_{m'}(0)\rangle_0 + \langle \bar{B}_n(t)\bar{B}^\dagger_{m'}(0)\rangle_0 \times \langle \bar{B}_m(t)\bar{B}^\dagger_{n'}(0)\rangle_0] , \tag{3.12b}$$

where the subscript 0 implies that the evolution is with respect to the free-boson material Hamiltonian (Eq. (3.1a) together with (3.12a)).

The one-particle Green functions in Eq. (3.12b) are identical for the system of free bosons and the Frenkel excitons, since the one-particle states are the same in both systems. The two-exciton scattering matrix can be expressed in terms of the one-exciton Green function in the following way:

$$\bar{\Gamma}_{mn}(\omega) = -2\{[\bar{F}(\omega)]^{-1}\}_{mn}, \qquad \bar{F}_{mn}(\omega) \equiv \int \frac{d\omega'}{2\pi i} G_{mn}(\omega')G_{mn}(\omega - \omega') . \tag{3.13a,b}$$

Eqs. (3.8) and (3.10), together with Eqs. (3.13), express the exact optical response of molecular aggregates in terms of the one-exciton Green function $G(\omega)$. We will denote these the Green function expressions (GFE). It was shown in [46] that Eq. (3.8), together with (3.10) and (3.13), still hold even when radiative decay is incorporated. The only difference is an additional contribution to the self-energy of the one-exciton Green function $G(\omega)$ representing the exciton interaction with the transverse electromagnetic field.

4. Application to aggregates with static diagonal disorder

In this section we consider the optical response of molecular assemblies with static disorder [73]. We specify the material Hamiltonian $\hat{H}_m$ by considering an assembly of two-level systems interacting with additional degrees of freedom, denoted q:

$$\hat{H}_m(q) = \sum_n \Omega_n(q)\hat{B}^\dagger_n\hat{B}_n + \sum_{m\neq n} J_{mn}(q)\hat{B}^\dagger_m\hat{B}_n + \hat{H}'(q) . \tag{4.1}$$

q represent a collection of coordinates (e.g., solvent, protein, etc.) which describe static disorder. q can also represent dynamic degrees of freedom as long as their typical time scale is sufficiently slow, so that their motions can be neglected on the time scale relevant for a particular measurement. For static disorder one can treat q as a set of classical variables describing different realizations. The Hamiltonian $\hat{H}_m(q)$ and the equilibrium density matrix $\hat{\rho}(q)$ depend on q parametrically. When motions of the other degrees of freedom cannot be neglected, we need to treat

q as operators and the problem becomes much more complex. This will be considered in later sections.

Instead of the Hamiltonian $\hat{H}'(q)$ in Eq. (4.1) we introduce the weight function $\exp[-F(q)]$, where F is the free energy; describing the probabilities of different realizations of disorder, and set $\hat{H}'(q) = 0$. The procedure now consists of two steps. We first evaluate the quantum mechanical expectation value of an operator representing an observable. The expectation value depends on the realization of the static degrees of freedom q. Let $\tilde{Q}(q, t)$ be a Heisenberg operator representing an observable (it depends on q through Eqs. (2.6) and (2.7) since $\hat{H}_m$ depends on q). The q-dependent expectation value $\langle \tilde{Q}(q, t) \rangle$ is defined as follows:

$$Q(q, t) \equiv \langle \tilde{Q}(q, t) \rangle \equiv \mathrm{Tr}\{\tilde{Q}(q, t)\hat{\rho}(q)\} . \tag{4.2a}$$

In the second step we average the q-dependent expectation value over all possible realizations of q. This is formally written as

$$Q(t) = \langle Q(q, t) \rangle_F , \tag{4.2b}$$

where $\langle \cdots \rangle_F$ represents the statistical average

$$\langle Q(q, t) \rangle_F \equiv Z^{-1} \int dq \exp[-F(q)] Q(q, t) \quad Z \equiv \int dq \exp[-F(q)] . \tag{4.2c,d}$$

The fact that the computation of the signal can be divided into two steps simplifies the problem considerably. When evaluating quantum expectation values we do not actually worry about the additional degrees of freedom, since they only enter as parameters in the Hamiltonian; when performing the averaging over disorder (Eq. (4.2)), we no longer make quantum mechanical calculations.

Our starting point will be Eq. (2.24a) with a slight modification: both the polarization and the optical response function $R^{(n)}$ now depend on the q degrees of freedom. Averaging Eq. (2.24a) over disorder we obtain the signal $P(\boldsymbol{r}, t) \equiv \langle P(\boldsymbol{r}, t; q) \rangle_F$ again in a form of Eq. (2.24a), but with

$$\begin{aligned} R^{(n)}(\boldsymbol{r}t; \boldsymbol{r}_1 t_1, \ldots, \boldsymbol{r}_n t_n) &\equiv Z^{-1} \int dq \exp[-F(q)] R^{(n)}(\boldsymbol{r}t; \boldsymbol{r}_1 t_1, \ldots, \boldsymbol{r}_n t_n; q) \\ &\equiv \langle R^{(n)}(\boldsymbol{r}t; \boldsymbol{r}_1 t_1, \ldots, \boldsymbol{r}_n t_n; q) \rangle_F . \end{aligned} \tag{4.3}$$

To find the optical response functions we should first compute $R^{(n)}(q)$ from Eq. (2.24a), fixing q in the Hamiltonian (4.1) with $H'(q) = 0$, and then average them in accordance with Eq. (4.2).

In a disordered system, the response functions in Eqs. (3.8) and (3.10) depend on q through the q-dependence of $\Omega_n(q)$ and $J_{mn}(q)$. The statistically averaged response functions of a disordered assemblies can be written as

$$R_{nm_1}(\omega) = Z^{-1} \int dq [-F(q)] \mu^2 \{G_{nm_1}(\omega; q) + G^*_{m_1 n}(-\omega; q)\} , \tag{4.4a}$$

$$\begin{aligned} R_{nm_1m_2m_3}(-\omega_s; \omega_1, -\omega_2, \omega_3) = Z^{-1} \tfrac{1}{6} \mu^4 \sum_{\substack{\text{perm} \\ m,\omega_i}} \sum_{n'n''} \int dq \exp[-F(q)] \\ \times G_{nn'}(\omega_s; q) G^*_{n'm_2}(\omega_2; q) G_{n''m_3}(\omega_3; q) \\ \times G_{n''m_1}(\omega_1; q) \bar{\Gamma}_{n'n''}(\omega_1 + \omega_3; q) + \text{c'.c'.} \end{aligned} \tag{4.4b}$$

Eq. (4.4) constitute our most general expressions for the optical response of disordered molecular aggregates. The averaging can be carried out numerically using, e.g., Monte Carlo simulations for different models of disorder [74] or using an extension of the coherent potential approximation to higher order [75]. Below we adopt a simple model of weak Gaussian diagonal disorder, which allows a diagrammatic analytical evaluation of the necessary averages. In this model, the interaction parameters J_{mn} are held fixed, and only the excitation energies Ω_n are affected by the bath coordinate q. We thus have

$$\Omega_n = \Omega + U_n. \tag{4.5a}$$

The coordinates representing static disorder are now represented by U_n, i.e., $q = \{U_n\}$, and the free energy $F(q) = F(\{U_n\})$ is taken to be

$$F(\{U_n\}) = \frac{1}{2\sigma^2}\sum_n U_n^2, \tag{4.5b}$$

where the variance parameter σ determines the strength of site-energy fluctuations. It follows from Eqs. (4.5b) and (4.2) that

$$\langle U_n\rangle_F = 0\,, \qquad \langle U_m U_n\rangle_F = \sigma^2\delta_{mn}, \tag{4.5c}$$

To perform the statistical averaging over disorder, we start with the GFE for the optical response (Eqs. (3.8), (3.10) and (3.13)), and expand the one-exciton Green functions in powers of U_m. We then average the products $\langle U_{m_1}\cdots U_{m_i}\rangle_F$ using Eq. (4.5c) and the Gaussian statistics of correlation functions of U's, which implies that they can be factorized into products of binary correlation functions $\langle U_{m_{i_1}} U_{m_{i_2}}\rangle_F$. Diagrammatic perturbation theory can then be developed. Assuming weak disorder, we will usually take into account the first nonvanishing corrections. Higher-order terms will be considered only if the small parameter related to disorder is compensated by a large resonant factor. We then obtain the following expressions for the optical response:

$$R_{nm_1}(\omega) = \mu^2[\tilde{G}_{nm_1}(\omega) + \tilde{G}^*_{m_1 n}(-\omega)]\,, \quad \tilde{G}_{mn}(\omega) \equiv \langle G_{mn}(\omega)\rangle_F. \tag{4.6a, b}$$

$\tilde{G}_{mn}$ is given by

$$\tilde{G}_{mn}(\omega) = [(\omega - h - \Sigma(\omega))^{-1}]_{mn}, \quad h_{mn} \equiv \Omega\delta_{mn} + J_{mn}(1 - \delta_{mn}). \tag{4.7a, b}$$

The self-energy $\Sigma(\omega)$ is obtained by solving the self-consistent equation

$$\Sigma_{mn}(\omega) = \delta_{mn}\sigma^2[(\omega - h - \Sigma(\omega))^{-1}]_{nn}. \tag{4.7c}$$

Eq. (4.7c) gives the self-energy Σ and the Green function $\tilde{G}$ by taking into account only perturbative contributions described by diagrams without intersections of dashed lines (see Appendix A and Fig. 22a) [64, 76].

The third-order response can be recast as a sum of three contributions

$$R = R^{(a)} + R^{(b)} + R^{(c)} + \text{c'.c'.}, \tag{4.8a}$$

with

$$R^{(a)}_{nm_1m_2m_3}(-\omega_s; \omega_1, -\omega_2, \omega_3) = \tfrac{1}{6}\mu^4 \sum_{\text{perm}}\sum_{n'n''} \tilde{G}_{nn'}(\omega_s)\tilde{G}^*_{n'm_2}(\omega_2)\tilde{G}_{n''m_3}(\omega_3)\tilde{G}_{n''m_1}(\omega_1) \times \bar{\Gamma}_{n'n''}(\omega_1 + \omega_3)\,, \tag{4.8b}$$

$$R^{(b)}_{nm_1m_2m_3}(-\omega_s;\omega_1,-\omega_2,\omega_3)=\mu^4\sum_{n'n''}\tilde{G}_{nn'}(\omega_s)\tilde{G}_{n''m_3}(\omega_3)\langle\langle G_{n'm_1}(\omega_1)G^*_{n''m_2}(\omega_2)\rangle\rangle \times\bar{\Gamma}_{n'n''}(\omega_1+\omega_3)\,, \tag{4.8c}$$

$$R^{(c)}_{nm_1m_2m_3}(-\omega_s;\omega_1,-\omega_2,\omega_3)=\mu^4\sum_{n'n''}\langle\langle G_{nn'}(\omega_s)G^*_{n''m_2}(\omega_2)\rangle\rangle\tilde{G}_{n''m_3}(\omega_3)\tilde{G}_{n'm_1}(\omega_1) \times\bar{\Gamma}_{n'n''}(\omega_1+\omega_3) \tag{4.8d}$$

The two-exciton scattering matrix $\bar{\Gamma}$ is given by

$$\bar{\Gamma}_{n'n''}(\omega)\equiv\int\frac{d\omega'}{2\pi i}\tilde{G}_{n'n''}(\omega')\tilde{G}_{n\,n''}(\omega-\omega')\,. \tag{4.9a}$$

and symbol $\langle\langle\cdots\rangle\rangle$ denotes the irreducible average:

$$\langle\langle G(\omega_1)G^*(\omega_2)\rangle\rangle\equiv\langle G(\omega_1)G^*(\omega_2)\rangle_F-\tilde{G}(\omega_1)\tilde{G}(\omega_2)\,. \tag{4.9b}$$

The irreducible Green function $\langle\langle G(\omega_1)G^*(\omega_2)\rangle\rangle$ can be expressed in terms of $\tilde{G}(\omega)$ by invoking the ladder approximation (see Eq. (4.13)).

The expressions for the response functions greatly simplify for translational invariant systems, i.e., periodic nanostructure. In the following we consider either infinite d-dimensional lattices for $d=1,2$ or finite d-dimensional lattices with size much smaller than the wavelength and periodic boundary conditions for $d=1,2,3$. We shall switch to momentum ($\boldsymbol{k}$) space, with lattice constant a, and adopt the following convention; for an arbitrary function f we have for an infinite lattice

$$f(n)=\left(\frac{a}{2\pi}\right)^d\int d^dk f(\boldsymbol{k})\exp(i\boldsymbol{k}\cdot\boldsymbol{R}_n)\,, \tag{4.10a}$$

and for a lattice with N sites and periodic boundary conditions

$$f(n)=\frac{1}{N}\sum_n e^{i\boldsymbol{k}\cdot\boldsymbol{R}_n}f(\boldsymbol{k})\,. \tag{4.10b}$$

The linear response function in the momentum domain has the form:

$$R(\omega,\boldsymbol{k})=\mu^2[G(\omega,\boldsymbol{k})+G^*(-\omega,-\boldsymbol{k})]\,. \tag{4.11}$$

The one-exciton Green function $G(\omega,\boldsymbol{k})$ is given by

$$G(\omega,\boldsymbol{k})=1/(\omega-\varepsilon(\boldsymbol{k})-\Sigma(\omega)+i\Gamma(\boldsymbol{k})/2) \tag{4.12a}$$

where $\varepsilon(\boldsymbol{k})$ is the exciton energy

$$\varepsilon(\boldsymbol{k})\equiv\Omega+\sum_n J_{no}\exp(i\boldsymbol{k}\cdot\boldsymbol{R}_n)\,. \tag{4.12b}$$

$\Gamma(\boldsymbol{k})$ is the momentum-dependent inverse exciton lifetime, which is introduced here phenomenologically. The self-energy induced by disorder satisfies the self-consistent equation [Eq. (4.7c)]

$$\Sigma(\omega)=\sigma^2\int d\boldsymbol{k}\,\frac{1}{\omega-\varepsilon(\boldsymbol{k})-\Sigma(\omega)+i\Gamma(\boldsymbol{k})/2}\,. \tag{4.12c}$$

Switching to k space and evaluating the irreducible Green functions $\langle\langle G(\omega_1)G^*(\omega_2)\rangle\rangle$ we obtain (see Appendix A):

$$\left\langle\left\langle G_{n'm_1}\left(\Omega+\frac{\omega}{2}\right)G^*_{n''m_2}\left(\Omega-\frac{\omega}{2}\right)\right\rangle\right\rangle$$
$$=\left(\frac{a}{2\pi}\right)^{3d}\int \mathrm{d}\boldsymbol{p}\,\mathrm{d}\boldsymbol{p}'\,\mathrm{d}\boldsymbol{q}\,L(\boldsymbol{p},\boldsymbol{p}';\boldsymbol{q},\Omega,\omega)\exp\{\mathrm{i}[\boldsymbol{p}\cdot(\boldsymbol{R}_{m_1}-R_{n'})-\boldsymbol{p}'\cdot(\boldsymbol{R}_{n''}-\boldsymbol{R}_{m_2})$$
$$+\tfrac{1}{2}\boldsymbol{q}\cdot(\boldsymbol{R}_{m_1}-\boldsymbol{R}_{n''}+\boldsymbol{R}_{n'}-\boldsymbol{R}_{m_2})]\}\,. \tag{4.13a}$$

For small frequencies ω, $L(\boldsymbol{p},\boldsymbol{p}';\boldsymbol{q},\Omega,\omega)$ has the form

$$L(\boldsymbol{p},\boldsymbol{p}';\boldsymbol{q},\Omega,\omega)=L_0(\boldsymbol{p},\boldsymbol{p}';\boldsymbol{q},\omega,\Omega)\,G\left(\Omega+\frac{\omega}{2},\boldsymbol{p}+\frac{\boldsymbol{q}}{2}\right)G^*\left(\Omega-\frac{\omega}{2},\boldsymbol{p}-\frac{\boldsymbol{q}}{2}\right)$$
$$\times G\left(\Omega+\frac{\omega}{2},\boldsymbol{p}'+\frac{\boldsymbol{q}}{2}\right)G^*\left(\Omega-\frac{\omega}{2},\boldsymbol{p}'-\frac{\boldsymbol{q}}{2}\right), \tag{4.13b}$$

where

$$L_0(\boldsymbol{p},\boldsymbol{p}';\boldsymbol{q},\Omega,\omega)=(2\mathrm{i}\sigma^2|\mathrm{Im}[\Sigma(\Omega)]|)/[\omega+\mathrm{i}D(\Omega)\boldsymbol{q}^2+\mathrm{i}\Gamma_0(\Omega)] \tag{4.13c}$$

when $\boldsymbol{q}$ is small, i.e., $D(\Omega)\boldsymbol{q}^2 \ll |\mathrm{Im}\,\Sigma(\Omega)|$, and

$$L_0(\boldsymbol{p},\boldsymbol{p}';\boldsymbol{q},\Omega,\omega)=(2\mathrm{i}\sigma^2|\mathrm{Im}[\Sigma(\Omega)]|)/[\omega+\mathrm{i}D(\Omega)(\boldsymbol{p}+\boldsymbol{p}')^2+\mathrm{i}\Gamma_0(\Omega)] \tag{4.13d}$$

when $(\boldsymbol{p}+\boldsymbol{p}')$ is small, i.e., $D(\Omega)(\boldsymbol{p}+\boldsymbol{p}')^2 \ll |\mathrm{Im}\,\Sigma(\Omega)|$.

Substituting Eq. (4.13) into Eq. (4.8) we obtain the optical response function in k space

$$R^{(i)}(-\omega_s-\boldsymbol{k}_s;\omega_1\boldsymbol{k}_1,\ -\omega_2-\boldsymbol{k}_2,\omega_3\boldsymbol{k}_3)$$
$$=\mu^4 G(\omega_1,\boldsymbol{k}_1)G^*(\omega_2,\boldsymbol{k}_2)G(\omega_3,\boldsymbol{k}_3)G(\omega_s,\boldsymbol{k}_s)\bar{\Gamma}^{(i)}(-\omega_s-\boldsymbol{k}_s;\omega_1\boldsymbol{k}_1,\ -\omega_2-\boldsymbol{k}_2,\omega_3\boldsymbol{k}_3)\,,$$
$$i=\mathrm{a},\mathrm{b},\mathrm{c} \tag{4.14a}$$

where $\boldsymbol{k}_s=\boldsymbol{k}_1-\boldsymbol{k}_2+\boldsymbol{k}_3$ and $\omega_s=\omega_1-\omega_2+\omega_3$.

$$\bar{\Gamma}^{(\mathrm{a})}(-\omega_s-\boldsymbol{k}_s,\omega_1\boldsymbol{k}_1,\ -\omega_2-\boldsymbol{k}_2,\omega_3\boldsymbol{k}_3)=\bar{\Gamma}(\omega_1+\omega_3,\boldsymbol{k}_1+\boldsymbol{k}_3)\,, \tag{4.14b}$$

$$\bar{\Gamma}^{(\mathrm{b})}(-\omega_s-\boldsymbol{k}_s;\omega_1\boldsymbol{k}_1,\ -\omega_2-\boldsymbol{k}_2,\omega_3\boldsymbol{k}_3)$$
$$=\frac{\mathrm{i}\sigma^2}{\omega_1-\omega_2+\mathrm{i}\Gamma_0(\Omega_{12})+\mathrm{i}(\boldsymbol{k}_1-\boldsymbol{k}_2)^2D(\Omega_{12})}\int \mathrm{d}\boldsymbol{p}\,2\pi\delta[\Omega_{12}-\varepsilon(\boldsymbol{p})]\bar{\Gamma}(\omega_3+\Omega_{12},\boldsymbol{p}+\boldsymbol{k}_3)\,, \tag{4.14c}$$

and

$$\bar{\Gamma}^{(\mathrm{c})}(-\omega_s-\boldsymbol{k}_s,\omega_1\boldsymbol{k}_1,\ -\omega_2-\boldsymbol{k}_2,\omega_3\boldsymbol{k}_3)$$
$$=\frac{2|\mathrm{Im}\,\Sigma(\omega_2)|\mathrm{i}}{\omega_1+\omega_3-2\omega_2+\mathrm{i}\Gamma_0(\omega_2)+\mathrm{i}(\boldsymbol{k}_1+\boldsymbol{k}_3)^2D(\omega_2)}\,\bar{\Gamma}(\omega_1+\omega_3,\boldsymbol{k}_1+\boldsymbol{k}_3)\,. \tag{4.14d}$$

Here

$$\bar{\Gamma}(\omega, \boldsymbol{k}) = -2\left\{\int \frac{d\omega'}{2\pi i} d\boldsymbol{p}\, G(\omega', \boldsymbol{p}) G(\omega - \omega', \boldsymbol{k} - \boldsymbol{p})\right\}^{-1}, \tag{4.14e}$$

$$\Omega_{12} = \tfrac{1}{2}(\omega_1 + \omega_2), \tag{4.15a}$$

$\Gamma_0(\omega)$ is a frequency-dependent exciton inverse lifetime averaged over momentum [23, 67]

$$\Gamma_0(\omega) \equiv \int d\boldsymbol{p}\, \Gamma(\boldsymbol{p}) |G(\omega, \boldsymbol{p})|^2 \left\{\int d\boldsymbol{p}' |G(\omega, \boldsymbol{p}')|^2\right\}^{-1}, \tag{4.15b}$$

and $D(\omega)$ is

$$D(\omega) \equiv \sigma^2 |\operatorname{Im} \Sigma(\omega)| \int d\boldsymbol{p} \frac{\partial \varepsilon(\boldsymbol{p})}{\partial(\boldsymbol{p})} \frac{\partial \varepsilon(\boldsymbol{p})}{\partial(\boldsymbol{p})} |G(\omega, \boldsymbol{p})|^4 . \tag{4.15c}$$

In order to clarify the physical significance of $D(\omega)$ and $\Gamma_0(\omega)$, let us consider the following dynamical variable:

$$n(\boldsymbol{p}, \boldsymbol{q}; t) \equiv \sum_{mn} \langle\langle \tilde{B}_m^{\dagger} \tilde{B}_n \rangle\rangle_F \exp\{i[\boldsymbol{p} \cdot (\boldsymbol{R}_m - \boldsymbol{R}_n) + \tfrac{1}{2}\boldsymbol{q} \cdot (\boldsymbol{R}_m + \boldsymbol{R}_n)\}, \tag{4.16a}$$

where $\langle \cdots \rangle$ stands for the quantum mechanical average and $\langle \cdots \rangle_F$ for the average over disorder. This variable represents the single-exciton density matrix. $\boldsymbol{p}$ represents the exciton momentum (through the Wigner representation of the density matrix) [5] and $\boldsymbol{q}$ is the wave vector associated with its spatial profile. In the following we would like to focus on energy rather than momentum. We shall, therefore, introduce the exciton density in position and energy space

$$n(\boldsymbol{q}, \omega; t) \equiv 2\pi \int d\boldsymbol{p}\, n(\boldsymbol{p}, \boldsymbol{q}; t) \delta[\omega - \varepsilon(\boldsymbol{p})] . \tag{4.16b}$$

Eq. (4.13) imply that the exciton density satisfies the equation

$$\partial n(\boldsymbol{q}, \omega; t)/\partial t = -[D(\omega)\boldsymbol{q}^2 + \Gamma_0(\omega)] n(\boldsymbol{q}, \omega; t) \tag{4.16c}$$

Eq. (4.16c) is the diffusion equation for the exciton density with a fixed energy ω, written in momentum space. This shows that $D(\omega)$ is the energy-dependent diffusion coefficient, and $\Gamma_0(\omega)$ is the inverse exciton lifetime representing decay processes that do not conserve the number of excitons. Since elastic scattering processes conserve exciton energy, the spatially inhomogeneous exciton density created with a given exciton energy ω evolves without changing the energy, and the diffusion coefficient and the inverse lifetime describing this evolution through Eq. (4.16c) depend on ω (see Eqs. (4.15b) and (4.15c). Eqs. (4.15b) and (4.15c) can be simplified further when the exciton velocity and decay rate change slowly compared with the exciton scattering rate

$$\Gamma_0(\omega) = \int d\boldsymbol{p}\, \delta[\omega - \varepsilon(\boldsymbol{p})] \Gamma(\boldsymbol{p}) \left\{\int d\boldsymbol{p}'\, \delta(\omega - \varepsilon(\boldsymbol{p}'))\right\}^{-1}, \tag{4.17a}$$

$$D(\omega) = \frac{\pi \sigma^2}{|\operatorname{Im} \Sigma(\omega)|^2} \int d\boldsymbol{p}\, \delta(\omega - \varepsilon(\boldsymbol{p})) \frac{\partial \varepsilon(\boldsymbol{p})}{\partial \boldsymbol{p}} \frac{\partial \varepsilon(\boldsymbol{p})}{\partial \boldsymbol{p}} . \tag{4.17b}$$

In deriving Eq. (4.17) we have used that $G(\omega, \boldsymbol{p})$ is strongly peaked at $\omega = \varepsilon(\boldsymbol{p})$ with the width given by $|\mathrm{Im}\,\Sigma(\omega)|$.

At this point it will be instructive to compare our results with the conventional (and the much simpler) local field approximation commonly used in the calculation of optical susceptibilities. This approach is based on calculating the polarizability γ of a single molecule interacting with a local field $E_{\mathrm{L}}(\omega\, \boldsymbol{k})$. All many-body effects are then lumped into the local field correction factor $\Delta(\omega, \boldsymbol{k})$ which is the ratio of the local field and the average (Maxwell) field $E(\omega, \boldsymbol{k})$

$$E_{\mathrm{L}}(\omega, \boldsymbol{k}) = \Delta(\omega, \boldsymbol{k}) E(\omega, \boldsymbol{k}) ,$$

Evaluating Δ using the procedure of Lorentz [77] allows us to compute the susceptibilities. It has been shown [5] that the local field approximation (LFA) can be obtained using the equations of motion framework by making a factorization $\langle \hat{B}_n \hat{B}_m \rangle = \langle \hat{B}_n \rangle \langle \hat{B}_m \rangle$ in Eq. (3.5a); Eq. (3.5b) then becomes redundant. The LFA is recovered from Eq. (4.14) by setting $R^{(\mathrm{b})} = R^{(\mathrm{c})} = 0$ and

$$\bar{\Gamma}(\omega, \boldsymbol{k}) = -2\left\{\omega - \int \mathrm{d}\boldsymbol{q}\, \{\varepsilon(\boldsymbol{q}) + \varepsilon(\boldsymbol{k} - \boldsymbol{q}) - \mathrm{i}\Gamma(\boldsymbol{q})/2 - \mathrm{i}\Gamma(\boldsymbol{k} - \boldsymbol{q})/2\}\right\} . \tag{4.18a}$$

When these approximations are made, we can recast the nonlinear response with the LFA in the form [5]:

$$R(-\omega_{\mathrm{s}} - \boldsymbol{k}_{\mathrm{s}}; \omega_1 \boldsymbol{k}_1, -\omega_2 - \boldsymbol{k}_2, \omega_3 \boldsymbol{k}_3) =$$
$$(2\pi/a)^d \Delta(\omega_{\mathrm{s}} \boldsymbol{k}_{\mathrm{s}}) \Delta(\omega_1 \boldsymbol{k}_1) \Delta(-\omega_2 - \boldsymbol{k}_2) \Delta(\omega_3 \boldsymbol{k}_3) \gamma(-\omega_{\mathrm{s}}; \omega_1, -\omega_2, \omega_3) , \tag{4.18b}$$

where γ is the third-order polarizability of a single molecule.

$$\gamma(-\omega_{\mathrm{s}}; \omega_1, -\omega_2, \omega_3)$$
$$= -\frac{1}{6} \sum_{\substack{\mathrm{perm} \\ \omega_i}} \frac{1}{\omega_1 - \Omega + \mathrm{i}\eta} \frac{1}{\omega_3 - \Omega + \mathrm{i}\eta} \frac{1}{\omega_2 - \Omega - \mathrm{i}\eta} \frac{1}{\omega_{\mathrm{s}} - \Omega + \mathrm{i}\eta} 2(\omega_1 + \omega_3 - 2\Omega) + \mathrm{c'.c'.} , \tag{4.18c}$$

and

$$\Delta(\omega, \boldsymbol{k}) \equiv \frac{(\omega + \mathrm{i}\eta)^2 - \Omega^2}{(\omega + \mathrm{i}\eta)^2 - [\varepsilon(\boldsymbol{k})]^2} . \tag{4.18d}$$

Disorder effects can sometimes be accounted for within the LFA by averaging Eq. (4.18b) over a statistical distribution of the local field (i.e., the fourth moment of Δ) [78].

We have expressed the third order nonlinear optical response of a disordered molecular assembly in a form of a sum of three contributions. $R^{(\mathrm{a})}$ contains one- and three-photon resonances on one-exciton states ($G(\omega_1)$, $G^*(\omega_2)$, $G(\omega_3)$, $G(\omega_{\mathrm{s}})$) and two-photon resonances on two-exciton states ($\bar{\Gamma}(\omega_1 + \omega_3)$). As can be seen from Eq. (4.18a), the LFA completely misses all two-photon resonances whereas within the GFE they are rigorously incorporated. $R^{(\mathrm{b})}$ and $R^{(\mathrm{c})}$ show additional resonances at $\omega_1 \approx \omega_2$ and $\omega_1 + \omega_3 \approx 2\omega_2$ respectively. These are collective many-body resonances which are not associated with some specific pairs of eigenstates of the system. This point will be clarified in Sections 11 and 12, where we rederive these resonances using the conventional

sum over states expression for optical susceptibilities [54, 37]. We shall also show later that these two resonances have a different nature. In the present model the two resonances have a comparable linewidth related to the inverse exciton lifetime Γ_0. However, this is no longer the case once inelastic exciton scattering by interaction with phonons is introduced. It will be shown in Section 10 that only the $\omega_1 + \omega_3 \approx 2\omega_2$ resonance is broadened by phonons. Another important feature is that, as one can see from Eqs. 4.14(c) and (d), these resonances have prefactors related to $\bar{\Gamma}$. In the LFA $\bar{\Gamma}$ is almost real, whereas in reality $\bar{\Gamma}$ has an imaginary part due to the two-exciton states. This means that by performing phase-controlled four-wave mixing, one can observe the breakdown of the LFA by looking for the signal in the resonant region. Both resonances show up when ω_2 is inside the one-exciton band. If ω_3 is off resonant (far from the one-exciton band) and $\omega_1 + \omega_3$ is far from the two-exciton band and $\bar{\Gamma}(\omega_1 + \omega_3)$ can be taken in the LFA. The LFA result for the $\omega_1 = \omega_2$ resonance in this case was obtained in [56]. Our present result holds when ω_3 is resonant as well. Since in the resonant expression near $\omega_1 + \omega_3 = 2\omega_2$ the signal is proportional to $\bar{\Gamma}(\omega_1 + \omega_3)$ and $\omega_1 + \omega_3$ is inside the two-exciton band the LFA always fails, as can be easily verified in a phase-controlled measurement.

Resonances associated with $\bar{\Gamma}^{(c)}$

In the examples considered below we focus on resonances associated with $\bar{\Gamma}^{(c)}$, and discuss their observation by frequency-domain and time-domain four-wave mixing. Resonances associated with $\bar{\Gamma}^{(a)}$ and $\bar{\Gamma}^{(b)}$ will be considered later, after we introduce exciton–phonon coupling.

The heterodyne (Eq. (2.20a)) four-wave mixing signal in the vicinity of the $\omega_1 + \omega_3 - 2\omega_2 \approx 0$ resonance for a disordered J-aggregate is plotted as a function of $\omega_1 + \omega_3 - 2\omega_2$ in Fig. 1 (solid

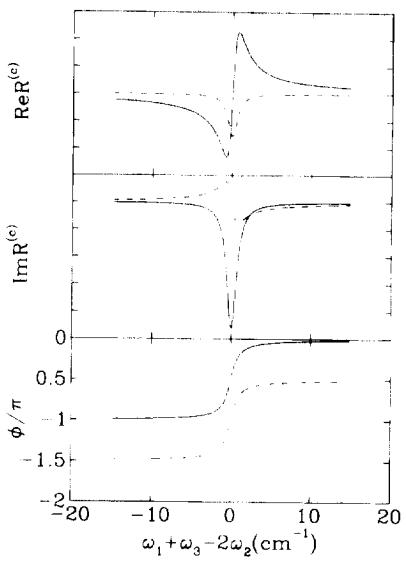

Fig. 1. The real part, imaginary part, and the phase of the heterodyne phase conjugate signal $S_{het}(\boldsymbol{k}_s\omega_s)$ given by $R^{(c)}$ for a 1-D lattice with Gaussian diagonal disorder [Eqs. 4.14(a) and (d)] as a function of detuning. $\sigma/J = 0.3, \omega_2 = 200\ \text{cm}^{-1}$, $\eta = 0.05|\text{Im}\,\Sigma(\omega_2)| = 0.74\ \text{cm}^{-1}$. Solid line is the result of Green function formulas, and the dash line is the result of LFA. The phase ϕ is defined by $\tan\phi = \text{Im}(R^{(c)})/\text{Re}(R^{(c)})$.

line corresponds to the exact theory, dashed to the LFA). The external electric field is represented as a sum of three coherent waves

$$\mathscr{E}(\boldsymbol{r}, t) = E_1 \exp(-i\omega_1 t + i\boldsymbol{k}_1 \cdot \boldsymbol{r}) + E_2 \exp(-i\omega_2 t + i\boldsymbol{k}_2 \cdot \boldsymbol{r}) + E_3 \exp(-i\omega_3 t + i\boldsymbol{k}_3 \cdot r) + \text{c.c.} \tag{4.19}$$

Taking the amplitudes $E_1 = E_2 = E_3$ and the amplitude of the heterodyne field $E_h(\boldsymbol{k}_s\omega_s) = E_1 \exp(i\varphi)$ and looking for the signal at $\boldsymbol{k}_s = \boldsymbol{k}_1 - \boldsymbol{k}_2 + \boldsymbol{k}_3$ we obtain from Eq. (2.20a)

$$S_{het}(\boldsymbol{k}_s\omega_s) = |E_1|^4 \mathrm{Re}(R^{(c)}), \quad \varphi = 0; \qquad S_{het}(\boldsymbol{k}_s\omega_s) = |E_1|^4 \mathrm{Im}(R^{(c)}), \quad \varphi = \frac{\pi}{2}. \tag{4.20a,b}$$

When the exact theory gives a Lorentzian form of the resonance the LFA gives a dispersive behavior and vice versa. The reason is that in the LFA $\bar{\Gamma}(2\omega)$ is practically real, but for the exact theory $\Gamma(2\omega)$ is mostly imaginary when ω is inside the exciton band. This is a clear signature of the failure of the LFA.

This resonance may be observed also in the time domain where it shows up as a two-exciton photon echo. The electric field in a time-resolved four-wave mixing has the form

$$\mathscr{E}(\boldsymbol{r}, t) = \mathscr{E}_1(\boldsymbol{k}_1, t)\exp(i\boldsymbol{k}_1 \cdot \boldsymbol{r}) + \mathscr{E}_2(\boldsymbol{k}_2, t)\exp(i\boldsymbol{k}_2 \cdot \boldsymbol{r}) + \mathscr{E}_3(\boldsymbol{k}_3, t)\exp(i\boldsymbol{k}_3 \cdot \boldsymbol{r}) + \text{c.c.}, \tag{4.21a}$$

where

$$\mathscr{E}_m(\boldsymbol{k}_m, t) = E_m(t - \tau'_m)\exp(-i\Omega_m t), \quad m = 1, 2, 3, \tag{4.21b}$$

where Ω_m and τ'_m represent the carrier frequencies and the time delays of the pulses. The time-resolved four-wave mixing signal measured in the direction $\boldsymbol{k}_s = \boldsymbol{k}_1 - \boldsymbol{k}_2 + \boldsymbol{k}_3$ is related to the corresponding Fourier component of the polarization

$$P(\boldsymbol{k}_s, t) = \int_{-\infty}^{t}\int_{-\infty}^{t}\int_{-\infty}^{t} d\tau_1\, d\tau_2\, d\tau_3\, R(t - \boldsymbol{k}_s;\ \tau_1\boldsymbol{k}_1, \tau_2 - \boldsymbol{k}_2, \tau_3\boldsymbol{k}_3) \times \mathscr{E}_1(\tau_1)\mathscr{E}^*_2(\tau_2)\mathscr{E}_3(\tau_3) \tag{4.22a}$$

with

$$R(t - \boldsymbol{k}_s; \tau_1\boldsymbol{k}_1, \tau_2 - \boldsymbol{k}_2, \tau_3\boldsymbol{k}_3) \equiv \int \frac{d\omega_1\, d\omega_2\, d\omega_3}{(2\pi)^3} R(-\omega_s - \boldsymbol{k}_s; \omega_1\boldsymbol{k}_1, -\omega_2 - \boldsymbol{k}_2, \omega_3\boldsymbol{k}_3) \times \exp[-i\omega_1(t - \tau_1) + i\omega_2(t - \tau_2) - i\omega_3(t - \tau_3)]. \tag{4.22b}$$

In an ordinary photon echo experiment [43] one first comes at $t = -\tau$ with a short resonant $\boldsymbol{k}_2$ pulse and then at $t = 0$ with two short resonant pulses $\boldsymbol{k}_1$ and $\boldsymbol{k}_3$. This is represented by the choice $\tau'_1 = \tau'_3 = 0$, and $\tau'_2 = -\tau$. In the two-exciton photon echo experiment the $\boldsymbol{k}_1$ and $\boldsymbol{k}_3$ pulses are kept off-resonant, $\Omega_1 + \Omega_3$ being resonant with two-exciton states (i.e., $\Omega_1 + \Omega_3$ is inside the two-exciton band), and $\Omega_1 + \Omega_3 = 2\Omega_2$. To obtain the signal we substitute the $R^{(c)}$ contribution given by Eqs. 4.14(a) and (d) into the r.h.s. of Eq. (4.22b) and then substitute Eq. (4.22b) into Eq. (4.22a). Provided the pulses are short compared with $\Gamma_0^{-1}(\Omega_2)$, but with spectral width

narrower than the bandwidth W, the nonlinear polarization which is nonzero only provided $\tau_2' < \tau_1' = \tau_3'$ has the form

$$P_s(\boldsymbol{k}_s, t) = g(\Omega_1, \Omega_3; \Omega_2)\exp(-\Gamma_0(\Omega_2)t)I(t-\tau)\,, \tag{4.23a}$$

where

$$g(\Omega_1, \Omega_3; \Omega_2) \equiv 4\mu^4 G(\Omega_1)G(\Omega_3)\left\{\int d\boldsymbol{q}\, G(\Omega_2, \boldsymbol{q})\right\}^{-1} \mathrm{Im}\,[G(\Omega_2)]\,, \tag{4.23b}$$

with $I(t-\tau)$ given by

$$I(t-\tau) \equiv \int d\tau' E_1\left(\frac{\tau'}{2}\right)E_3\left(\frac{\tau'}{2}\right)E_2^*(\tau'+\tau-t)\,. \tag{4.23c}$$

The signal can also be written in the form of Eq. (4.22a) with

$$R(t\boldsymbol{k}_s; \tau_1\boldsymbol{k}_1, \tau_2-\boldsymbol{k}_2, \tau_3\boldsymbol{k}_3) = \exp[-\Gamma_0(\Omega_2)(t-\tau_1)]\theta(t-\tau_1)\delta(\tau_1-\tau_3)\delta(t-2\tau_1+\tau_2) \times g(\Omega_1, \Omega_3; \Omega_2)\,. \tag{4.23d}$$

For short pulses $I(t-\tau) = \delta(t-\tau)$ and the signal is peaked at $t=\tau$. Its decay rate with the delay time is given by the homogeneous dephasing rate $\Gamma_0(\Omega_2)$.

We denote this two-exciton echo because it is related to the strong correlation between the one- and two-exciton states. This point is discussed further in Sections 11 and 12. We will return to the two-exciton photon echo in Section 10 where we add coupling with phonons and show how the echo-decay rate is affected by inelastic exciton–phonon scattering.

5. Correlation function expressions for optical response functions

In the previous section we considered the optical response of molecular nanostructures with static disorder, i.e., when the additional degrees of freedom are slow. The calculation was carried out in two steps: we first evaluated the quantum expectation value for a given realization of disorder, and then averaging this expectation value over all possible realizations. The quantum part of the problem was solved in Section 3, making use of equations of motion for Heisenberg operators. The situation becomes more complicated when the additional degrees are not slow, since one has to solve the quantum problem in the expanded phase-space containing the additional degrees of freedom as well.

A major difficulty we face in this case is that once the additional degrees of freedom are eliminated, the equations of motion become retarded. This means that the time derivative of an exciton operator depends now on products of exciton operators at different times. It is then no longer possible to close the equations using the factorization procedure employed in the previous section. The many-body Green function approach [64, 79] provides a convenient and useful alternative. In this approach we formulate the optical response using multitime-correlation functions, which are then evaluated using diagrammatic techniques. This eventually amounts to factorizing higher correlation functions into lower order ones. This procedure is more general and less restrictive than the factorization of expectation values of products of operators at the same

time, which is made in the equations of motion approach. The diagrammatic approach allows us to treat the additional degrees of freedom as a dynamical disorder. This means that one can consider the evolution of the exciton system in a time-dependent external field related to the additional degrees of freedom, and then average the result over all possible trajectories of these degrees of freedom, with a certain weight. This picture arises naturally when the Green function formalism is recast using the path integral representation [79, 80].

In this section we derive compact expressions for the optical signals and response functions in terms of equilibrium correlation functions of the polarization operators in the isolated system without external sources. To that end, following [46] we introduce chronological Green functions on the Keldysh time loop [81, 82]. For operators $\hat{Q}^{(1)}, \ldots, \hat{Q}^{(n)}$ and indices $i_1, \ldots, i_n$ which assume the values $i = \mathrm{L}, \mathrm{R}$ we define the chronological correlation function $\langle \hat{Q}^{(1)}_{i_1}(t_1) \cdots \hat{Q}^{(1)}_{i_n}(t_n) \rangle$ as follows:

$$\langle \hat{Q}^{(1)}_{\mathrm{L}}(t_1) \cdots \hat{Q}^{(j)}_{\mathrm{L}}(t_j) \hat{Q}^{(j+1)}_{\mathrm{R}}(t_{j+1}) \cdots \hat{Q}^{(n)}_{\mathrm{R}}(t_n) \rangle$$
$$\equiv \mathrm{Tr}\{ T[\hat{Q}^{(1)}(t_1) \cdots \hat{Q}^{(j)}(t_j)] \hat{\rho} T'[\hat{Q}^{(j+1)}(t_{j+1}) \cdots \hat{Q}^{(n)}(t_n)] \}, \tag{5.1}$$

The indices L and R denote whether the operator appears to the left or to the right of the density matrix. The operator T stands for chronological time ordering. It acts on the "left" operators $\hat{Q}^{(1)}(t_1), \ldots, \hat{Q}^{(j)}(t_j)$ and rearranges them so that the earliest time appears on the right and the latest time on the left. The operator T' stands for antichronological time ordering. It acts on the "right" operators $\hat{Q}^{(j+1)}(t_{j+1}), \ldots, \hat{Q}^{(n)}(t_n)$ and rearranges them such that the earliest time is to the left and the latest time to the right. Since the order of operators is uniquely determined by the L and R indices and by T and T', then the chronological-correlation function is invariant with respect to the ordering of operators in the l.h.s. of Eq. (5.1). We can similarly define another correlation function $\langle \tilde{Q}^{(1)}_{i_1}(t_1) \cdots \tilde{Q}^{(n)}_{i_n}(t_n) \rangle$ using the same rules, except that the operators are now in the Heisenberg rather than the interaction picture [see Eq. (2.7)].

Alternatively we may change variables and define

$$Q_+ \equiv \tfrac{1}{2}(Q_{\mathrm{L}} + Q_{\mathrm{R}}), \qquad Q_- \equiv Q_{\mathrm{L}} - Q_{\mathrm{R}}. \tag{5.2a}$$

We will label these variables Q_α, where the Greek index α assumes the values $+$ and $-$. These indices are related to the Latin indices by the linear transformation

$$Q_\alpha = V_{\alpha i} Q_i \tag{5.2b}$$

where summation over repeating indices is assumed, and

$$V_{+,\mathrm{R}} = V_{+,\mathrm{L}} = \tfrac{1}{2}, \qquad V_{-,\mathrm{R}} = 1, \; V_{-,\mathrm{L}} = -1. \tag{5.2c}$$

Combining these with (5.1) we can define the correlation functions

$$\langle \hat{Q}^{(1)}_{\alpha_1}(t_1) \cdots \hat{Q}^{(n)}_{\alpha_n}(t_n) \rangle \equiv V_{\alpha_1 i_1} \cdots V_{\alpha_n i_n} \langle \hat{Q}^{(1)}_{i_1}(t_1) \cdots \hat{Q}^{(n)}_{i_n}(t_n) \rangle . \tag{5.3}$$

Using the present notation, we can recast the scattered field and the coherent signal defined in Section 2 as:

$$E_{\mathrm{s}}(\boldsymbol{r}, t) = \mathrm{Tr}(\tilde{E}(\boldsymbol{r}, t)\hat{\rho}) = \langle \tilde{E}_+(\boldsymbol{r}, t) \rangle , \tag{5.4a}$$

$$I_{\mathrm{c}}(\boldsymbol{r}_1 t_1, \boldsymbol{r}_2 t_2) = \mathrm{Tr}\{ [\tilde{E}(\boldsymbol{r}_1, t_1)\tilde{E}(\boldsymbol{r}_2, t_2) + \tilde{E}(\boldsymbol{r}_2, t_2)\tilde{E}(\boldsymbol{r}_1, t_1)]\hat{\rho} \}$$
$$= 2\langle \tilde{E}_+(\boldsymbol{r}_1, t_1)\tilde{E}_+(\boldsymbol{r}_2, t_2) \rangle . \tag{5.4b}$$

the polarization assumes the form

$$P(\boldsymbol{r}, t) = \mathrm{Tr}(\tilde{P}(\boldsymbol{r}, t)\hat{\rho}) = \langle \tilde{P}_-(\boldsymbol{r}, t)\rangle \,, \tag{5.5a}$$

and the polarization correlation function is

$$\begin{aligned}\mathscr{C}_p(\boldsymbol{r}_1 t_1, \boldsymbol{r}_2 t_2) &= \tfrac{1}{2}\mathrm{Tr}\{[\tilde{P}(\boldsymbol{r}_1, t_1)\tilde{P}(\boldsymbol{r}_2, t_2) + \tilde{P}(\boldsymbol{r}_2, t_2)\tilde{P}(\boldsymbol{r}_1, t_1)]\hat{\rho}\} \\ &= \langle \tilde{P}_+(\boldsymbol{r}_1, t_1)\tilde{P}_+(\boldsymbol{r}_2, t_2)\rangle . \end{aligned} \tag{5.5b}$$

We next express the signals in terms of correlation functions of the polarization operators in the isolated system without external sources ($P_{\mathrm{ext}} = 0$). To that end, we will use a general relation, derived in Appendix B which connects system correlation functions calculated with and without P_{ext}. This relation has the following form for arbitrary operators $\hat{Q}^{(1)}, \ldots, \hat{Q}^{(n)}$ [46]:

$$\langle \tilde{Q}^{(1)}_{\chi_1}(t_1)\cdots \tilde{Q}^{(n)}_{\chi_n}(t_n)\rangle = \left\langle \hat{Q}_{\chi_1}(t_1)\cdots \hat{Q}_{\chi_n}(t_n)\exp\left\{ \mathrm{i}\int \mathrm{d}\boldsymbol{r}\int_{\chi}^{\infty} \mathrm{d}t\, \mathscr{E}(\boldsymbol{r}, t)\hat{P}_-(\boldsymbol{r}, t)\right\}\right\rangle , \tag{5.6}$$

where $\mathscr{E}(\boldsymbol{r}, t)$ is the external field given by the solution of the Maxwell equations with P_{ext} as the only source (Eq. (2.23)).

Using the expressions derived in Secion 2 which relate the optical signals to P and $\mathscr{C}_p$, Eq. (5.5) together with Eq. (5.6) close the system of equations which relate the optical signals to correlation functions of the polarization.

Finally we express the response functions in terms of correlation functions of the polarization operators in the isolated system ($P_{\mathrm{ext}} = 0$). Substituting Eq. (5.6) into Eq. (5.5), expanding the exponent in Eq. (5.6) in powers of the external field, and comparing the expansions with Eq. (2.24) we obtain the correlation function expressions for the optical response functions

$$R^{(n)}(\boldsymbol{r}t; \boldsymbol{r}_1 t_1, \ldots, \boldsymbol{r}_n t_n) = \mathrm{i}^n\langle \hat{P}_+(\boldsymbol{r}, t)\hat{P}_-(\boldsymbol{r}_1, t_1)\cdots \hat{P}_-(\boldsymbol{r}_n, t_n)\rangle \,, \tag{5.7a}$$

$$R^{(n)}_{\mathrm{c}}(\boldsymbol{r}t, \boldsymbol{r}'t'; \boldsymbol{r}_1 t_1, \ldots, \boldsymbol{r}_n t_n) = \mathrm{i}^n\langle \hat{P}_+(\boldsymbol{r}, t)\hat{P}_+(\boldsymbol{r}', t')\hat{P}_-(\boldsymbol{r}_1, t_1)\cdots \hat{P}_-(\boldsymbol{r}_n, t_n)\rangle \,. \tag{5.7b}$$

In the following sections we will consider the third-order nonlinear optical response function $R^{(3)}$ responsible for coherent four-wave mixing signal, and the correlation signal linear in the intensity of the external field which is given by the response function $R^{(2)}_{\mathrm{c}}$. Both response functions are given by four-point correlation functions of the polarization, but with different indices. This implies that they are given by different combinations of four-point correlation functions.

$$R^{(3)}(\boldsymbol{r}t; \boldsymbol{r}_1 t_1, \boldsymbol{r}_2 t_2, \boldsymbol{r}_3 t_3) = \langle \hat{P}_+(\boldsymbol{r}, t)\hat{P}_-(\boldsymbol{r}_1, t_1)\hat{P}_-(\boldsymbol{r}_2, t_2)\hat{P}_-(\boldsymbol{r}_3, t_3)\rangle, \tag{5.8a}$$

$$R^{(2)}_{\mathrm{c}}(\boldsymbol{r}t, \boldsymbol{r}'t'; \boldsymbol{r}_1 t_1, \boldsymbol{r}_2 t_2) = \langle \hat{P}_-(\boldsymbol{r}, t)\hat{P}_+(\boldsymbol{r}', t')\hat{P}_-(\boldsymbol{r}_1, t_1)\hat{P}_-(\boldsymbol{r}_2, t_2)\rangle. \tag{5.8b}$$

It will be shown in Section 9 that $R^{(2)}_{\mathrm{c}}$ determines the time- and frequency-resolved fluorescence spectrum as well. Eq. (5.8) allow, therefore, a direct comparison of four-wave mixing and fluorescence spectroscopy.

6. Response functions of Frenkel excitons coupled to a dynamical bath

In this section we derive formal expressions for the linear and the third-order nonlinear optical response of molecular nanostructures interacting with additional degrees of freedom, by evaluating

the correlation functions in the expressions for the optical response [Eq. (5.7a)] derived in the previous section. Our goal is to generalize the GFE of Section 3 which holds for static disorder, to incorporate additional dynamical degrees of freedom with an arbitrary time scale. To that end we return to the Hamiltonian of Eq. (4.1) but now we assume that the variables q are operators related to the additional dynamical variables. The non-boson character of the exciton operators greatly complicates the calculation. To overcome this difficulty we use the following procedure [46, 56]: instead of the exciton Hamiltonian (3.1a) with commutation relations (3.1b), we introduce a different Hamiltonian which describes a system of bosons with on-site interaction controlled by the parameter g:

$$\hat{H}_m(q) = \sum_n \Omega_n(q)\hat{C}_n^\dagger \hat{C}_n + \sum_{m \neq n} J_{mn}(q)\hat{C}_m^\dagger \hat{C}_n + \frac{g}{2}\sum_n (\hat{C}_n^\dagger)^2 \hat{C}_n^2 + H'(q)\,, \tag{6.1a}$$

$$[\hat{C}_n, \hat{C}_m^\dagger] = \delta_{nm}\,. \tag{6.1b}$$

The excitons described by Eq. (3.1) behave as hard core bosons; states with more than one exciton occupying the same site are excluded. In contrast, the present Hamiltonian allows two excitons to reside on the nth site, but for $g > 0$ it adds a penalty: the energy of that state $(2\Omega_n + g)$ is higher by an amount g. We have thus changed the hard core boson model to a soft core model. As g increases, the occupation of these states becomes less and less likely. We shall calculate the response function corresponding to the Hamiltonian (6.1). By sending $g \to \infty$ at the end we then recover the results of the Hamiltonian (4.1).[3]

The linear and the third-order optical response are given by Eq. (3.6). Making use of the correlation functions (Eq. (5.7a)) and Eq. (3.2), we obtain the following expressions for R_{nm_1} and $R_{nm_1m_2m_3}$:

$$R_{nm_1}(t; t_1) = \mathrm{i}\mu^2 \langle (\hat{C}_{n+}(t) + \hat{C}_{n+}^+(t))(\hat{C}_{m_1}(t_1) + \hat{C}_{m_1}^+(t_1))\rangle\,, \tag{6.2a}$$

$$\begin{aligned} R_{nm_1m_2m_3}(t; t_1, t_2, t_3) = \mathrm{i}^3\mu^4 \langle &(\hat{C}_{n+}(t) + \hat{C}_{n+}^+(t))(\hat{C}_{m_1}^-(t_1) + \hat{C}_{m_1}(t_1)) \\ &\times (\hat{C}_{m_2}^-(t_2)) + \hat{C}_{m_2}^+(t_2))(\hat{C}_{m_3}(t_3) + \hat{C}_{m_3}^+(t_3))\rangle\,. \end{aligned} \tag{6.2b}$$

In Appendix C we calculate the correlation functions which appear in Eq. (6.2b) using the Green function technique; here we present a brief sketch of the derivation and comment on the results. We start with a perturbative expansion in the interaction of excitons with the additional degrees of freedom (hereafter denoted the exciton–phonon interaction). In complete analogy with the treatment of static disorder in Section 4, we will take into account the higher-order terms in the perturbation theory only if they are compensated by large resonant factors. Otherwise we truncate the expansion to lowest order. If we adopt the path integral approach introduced in Appendix B [46, 79, 80], we can visualize the problem in a manner very close to the problem of static disorder; we then look for the optical response of a system of Frenkel excitons with time-dependent parameters Ω_n and J_{mn}. This time-dependence reflects the time evolution of the coordinates q, i.e., $\Omega_n = \Omega_n(q(t))$, $J_{mn} = J_{mn}(q(t))$. The optical response of the system can then be

[3] In addition, the Hamiltonian (5.1) for $g < 0$ can describe two-particle bound states (biexcitons) [20, 83]. These will not be considered here.

obtained by averaging it over all possible trajectories $q(t)$ with the weight $\exp[iS[q(t)]]$, where $S[q(t)]$ is the classical action of the additional degrees of freedom.[4]

The linear response is given by

$$R_{nm_1}(\omega) = \mu^2[G_{nm_1}(\omega) + G^*_{m_1 n}(-\omega)] \,. \tag{6.3a}$$

where the one-exciton Green function G is defined as follows:

$$G_{mn}(\omega) = -i\int_0^\infty dt\, \exp(i\omega t)\, \langle \hat{C}_m(t)\hat{C}^+_n(0)\rangle_0 \,. \tag{6.3b}$$

The notation $\langle \cdots \rangle_0$ in Eq. (6.3b) implies that the correlation functions are evaluated for the free boson system with the Hamiltonian given by Eq. (6.1) with $g = 0$. Interactions among excitons due to their non-boson nature do not affect the linear response, which is determined by the dynamics of a single exciton.

Making the same factorization as in Eq. (4.8), we obtain the following expressions for the third-order response:

$$R = R^{(a)} + R^{(b)} + R^{(c)} + R^{(d)} + \text{c.c.} \,, \tag{6.4a}$$

$$R^{(a)}_{mm_1m_2m_3}(-\omega_s;\omega_1,-\omega_2,\omega_3) = \mu^4 \sum_{\substack{\text{perm}\\ m_i,\omega_i}} \sum_{n'n''} G_{nn'}(\omega_s) G^*_{n''m_2}(\omega_2)\, G_{n''m_3}(\omega_3) G_{n'm_1}(\omega_1)\, \bar{\Gamma}_{n'n''}(\omega_1+\omega_3) \,, \tag{6.4b}$$

$$R^{(b)}_{nm_1m_2m_3}(-\omega_s;\omega_1,-\omega_2,\omega_3) = \mu^4 \int \frac{d\omega'}{2\pi} \sum_{n'n''} G_{nn'}(\omega_s) G_{n''m_3}(\omega_3)\, \mathscr{G}^{(2)}_{m_1m_2n'n''}\left(\frac{\omega_1+\omega_2}{2}, \omega' - \frac{\omega_1+\omega_2}{2}, \omega_1-\omega_2\right) \times \bar{\Gamma}_{n'n''}(\omega_3+\omega') \,, \tag{6.4c}$$

$$R^{(c)}_{nm_1m_2m_3}(-\omega_s;\omega_1,-\omega_2,\omega_3) = \mu^4 \int \frac{d\omega'}{2\pi} \sum_{n'n''} G_{n''m_3}(\omega_3) G_{n''m_1}(\omega_1)\, \mathscr{G}^{(2)}_{n'm_2nn}\left(\frac{\omega'+\omega_2}{2}, \omega_1+\omega_3 - \frac{\omega_2+\omega'}{2}, \omega'-\omega_2\right) \times \bar{\Gamma}_{n'n''}(\omega_1+\omega_3) \,. \tag{6.4d}$$

$$R^{(d)}_{nm_1m_2m_3}(-\omega_s;\omega_1,-\omega_2,\omega_3) = \mathscr{G}^{(2)}_{m_1m_2nm_3}\left(\frac{\omega_1+\omega_2}{2}, \frac{\omega_3+\omega_s}{2}; \omega_1-\omega_2\right), \tag{6.4e}$$

In addition to the one-exciton Green function G, the nonlinear response function depends also on two additional quantities; the two-exciton scattering matrix $\bar{\Gamma}_{mn}(\omega)$ and $\mathscr{G}^{(2)}$. They are given by

$$\bar{\Gamma}_{mn}(\omega) = -2\{[\bar{F}(\omega)]^{-1}\}_{mn} \,, \qquad \bar{F}_{mn}(\omega) = \int \frac{d\omega'}{2\pi i}\, G_{mn}(\omega')\, G_{mn}(\omega-\omega') \,, \tag{6.5a, b}$$

[4] Strictly speaking, one should average over pairs of trajectories $q_L(t)$, $q_R(t)$ corresponding to the quantum dynamics of the bra- and the ket-vectors of the density matrix. The exact formal procedure is outlined in Appendix C, however, the simplified picture given here is qualitatively correct.

and

$$\mathscr{G}^{(2)}_{mnm'n'\alpha}(\Omega,\Omega';\omega) = \int_0^\infty dt_1\,dt_2\,dt_3\,\mathscr{G}^{(2)}_{mnm'n'\alpha}(t_1,t_2,t_3,t_4)\exp\{i\Omega(t_1-t_2)-i\Omega'(t_3-t_4) - \frac{i\omega}{2}(t_1+t_2-t_3-t_4)\}, \tag{6.6a}$$

where

$$\mathscr{G}^{(2)}_{mnm'n'\alpha}(t_1,t_2,t_3,t_4) \equiv \langle \hat{C}^+_{m-}(t_1)\hat{C}_{n-}(t_2)\hat{C}_{m'+}(t_3)\hat{C}^+_{n'\alpha}(t_4)\rangle_0 - \langle \hat{C}^+_{m-}(t_1)\hat{C}_{m'+}(t_3)\rangle_0\langle \hat{C}_{n-}(t_2)\hat{C}^+_{n'\alpha}(t_4)\rangle_0 . \tag{6.6b}$$

Note that in the absence of additional degrees of freedom $\mathscr{G}^{(2)} = 0$ so that $R = R^{(a)}$ (see Eq. (6.4)). $R^{(b)}$, $R^{(c)}$ and $R^{(d)}$ are therefore new terms induced by the additional degrees of freedom. Eq. (6.4) generalize Eq. (4.8), derived for static disorder, for the case of dynamical disorder. $R^{(b)}$ for off-resonant ω_3 in the static limit, within the local field approximation was calculated in [56]. Eq. (6.4) express the four-wave mixing signals in terms of one- and two-exciton Green functions G and $\mathscr{G}^{(2)}$. In the coming sections we will evaluate these Green functions for different models, and analyze the signatures of exciton–phonon interaction and static disorder in four-wave mixing.

Let us compare the dynamical case with the previous case of static disorder. $\bar{\Gamma}_{mn}$ is still the two-exciton scattering matrix related to the kinematic exciton–exciton interaction due to the Pauli exclusion principle. The Green function $\mathscr{G}^{(2)}$ is the two-exciton Green function if excitons are considered as free bosons interacting with phonons. $\mathscr{G}^{(2)}$ is analogous to $\langle\langle GG^*\rangle\rangle$ in Eq. (4.8). The difference is that, for static disorder, as indicated in Section 4, the averaging can be carried out in two steps: quantum mechanical averaging which gives the product GG^* is followed by averaging over realizations of static disorder which leads to $\langle\langle GG^*\rangle\rangle$. In the case of dynamical disorder both steps need to be carried out simultaneously; for this reason we have to introduce the two-particle Green function $\mathscr{G}^{(2)}$.

Another characteristic of dynamical disorder is the appearance of a new contribution $R^{(d)}$. This represents the optical response of a system of excitons modeled as free bosons interacting with phonons. The nonlinear response of a system of free bosons vanishes since the system is harmonic. Exciton–phonon interaction destroys the harmonic picture since the bosons interact via phonon exchange, which induces the nonlinear response. When the additional degrees of freedom slow down, this contribution is reduced and for static disorder it eventually vanishes. This can be rationalized by the following argument: for each realization of static disorder, the system of free bosons is harmonic; its nonlinear response vanishes and it remains so even after averaging over disorder. When the exciton–phonon interaction is weaker than the exciton–exciton interaction, $R^{(d)}$ is much smaller than $R^{(b)}$ and $R^{(c)}$.

The Green function $\mathscr{G}^{(2)}$ can be most conveniently calculated using the Bethe–Salpeter equation [64]:

$$\mathscr{G}^{(2)}_{mnm'n'}(\Omega,\Omega';\omega) = \sum_{aa'bb'} G_{am}\left(\Omega+\frac{\omega}{2}\right)G^*_{nb}\left(\Omega-\frac{\omega}{2}\right)G_{m'a'}\left(\Omega'+\frac{\omega}{2}\right)G^*_{b'n'}\left(\Omega'-\frac{\omega}{2}\right)Q_{aba'b'}(\Omega,\Omega';\omega), \tag{6.7a}$$

with

$$Q_{aba'b'}(\Omega, \Omega'; \omega) = U_{aba'b}(\Omega, \Omega'; \omega) + \sum_{mnm'n'} \int \frac{d\Omega''}{2\pi} U_{abmn}(\Omega, \Omega''; \omega) G_{m'm}\left(\Omega'' + \frac{\omega}{2}\right) G^*_{n'n}\left(\Omega'' - \frac{\omega}{2}\right) Q_{m'n'a'b'}(\Omega'', \Omega'; \omega) . \quad (6.7b)$$

In Eq. (6.7) Q is the one particle irreducible two-exciton Green function and U is an irreducible vertex. $\mathcal{G}^{(2)}$ is evaluated by first calculating the vertex U perturbatively in the exciton–phonon interaction, then solving Eq. (6.7b) for Q, which when substituted in (6.7a) finally yields $\mathcal{G}^{(2)}$. This calculation will be carried out in the next section for a specific model of exciton–phonon interaction.

7. Phonon effects in the optical response of periodic assemblies

In this section we apply our Green function expressions (Eqs. (6.3)–(6.6)) to explore the signatures of exciton–phonon interaction in four-wave mixing spectroscopy of periodic nanostructures. We will consider the same model introduced in Section 4, but replace the static disorder with exciton–phonon interaction. We also use the same convention for transformation to momentum domain (Eq. (4.10)).

We adopt a model of harmonic phonons, with exciton–phonon interaction linear in the phonon operators. The matter Hamiltonian $\hat{H}_m$ is [1]

$$\hat{H}_m = \Omega \sum_m \hat{C}^\dagger_m \hat{C}_m + \sum_{m \neq n} J_{mn} \hat{C}^\dagger_m \hat{C}_n + \sum_{m,n} \Omega_{mn} \hat{b}^\dagger_m \hat{b}_n + \sum_{mn1} V_{mn1} \hat{C}^\dagger_m \hat{C}_n (\hat{b}^\dagger_1 + \hat{b}_1) + \frac{g}{2} \sum_n (\hat{C}^\dagger_n)^2 \hat{C}^2_n \quad (7.1a)$$

The first three terms represent the free excitons and phonons energy, the fourth is the exciton–phonon interaction, and the last term describes the direct exciton–exciton interaction. The sum over m and n in the fourth term includes diagonal on-site coupling ($n = m$) as well as off diagonal coupling $n \neq m$. Optical phonons usually couple through the former terms and accoustic phonons through the latter [1].

In the momentum domain, the Hamiltonian assumes the form

$$\hat{H}_m = \int d\boldsymbol{q} \{\varepsilon(\boldsymbol{q}) \hat{C}^+_{\boldsymbol{q}} \hat{C}_{\boldsymbol{q}} + \Omega(\boldsymbol{q}) \hat{b}^+_{\boldsymbol{q}} \hat{b}_{\boldsymbol{q}}\} + \int d\boldsymbol{q}\, d\boldsymbol{p}\, V(\boldsymbol{q}, \boldsymbol{q}-\boldsymbol{p}) \{\hat{C}^+_{\boldsymbol{p}} \hat{C}_{\boldsymbol{q}} \hat{b}^+_{\boldsymbol{q}-\boldsymbol{p}} + V^*(\boldsymbol{q}, \boldsymbol{q}-\boldsymbol{p}) \hat{C}^+_{\boldsymbol{q}} \hat{C}_{\boldsymbol{p}} b_{\boldsymbol{q}-\boldsymbol{p}}\} + \frac{g}{2} \int d\boldsymbol{q}'\, d\boldsymbol{q}''\, d\boldsymbol{q}\, \hat{C}^+_{\boldsymbol{q}'} \hat{C}^+_{\boldsymbol{q}''} \hat{C}_{\boldsymbol{q}} \hat{C}_{\boldsymbol{q}'+\boldsymbol{q}''-\boldsymbol{q}} . \quad (7.1b)$$

where $\varepsilon(\boldsymbol{q})$ is the exciton energy defined in Eq. (4.12b) and

$$V(\boldsymbol{q}, \boldsymbol{q}-\boldsymbol{p}) \equiv \sum_{mn} \exp[i\boldsymbol{q} \cdot (\boldsymbol{R}_n - \boldsymbol{R}_1) - i\boldsymbol{p} \cdot (\boldsymbol{R}_m - \boldsymbol{R}_1)] V_{mn1} . \quad (7.1c)$$

In this section we will work with the model Hamiltonian (Eq. (7.1)); however, the results hold as well for the more general model defined by Eq. (6.1).

The linear response function is given by Eq. (4.11), where the one-exciton Green function in momentum space is

$$G(\omega, \boldsymbol{k}) = \frac{1}{\omega - \varepsilon(\boldsymbol{k}) - \Sigma(\omega, \boldsymbol{k}) + \mathrm{i}\Gamma(\boldsymbol{k})/2} . \tag{7.2a}$$

Here $\Gamma(\boldsymbol{k})$ is the imaginary part of the self-energy representing finite exciton lifetime, either due to spontaneous emission (coupling to the electromagnetic field degrees of freedom) or to other relaxation mechanisms which do not conserve the number of excitons, and $\Sigma(\omega, \boldsymbol{k})$ is the phonon-induced exciton self-energy.

Neglecting the real part of the self-energy, the one-exciton Green function G becomes

$$G(\omega, \boldsymbol{k}) = \frac{1}{\omega - \varepsilon(\boldsymbol{k}) + \mathrm{i}\Sigma(\boldsymbol{k}) + \mathrm{i}\Gamma(\boldsymbol{k})/2} , \quad \Sigma(\boldsymbol{k}) \equiv |\operatorname{Im} \Sigma(\varepsilon(\boldsymbol{k}), \boldsymbol{k})| . \tag{7.2b,c}$$

The exciton self-energy is given by (see Appendix D):

$$\Sigma(\boldsymbol{k}) = \tfrac{1}{2} \int \mathscr{I}(\boldsymbol{p}, \boldsymbol{k}) \, \mathrm{d}\boldsymbol{p} . \tag{7.2d}$$

The function $\mathscr{I}(\boldsymbol{p}, \boldsymbol{k})$ given in Eq. (E.3a), is the kernel of the Boltzmann equation (Eq. (7.5b)). One can derive Eq. (7.2d) by calculating Σ and $\mathscr{I}$ perturbatively using the present model of exciton–phonon coupling. However, this equation is more general and applies to any model of exciton–phonon scattering which conserves the number of excitons. It represents the total scattering rate of excitons with momentum $\boldsymbol{k}$.

To derive expressions for the nonlinear response we can follow the procedure described at the end of Section 6 for evaluating the two-exciton Green function $\mathscr{G}^{(2)}$. However, the procedure can be simplified considerably (see Appendix D) if we assume that exciton transport due to exciton–phonon coupling, described by the Green function $\mathscr{G}^{(2)}$ is slow. Instead of solving the Bethe–Salpeter equation (6.7b), we expand the solution in powers of U. We can then perform exact integrations over frequencies in all the terms, taking into account only the one-exciton poles of the Green functions. In the resulting expansion we are left with integrations over momenta. Summing the resulting expansion to all orders is equivalent to solving the Boltzmann equation.

The nonlinear optical response function is given by

$$\begin{aligned} &R(-\omega_s - \boldsymbol{k}_s; \omega_1 \boldsymbol{k}_1, \; -\omega_2 - \boldsymbol{k}_2, \omega_3 \boldsymbol{k}_3) \\ &\quad = \sum_{j=a,b,c,d} R^{(j)}(-\omega_s - \boldsymbol{k}_s; \omega_1 \boldsymbol{k}_1, \; -\omega_2 - \boldsymbol{k}_2, \omega_3 \boldsymbol{k}_3) + \mathrm{c'.c'.} , \end{aligned} \tag{7.3a}$$

where $R^{(j)}$ are given by Eq. (4.14a). Since the single exciton Green function is given by Eq. (7.2b), we shall focus on the calculation of $\bar{\Gamma}^{(j)}$. As in the case of static disorder Eq. (4.14b), $\bar{\Gamma}^{(a)}$ is equal to the two-exciton scattering matrix $\bar{\Gamma}$.

$$\bar{\Gamma}^{(a)}(-\omega_s - \boldsymbol{k}_s, \omega_1 \boldsymbol{k}_1, \; -\omega_2 - \boldsymbol{k}_2, \omega_3 \boldsymbol{k}_3) = \bar{\Gamma}(\omega_1 + \omega_3, \boldsymbol{k}_1 + \boldsymbol{k}_3) \tag{7.3b}$$

This can be expressed in terms of the one-exciton Green function G:

$$\bar{\Gamma}(\omega, \boldsymbol{k}) = -2 \left\{ \int \frac{\mathrm{d}\omega'}{2\pi \mathrm{i}} \, \mathrm{d}\boldsymbol{p} \; G(\omega', \boldsymbol{p}) \, G(\omega - \omega', \boldsymbol{k} - \boldsymbol{p}) \right\}^{-1} , \tag{7.3c}$$

The contribution $\bar{\Gamma}^{(c)}$ vanishes in the absence of static disorder, since there are no large resonant factors (we will discuss it in detail in Section 9)

$$\bar{\Gamma}^{(c)} = 0 . \tag{7.3d}$$

The other two contributions are given by

$$\bar{\Gamma}^{(b)}(-\omega_s - \boldsymbol{k}_s, -\omega_1 \boldsymbol{k}_1, -\omega_2, -\boldsymbol{k}_2, \omega_3 \boldsymbol{k}_3)$$

$$= \int d\boldsymbol{p}'\, d\boldsymbol{p}\, g(\boldsymbol{p}', \boldsymbol{k}; \tfrac{1}{2}(\omega_1 + \omega_2))\, \mathscr{L}(\boldsymbol{p}, \boldsymbol{p}'; \boldsymbol{q}\omega)\, \bar{\Gamma}(\varepsilon(\boldsymbol{p}) + \omega_3; \boldsymbol{p} + \boldsymbol{k}_3) , \tag{7.3e}$$

$$\bar{\Gamma}^{(d)}(-\omega_s - \boldsymbol{k}_s, \omega_1 \boldsymbol{k}_1, -\omega_2 - \boldsymbol{k}_2, \omega_3 \boldsymbol{k}_3) = g_0(\boldsymbol{k}_s, \boldsymbol{k}; \omega_s, \tfrac{1}{2}(\omega_1 + \omega_2))$$

$$+ \int d\boldsymbol{p}'\, d\boldsymbol{p}''\, g_d(\boldsymbol{k}_s, \boldsymbol{p}'; \omega_s)\, \mathscr{L}(\boldsymbol{p}', \boldsymbol{p}''; \boldsymbol{q}\omega)\, g(\boldsymbol{p}'', \boldsymbol{k}; \tfrac{1}{2}(\omega_1 + \omega_2)) , \tag{7.3f}$$

where $\boldsymbol{k} \equiv \frac{1}{2}(\boldsymbol{k}_1 + \boldsymbol{k}_2), \boldsymbol{q} \equiv \boldsymbol{k}_1 - \boldsymbol{k}_2, \omega \equiv \omega_1 - \omega_2$ in Eqs. 7.3(e) and (f).

The correlation function $\mathscr{L}(\boldsymbol{p}, \boldsymbol{p}'; \boldsymbol{q}\omega)$ in Eq. (7.3) is defined by

$$\mathscr{L}(\boldsymbol{p}, \boldsymbol{p}'; \boldsymbol{q}\omega) \equiv \sum_{mnm'} \int dt \exp\{i\omega t + i\boldsymbol{p}\cdot(\boldsymbol{R}_m - \boldsymbol{R}_n) - i\boldsymbol{p}'\cdot(\boldsymbol{R}_{m'} - \boldsymbol{R}_{n'})$$

$$+ \frac{i}{2}\boldsymbol{q}\cdot(\boldsymbol{R}_m + \boldsymbol{R}_n - \boldsymbol{R}_{m'} - \boldsymbol{R}_{n'})\} \langle \hat{C}^{\dagger}_{m-}(0)\hat{C}_{n-}(0)\hat{C}^{\dagger}_{m'+}(t)\hat{C}^{\dagger}_{n'+}(t)\rangle_0 , \tag{7.4}$$

and it satisfies the equation

$$-i[\omega - \varepsilon(\boldsymbol{p} + \boldsymbol{q}/2) + \varepsilon(\boldsymbol{p} - \boldsymbol{q}/2)]\, \mathscr{L}(\boldsymbol{p}, \boldsymbol{p}'; \boldsymbol{q}\omega)$$

$$+ \left[\int d\boldsymbol{p}''\, \mathscr{J}(\boldsymbol{p}'', \boldsymbol{p}) + \Gamma(\boldsymbol{p}) \right] \mathscr{L}(\boldsymbol{p}, \boldsymbol{p}'; \boldsymbol{q}\omega) - \int d\boldsymbol{p}''\, \mathscr{J}(\boldsymbol{p}, \boldsymbol{p}'')\, \mathscr{L}(\boldsymbol{p}'', \boldsymbol{p}'; \boldsymbol{q}\omega) = \delta(\boldsymbol{p} - \boldsymbol{p}') . \tag{7.5a}$$

To clarify the physical significance of $\mathscr{L}$ let us consider the single-exciton density matrix in the momentum domain $n(\boldsymbol{p}, \boldsymbol{q}, t)$, defined by Eq. (4.16a). This satisfies the Boltzmann equation [5]:

$$\left\{ \frac{\partial}{\partial t} + i[\varepsilon(\boldsymbol{p} + \boldsymbol{q}/2) - \varepsilon(\boldsymbol{p} - \boldsymbol{q}/2)] \right\} n(\boldsymbol{p}, \boldsymbol{q}, t)$$

$$= -\int d\boldsymbol{p}''\, [\mathscr{J}(\boldsymbol{p}'', \boldsymbol{p}) n(\boldsymbol{p}, \boldsymbol{q}, t) - \mathscr{J}(\boldsymbol{p}, \boldsymbol{p}'') n(\boldsymbol{p}'', \boldsymbol{q}, t)] - \Gamma(\boldsymbol{p}) n(\boldsymbol{p}, \boldsymbol{q}, t) \tag{7.5b}$$

By comparing Eqs. 7.5(a) and (b), we note that $\mathscr{L}$ is the Green function of the Boltzmann equation

$$n(\boldsymbol{p}, \boldsymbol{q}, t) = \int d\boldsymbol{p}'\, \mathscr{L}(\boldsymbol{p}, \boldsymbol{p}'; \boldsymbol{q}, t - t_0) n(\boldsymbol{p}', \boldsymbol{q}, t_0) , \tag{7.6a}$$

where

$$\mathscr{L}(\boldsymbol{p}, \boldsymbol{p}'; \boldsymbol{q}t) \equiv \int \frac{d\omega}{2\pi} e^{-i\omega t}\, \mathscr{L}(\boldsymbol{p}, \boldsymbol{p}'; \boldsymbol{q}\omega) . \tag{7.6b}$$

The other auxiliary functions necessary for evaluating the response function ($\not{f}$, g, g_s, g_d and g_0) are expressed in terms of the vertex function U in Appendix D, and are then evaluated for some specific models of the exciton–phonon interaction in Appendix E.

The physical reason why we end up with the Boltzmann equation is as follows: Recasting Eq. (6.4c) in the time domain we find that since $\bar{\Gamma}(t'' - t')$ (the Fourier transform of $\bar{\Gamma}(\omega)$) is nonzero only for a very short time $|t'' - t'| \sim W^{-1}$, W being the exciton bandwidth, $R^{(b)}$ may be expressed in terms of the Green function $\mathscr{G}^{(2)}(t_1, t_2, t'', t')$ for $|t'' - t'| \sim W^{-1}$, and we can set $t'' = t' = t$ to get $\mathscr{G}^{(2)}(t_1, t_2, t, t)$. This describes the evolution of the exciton variable $\langle B_n^\dagger(t) B_m(t) \rangle$, i.e., the single exciton density matrix, in the presence of the external field. Using standard approximations it can then be shown that the exciton density matrix satisfies the Boltzmann equation [5]. In the next section we apply these results to various frequency and time-domain four-wave mixing techniques.

8. Collective many-body resonances in four-wave mixing spectroscopy

In this section we consider resonances of the third-order optical response and present various frequency- and time-domain techniques which can be used to probe these resonances.

According to Eq. (7.3a), the optical response function has four contributions, given by the functions $\bar{\Gamma}^{(i)}$ with i = a, b, c, d. These are related to different resonances in the frequency domain, and show up in time-domain four-wave mixing spectroscopy as well.

The contribution $\bar{\Gamma}^{(c)}$ vanishes in the absence of static disorder (Eq. (7.3d)]. We have shown in Section 4 that in a disordered nanostructure without phonons, $\bar{\Gamma}^{(c)}$ is related to resonances at $\omega_1 + \omega_3 = 2\omega_2$. We will show in Section 10 that this resonance occurs when we have both static and dynamical disorder; its peak value is proportional to the static disorder strength and the width is proportional to the dynamical disorder strength. Similar to the resonance at $\omega_1 = \omega_2$, the $\omega_1 + \omega_3 = 2\omega_2$ resonance has a collective nature, as will be discussed in Sections 11 and 12. $\bar{\Gamma}^{(d)}$ is induced by the exciton–phonon interaction and does not include direct exciton–exciton scattering processes due to the Pauli exclusion principle, i.e., it describes the nonlinear response of free particles (bosons) interacting with phonons. This interesting contribution deserves a separate study and it will be not considered here.

At this point we should compare our Green function expressions (GFE) for the nonlinear optical response with the results obtained from the Heisenberg equations of motion for exciton operators using two factorization schemes. The local field approximation (LFA) which can be obtained starting with Eq. (3.5a) putting $\langle \tilde{B}\tilde{B} \rangle = \langle \tilde{B} \rangle \langle \tilde{B} \rangle$ (full factorization) and skipping Eq. (3.5b) is equivalent to taking the $\bar{\Gamma}^{(a)}$ contribution with $\bar{\Gamma}$ evaluated in the LFA (see Eq. (4.18a)). Therefore, LFA is a good approximation far from two-photon resonances. The $\bar{\Gamma}^{(a)}$ contribution in our GFE was obtained by Spano and Mukamel [14]. In this approximation the two-exciton states are taken into account explicitly (including the resonant region). However, the approach of [14] does not allow to take into account additional degrees of freedom. Exciton–phonon interaction was incorporated by Knoester and Mukamel [5] who invoked a factorization $\langle \tilde{B}^\dagger \tilde{B}\tilde{B} \rangle = \langle \tilde{B}^\dagger \tilde{B} \rangle \langle \tilde{B} \rangle$ in the equations of motion for the exciton operators. That result can be obtained from the GFE by taking the sum of $\bar{\Gamma}^{(a)} + \bar{\Gamma}^{(b)}$ with $\bar{\Gamma}$ evaluated in the LFA (Eq. (4.18a)). Since in this approximation $\bar{\Gamma}$ is evaluated using the LFA, but the approximation itself is different from LFA, we will denote it LFA′. The LFA′ takes into account additional degrees of freedom and leads to the degenerate

four-wave mixing resonances, however, since it describes the exciton–exciton scattering in the LFA, it does not apply near two-photon resonances. Note that neither the expressions of [14] nor the LFA′ can describe both degenerate four-wave mixing and two-photon resonances. The GFE which gives a reasonable description in the entire frequency range, have a form of a convolution of the two-exciton scattering matrix $\bar{\Gamma}$ which shows up in expressions of [14] and the Boltzmann equation Green function which shows up in the LFA′. In the GFE for $\bar{\Gamma}^{(c)}$ near the $\omega_1 + \omega_3 = 2\omega_2$, $\bar{\Gamma}(\omega_1 + \omega_3)$ resonance is always in the two-photon resonant region and, therefore, it cannot be evaluated in the LFA. The breakdown of the LFA for $\bar{\Gamma}^{(c)}$ was shown in Section 4 for the four-photon hole burning technique in the frequency domain ($\omega_1 + \omega_3 = 2\omega_2$ resonance) and for its time domain analogue; the two exciton echo.

In the remainder of the section we consider applications which demonstrate clearly the breakdown of the LFA and the LFA′. We will consider various frequency and time domain techniques testing the resonances of $R^{(a)}$ and $R^{(b)}$. We present numerical calculations for frequency domain nonlinear spectroscopy of an infinite one-dimensional molecular lattice, with nearest neighbor interactions, and exciton dispersion

$$\varepsilon(k) = \Omega_0 + 2J\cos(ka)\,. \tag{8.1a}$$

This system has only one optically active exciton state ($k = 0$). Depending on the sign of intermolecular coupling J, this state is either at the bottom of the band ($J < 0$) or at the top of the band ($J > 0$). In the context of molecular aggregates, these cases, which have a very different photophysics, are known as J-aggregates, and H-aggregates respectively. We shall consider coupling to either acoustic or optical phonons [1]. Acoustic phonons have the dispersion.

$$\Omega_{ac}(q) = \Omega_{ac}\sin|qa/2|\,, \tag{8.1b}$$

and the exciton–phonon coupling

$$V_{ac}(k, q) = V_{ac}(\cos[(k + q/2)a]\sin(qa/2)\sqrt{\sin|qa/2|})\,. \tag{8.1c}$$

The corresponding quantities for optical phonons are

$$\Omega_{op}(q) = \Omega_{op}\,, \qquad V_{op}(k, q) = V_{op}\cos[(k + q/2)a]\cos(qa/2)\,. \tag{8.1d, e}$$

We use typical parameters for anthracene [84], $W = -4J = 1250\ \mathrm{cm}^{-1}$ is the exciton bandwidth, $\Omega_{op} = 90\ \mathrm{cm}^{-1}$, and Ω_{ac} is taken to be the Dybe frequency $67\ \mathrm{cm}^{-1}$. Since the numerical calculations were performed on a finite lattice, the allowed momenta are discrete. Consequently, we need to broaden the Dirac delta function in Eq. (E.3) by assuming that the frequency of a phonon with momentum $\boldsymbol{p}$ has a Lorentzian distribution centered at $\Omega(\boldsymbol{p})$. This is equivalent to replacing the Dirac delta function by

$$\delta(\varepsilon) = (1/\pi)[\eta/(\varepsilon^2 + \eta^2)]\,, \tag{8.2}$$

where η is the phonon frequency distribution width. As $\eta \to 0$, the minimal lattice size beyond which the results converge increases to ∞. We choose $\eta = 10\ \mathrm{cm}^{-1}$ in our numerical calculations, and the results converge for lattice with more than 320 molecules (assuming periodic boundary conditions). In the numerical calculations, we studied separately the effects of acoustic and optical

phonons. We choose either $V_{op} = 140\,cm^{-1}$, $V_{op} = 0$ (corresponding to anthracene), or take $V_{op} = 0$, $V_{ac} = 140\,cm^{-1}$. Since the projections of the incident and signal wave vectors on the lattice line k_j, $k_s \sim 2\pi/\lambda$ (λ being the optical wavelength) are much smaller than the size of the Brillouin zone ($2\pi/a$), we will set all wave vectors to 0. For brevity, the response function in Eq. (7.3a) with $\boldsymbol{k}_s = \boldsymbol{k}_1 = \boldsymbol{k}_2 = \boldsymbol{k}_3 = 0$ will be denoted $R(-\omega_s; \omega_1, -\omega_2, \omega_3)$.

The specific techniques and resonances reported below were selected to demonstrate the breakdown and limitations of the LFA and LFA'. We will present the frequency-domain techniques together with the corresponding time-domain analogues.

As indicated in Section 2, the external field has a form of a sum of three waves in a frequency-domain experiment (see Eqs. (2.25) and (2.28)), and a sum of three pulses in a time-domain experiment (see Eqs. (2.25) and (2.27)). For simplicity we consider time domain measurements in which two of the pulses coincide temporarily so that we vary only one time delay. We shall distinguish between echo techniques in which pulses 1 and 3 coincide, and transient grating or pump probe techniques where pulses 1 and 2 coincide.

Resonances associated with $\bar{\Gamma}^{(a)}$

$\bar{\Gamma}^{(a)}$ is nonzero even in the absence of exciton–phonon interactions. These interactions modify $\bar{\Gamma}^{(a)}$ by the addition of the phonon self-energy in the single-exciton Green function G which enters $\bar{\Gamma}^{(a)} = \bar{\Gamma}$ through Eq. (7.3c). $\bar{\Gamma}^{(a)}(\omega)$ has an imaginary part when ω is inside the two-exciton band even in the absence of phonons, which is the evidence of two-photon resonances on two-exciton states.

(1) *Two exciton resonances.* To probe two-exciton states without interference from single-exciton transitions, we set $\omega_1 = \omega_2$, keep this frequency off resonance, and scan ω_3 so that $\omega_1 + \omega_3$ is resonant with the two-exciton band (two-photon resonance). In this case $\omega_s = \omega_3$. We assume $E_1 = E_2$ and in a heterodyne measurements take a replica of the third wave as a heterodyne field, i.e., $E_h = E_3 \exp(i\varphi)$. The heterodyne signal $S_{het}(\boldsymbol{k}_s, \omega_s)$ (see Eq. (2.20a)) has the form

$$S_{het}(\boldsymbol{k}_s\omega_s) = |E_1|^2 |E_3|^2 \operatorname{Re}\{\exp(-i\varphi) R^{(a)}(-\omega_3; \omega_1, -\omega_1, \omega_3)\} . \tag{8.3}$$

Since all frequencies (ω_1, ω_2, ω_3, and ω_s) are off-resonant, the Green functions $G(\omega_1)$, $G^*(\omega_2)$, $G(\omega_3)$ and $G(\omega_s)$ in Eq. (4.14a) become unimportant real prefactors, and for $\varphi = 0$ and $\varphi = \pi/2$ the signal $S_{het}(\boldsymbol{k}_s\omega_s) \propto \operatorname{Re}(\bar{\Gamma}(\omega_1 + \omega_3, 0))$ and $S_{het}(\boldsymbol{k}_s\omega_s) \propto \operatorname{Im}(\Gamma(\omega_1 + \omega_3, 0))$. The real part, the imaginary part, and the phase of $\bar{\Gamma}(\omega_1 + \omega_3, 0)$ as a function of $\Delta\omega = \omega_1 + \omega_3 - 2\Omega_0$ are displayed in Fig. 2. The dashed line is the result of the LFA with $\bar{\Gamma}^{(L)}(\omega_1 + \omega_3, \boldsymbol{k})$ given by Eq. (8.5b). Im $\bar{\Gamma}(\omega, 0)$ is nonzero when ω is tuned to the two-exciton band, and it carries information about the two-exciton states. In the LFA, Im $\bar{\Gamma}^{(L)}(\omega, \boldsymbol{k})$ is small, independent of ω, and carries no information about two-exciton states.

(2) *Interaction-induced two-exciton spectroscopy.* This is the time domain analogue of the frequency domain technique (1), which probes the two-exciton states in the time domain. Let us assume that pulses 1 and 3 overlap. We thus set $\tau_1' = \tau_3' = -\tau'$; $\tau_2' = 0$. For $\tau' < 0$ (pulse 2 first) this sequence represents the two-exciton echo discussed in Section 4. We will demonstrate in Sections 11 and 12 that the echo is a signature of strong correlations between one- and two-exciton states in disordered aggregates. The situation is, however, very different if we reverse the time order of the two pulses and take $\tau' > 0$ (pulses 1 and 3 first). Now the signal which vanishes for a two level

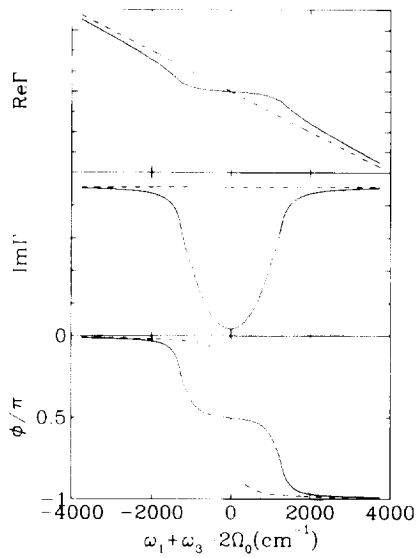

Fig. 2. Real part (upper panel), imaginary part (middle panel), and the phase of $\bar{\Gamma}(\omega_1 + \omega_3, 0)$ related to the heterodyne signal $S_{\rm het}(\boldsymbol{k}_s\omega_s)$ for a 1-D lattice with acoustic phonons as a function of $\Delta\omega = \omega_1 + \omega_3 - 2\Omega_0$. Solid line is the result of Green function formalism, and dash line is the result of the LFA. $V_{\rm ac} = 140\,{\rm cm}^{-1}$, $V_{\rm op} = 0$, $T = 100\,{\rm K}$, $\tan\phi \equiv {\rm Im}\,\bar{\Gamma}/{\rm Re}\,\bar{\Gamma}$.

system, provides a direct probe for two exciton dynamics. We shall, therefore, focus our analysis on this case. To avoid interference with single exciton transitions we tune all pulses to be off resonant with respect to the exciton band. However, we assume that $\omega_1 + \omega_3$ is tuned through the two exciton states. The optical polarization then becomes

$$P_s(\boldsymbol{k}_s, t) = \mu^4 \frac{1}{\Omega_1 - \varepsilon(0)} \frac{1}{\Omega_3 - \varepsilon(0)} \frac{1}{\Omega_2 - \varepsilon(0)} \frac{1}{\Omega_1 + \Omega_3 - \Omega_2 - \varepsilon(0)} E_2^*(t)$$

$$\times \Big\{ -2(\Omega_1 + \Omega_3 - 2\varepsilon_0 + 2i\Gamma_0) E_1(t+\tau') E_3(t+\tau') - 2i \frac{\partial}{\partial t} (E_1(t+\tau') E_3(t+\tau'))$$

$$+ \int d\tau\, \bar{\Gamma}_c(t + \tau' - \tau) E_1(\tau) E_3(\tau) \Big\} , \tag{8.4a}$$

where

$$\bar{\Gamma}_c(t) \equiv \int \frac{d\omega}{2\pi} e^{-i\omega t} \bar{\Gamma}_c(\omega) , \tag{8.4b}$$

$$\bar{\Gamma}_c(\omega) \equiv \bar{\Gamma}(\omega) - \bar{\Gamma}^{(L)}(\omega) , \quad \bar{\Gamma}^{(L)}(\omega) \equiv -2(\omega - 2\varepsilon_0 + 2i\Gamma_0) . \tag{8.5a, b}$$

Here

$$\varepsilon_0 \equiv \int d\boldsymbol{k}\, \varepsilon(\boldsymbol{k}) , \qquad \Gamma_0 \equiv \int d\boldsymbol{k}\, |{\rm Im}\, \Sigma(\boldsymbol{k})| . \tag{8.5c, d}$$

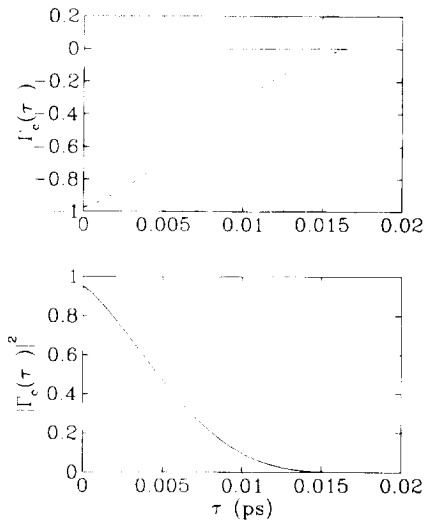

Fig. 3. $\bar{\Gamma}_c(\tau')$ related to the time-integrated heterodyne signal $S^I_{het}(\boldsymbol{k}_s; \tau')$ as a function of the time delay τ' for a 1-D H-aggregate described in Fig. 14. Upper panel shows the real (solid) and imaginary (dash) part of $\bar{\Gamma}_c(\tau')$. Lower panel shows $|\bar{\Gamma}_c(\tau')|^2$, related to the homodyne signal $S^I_{hom}(\boldsymbol{k}_s; \tau')$.

The function $\bar{\Gamma}_c(\omega) \to 0$ when $\omega \to \infty$, which implies that the LFA becomes exact for large detunings. The first two terms in Eq. (8.4a) give the signal in the LFA, which is nonzero only during the 1 and 3 pulses. The third term goes beyond the LFA. It varies on a time scale given by the inverse exciton bandwidth W^{-1}. If the pulses are shorter than W^{-1}, the signal at time delays $\tau' \sim W^{-1}$ is directly related to the deviations from the local field expression.

The signal with off-resonant pump, $\bar{\Gamma}_c(\tau')$, is displayed in Fig. 3. We assume that the forms of the 1 and 2 pulses are identical, i.e., $\Omega_1 = \Omega_2$, $E_1(t) = E_2(t)$ and take a replica of the third pulse as the heterodyne field, i.e., $E_h(\boldsymbol{k}_s, t) = E_3(t - t')\exp(i\varphi)$. The time-integrated heterodyne signal (see Eq. (2.20c)) $S^I_{het}(\boldsymbol{k}_s; \tau')$ as a function of the time delay τ' for short pulses can be obtained from Eq. (8.4a), and after omitting real off-resonant factors yields:

$$S^I_{het}(\boldsymbol{k}_s; \tau') \propto \left\{ \left| \int d\tau\, E_1(\tau) E_3(\tau) \right|^2 \mathrm{Re}\exp(-i\varphi)\bar{\Gamma}_c(\tau') \right\}. \tag{8.6}$$

Taking $\varphi = 0$ and $\varphi = \pi/2$ we obtain $S^I_{het}(\boldsymbol{k}_s; \tau') \propto \mathrm{Re}(\bar{\Gamma}_c(\tau'))$ and $S^I_{het}(\boldsymbol{k}_s; \tau') \propto \mathrm{Im}(\bar{\Gamma}_c(\tau'))$. $\bar{\Gamma}_c(\tau')$ is displayed in Fig. 3 (upper panel). The real part of $\bar{\Gamma}_c(\tau')$ is negligible compared with the imaginary part, and the signal decays in a time scale of the order of inverse exciton bandwidth.

For the time-integrated homodyne signal (Eq. (2.19e)) as a function of the time delay τ' we have $S^I_{hom}(\boldsymbol{k}_s, \tau') \propto |\bar{\Gamma}_c(\tau')|^2$, which is displayed in Fig. 3 (lower panel). When pulses 1 and 3 are resonant ($\Omega_1 = \Omega_3 = \varepsilon(0)$) and much shorter than the dephasing time, the polarization has the form

$$\begin{aligned} P(\boldsymbol{k}_s, t; \tau') = {} & \frac{\mu^4}{[\Omega_2 - \varepsilon(0)]^2} E_2^*(t) \int d\tau_1\, E_1(\tau_1) \int d\tau_3\, E_3(\tau_3) \\ & \times \{4[\varepsilon(0) - \varepsilon_0]\exp[-i2\varepsilon(0)(t + \tau') - 2\Sigma(0)(t + \tau')] \\ & + \int \frac{d\Omega}{2\pi i} \frac{\bar{\Gamma}_c(\Omega)}{\Omega - 2\varepsilon(0) + 2i\Sigma(0)} e^{-i\Omega(t+\tau')}\} \exp(i\Omega_2 t)\,. \end{aligned} \tag{8.7}$$

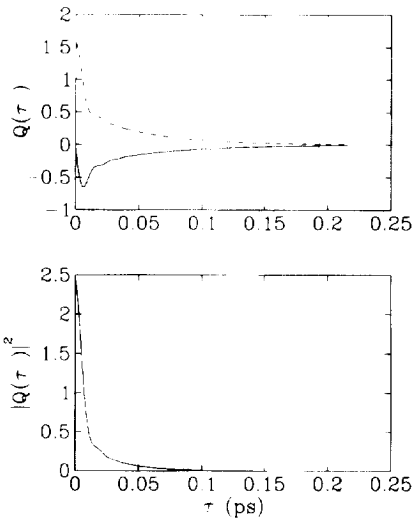

Fig. 4. The signal $Q(\tau')$ related to $S^{I}_{het}(\boldsymbol{k}_s;\tau')$ for the on-resonance excitation (Eq. (8.8)) for 1-D H-aggregate as described in Fig. 14. $V_{ac} = 140\ cm^{-1}$, $V_{op} = 0$. Upper panel shows that real (solid line) and imaginary (dash line) parts of $Q(\tau')$, and the lower panel shows $|Q(\tau')|^2$, related to $S^{I}_{hom}(\boldsymbol{k}_s;\tau')$.

We assume that the pulses 1 and 3 are identical, i.e. $E_3(t) = E_1(t)$, and the off-resonant pulse 2 has the same form as pulses 1 and 3, i.e., $E_2(t) = E_1(t)$. We choose the heterodyne pulse to have the same form and time delay as pulse 2, i.e., $\mathscr{E}_h(\boldsymbol{k}_s, t) = E_1(t-\tau')\exp(-i\Omega_s t + i\varphi)$. The time-integrated heterodyne signal (Eq. (2.20c)) as a function of the time delay τ' becomes

$$S^{I}_{het}(\boldsymbol{k}_s;\tau') = \frac{\mu^4}{[\Omega_2 - \varepsilon(0)]^2}\,\mathrm{Re}\left\{\int [E_1^*(\tau_1)]^2\,d\tau_1\left[\int E_1(\tau_1)\,d\tau_1\right]^2 \exp(-i\varphi)\,Q(\tau')\right\} \tag{8.8a}$$

where

$$Q(\tau') \equiv 4[\varepsilon(0) - \varepsilon_0]\exp(-2\Sigma(0)\tau') + \int \frac{d\Omega}{2\pi i}\,\frac{\bar{\Gamma}_c(\Omega)}{\Omega - 2\varepsilon(0) + 2i\Sigma(0)} \times \exp[-i(\Omega - 2\varepsilon(0))\tau'] \,. \tag{8.8b}$$

When the pulses have no phase modulation and for $\varphi = 0$ and $\varphi = \pi/2$ we have $S^{I}_{het}(\boldsymbol{k}_s;\tau') \propto \mathrm{Re}[Q(\tau')]$ and $S^{I}_{het}(\boldsymbol{k}_s;\tau') \propto \mathrm{Im}(Q(\tau'))$ respectively. For the time-integrated homodyne signal (see Eq. (2.19e)) $S^{I}_{hom}(\boldsymbol{k}_s;\tau') \propto |Q(\tau')|^2$.

The variation of the time-integrated signals with the delay time τ' is displayed in Fig. 4. In the LFA $S^{I}_{hom}(\boldsymbol{k}_s;\tau')$ decays exponentially with twice the single-exciton decay rate, i.e., $S^{I}_{het}(\boldsymbol{k}_s;\tau') \propto \exp\{-2\Sigma(0)\tau'\}$. In the GFE, $S_{het}(\boldsymbol{k}_s;\tau')$ decays nonexponentially, with an average decay rate faster than $2\Sigma(0)$. This means that the two-exciton decay rate is larger than the sum of two single-exciton decay rates [23].

Resonances associated with $\bar{\Gamma}^{(b)}$

The $\bar{\Gamma}^{(b)}$ contribution (Eq. (7.3e)) is proportional to the exciton–phonon coupling and it vanishes in the absence of exciton–phonon interaction. In Section 4, we calculated $\bar{\Gamma}^{(b)}$ and found it to be proportional to the value of static disorder. $\bar{\Gamma}^{(b)}$ is, therefore, a disorder-induced term; the disorder can be either static or dynamical. It was shown in Section 4 that $\bar{\Gamma}^{(b)}$ is related to the degenerate four-wave mixing resonance at $\omega_1 = \omega_2$ for static disorder (see [56]). We shall now show that the same resonance in $\bar{\Gamma}^{(b)}$ is induced by dynamical disorder as well.

According to Eq. (7.3e), $\bar{\Gamma}^{(b)}$ is given by a convolution of the function g, evaluated in Appendix E, the two-exciton scattering matrix $\bar{\Gamma}$, and the Green function $\mathscr{G}$ of the transport equation (Eq. (7.5)). The latter can be calculated numerically, however we can obtain the interesting asymptotic behavior analytically using the operator representation for $\mathscr{G}$. To that end we introduce a collision operator L_0 acting in the space of exciton distribution functions in momentum space $n(\boldsymbol{p})$:

$$(L_0)n(\boldsymbol{p}) \equiv -\left\{ \int d\boldsymbol{p}' \gamma(\boldsymbol{p}, \boldsymbol{p}') n(\boldsymbol{p}') - n(\boldsymbol{p}) \int d\boldsymbol{p}' \gamma(\boldsymbol{p}', \boldsymbol{p}) \right\}. \tag{8.9}$$

The Green function $\mathscr{G}$ can be expressed in terms of the right eigenmodes $\varphi_\alpha(\boldsymbol{p})$, the left eigenmodes (comodes) $\bar{\varphi}_\alpha(\boldsymbol{p})$ and the corresponding eigenvalues λ_α of the operator L_0 [85] (see Appendix D for details):

$$\mathscr{G}(\boldsymbol{p}, \boldsymbol{p}'; \boldsymbol{q}\omega) = i \sum_\alpha \frac{\varphi_\alpha(\boldsymbol{p}) \bar{\varphi}_\alpha(\boldsymbol{p}')}{\omega + i\lambda_\alpha + iS_\alpha(\boldsymbol{q})}, \tag{8.10a}$$

where

$$S_\alpha = 0 \quad \text{for } \alpha \neq 0, \tag{8.10b}$$

$$S_0 = \Gamma_0 + D_{ij} q_i q_j, \tag{8.10c}$$

$$\Gamma_0 \equiv C \int d\boldsymbol{p}\, \Gamma(\boldsymbol{p}) \exp[-\varepsilon(\boldsymbol{p})/kT], \tag{8.10d}$$

$$D_{ij} \equiv C \sum_\alpha \lambda_\alpha^{-1} \int d\boldsymbol{p}\, (\partial\varepsilon(\boldsymbol{p})/\partial \boldsymbol{p}_i) \varphi_\alpha(\boldsymbol{p}) \int d\boldsymbol{p}'\, (\partial\varepsilon(\boldsymbol{p}')/\partial \boldsymbol{p}'_j) \exp[-\varepsilon(\boldsymbol{p}')/kT] \bar{\varphi}_\alpha(\boldsymbol{p}'), \tag{8.10e}$$

$$C \equiv \left\{ \int d\boldsymbol{p} \exp[-\varepsilon(\boldsymbol{p})/kT] \right\}^{-1} \tag{8.10f}$$

Substituting Eq. (8.10a) into Eq. (7.3e) and making use of Eqs. (8.10b)–(8.10f) we obtain the following expression for $\bar{\Gamma}^{(b)}$ in terms of the eigenstates of the operator L_0.

$$\bar{\Gamma}^{(b)} = \bar{\Gamma}_s^{(b)} + \bar{\Gamma}_t^{(b)}, \tag{8.11a}$$

$$\begin{aligned} &\bar{\Gamma}_s^{(b)}(-\omega_s - \boldsymbol{k}_s, \omega_1 \boldsymbol{k}_1, -\omega_2 - \boldsymbol{k}_2, \omega_3 \boldsymbol{k}_3) \\ &\equiv \frac{iC}{\omega + i\Gamma_0 + iD\boldsymbol{q}^2} \int d\boldsymbol{p}'\, g(\boldsymbol{p}', \boldsymbol{k}; \tfrac{1}{2}(\omega_1 + \omega_2)) \\ &\quad \times \int d\boldsymbol{p} \exp[-\varepsilon(\boldsymbol{p})/kT] \bar{\Gamma}(\varepsilon(\boldsymbol{p}) + \omega_3, \boldsymbol{p} + \boldsymbol{k}_3), \end{aligned} \tag{8.11b}$$

$$\Gamma_{\mathrm{f}}^{(\mathrm{b})}(\omega_{\mathrm{s}}\boldsymbol{k}_{\mathrm{s}}, \omega_1\boldsymbol{k}_1, -\omega_2 - \boldsymbol{k}_2, \omega_3\boldsymbol{k}_3)$$

$$\equiv \mathrm{i}\sum_{\alpha\neq 0}\frac{1}{\omega + \mathrm{i}\lambda_\alpha}\int \mathrm{d}\boldsymbol{p}'\,\bar{\varphi}_\alpha(\boldsymbol{p}')\,g(\boldsymbol{p}', \boldsymbol{k}, \tfrac{1}{2}(\omega_1 + \omega_2))\int \mathrm{d}\boldsymbol{p}\,\varphi_\alpha(\boldsymbol{p})\,\bar{\Gamma}(\varepsilon(\boldsymbol{p}) + \omega_3, \boldsymbol{p} + \boldsymbol{k}_3)\,, \quad (8.11c)$$

where $\omega = \omega_1 - \omega_2$, $\boldsymbol{k} = \frac{1}{2}(\boldsymbol{k}_1 + \boldsymbol{k}_2)$ and $\boldsymbol{q} \equiv \boldsymbol{k}_1 - \boldsymbol{k}_2$.

We can obtain two asymptotic limits from Eq. (8.11). The first is when the frequency ω is much smaller than the dephasing rate, i.e. $|\omega| \ll \lambda_\alpha$ for $\alpha \neq 0$. In this case we can neglect the contribution $\bar{\Gamma}_{\mathrm{f}}^{(\mathrm{b})}$ and get

$$\bar{\Gamma}^{(\mathrm{b})} = \bar{\Gamma}_{\mathrm{s}}^{(\mathrm{b})}\,. \quad (8.12)$$

Another limiting case is when the third wave is off-resonant, i.e., $|\omega_3 - \varepsilon(\boldsymbol{p})| \gg W$, where W is the exciton bandwidth. In this case $\bar{\Gamma}$ does not depend on $\boldsymbol{p}$, and $\bar{\Gamma}_{\mathrm{f}}^{(\mathrm{b})} = 0$. Substituting the local field expression for $\bar{\Gamma} = -2(\omega_3 - \varepsilon_0)$ into Eq. (8.11b) and making use of Eq. (8.10f) we obtain:

$$\bar{\Gamma}^{(\mathrm{b})}(\omega_{\mathrm{s}}\boldsymbol{k}_{\mathrm{s}}, \omega_1\boldsymbol{k}_1, -\omega_2 - \boldsymbol{k}_2, \omega_3\boldsymbol{k}_3) = -2\int \mathrm{d}\boldsymbol{p}'\,g(\boldsymbol{p}', \boldsymbol{k}, \tfrac{1}{2}(\omega_1 + \omega_2))\frac{\mathrm{i}(\omega_3 - \varepsilon_0)}{\omega + \mathrm{i}\Gamma_0 + \mathrm{i}D\boldsymbol{q}^2}\,. \quad (8.13)$$

The case when we have both static and dynamical disorder (and the static disorder is dominant) will be considered in Section 10. The $\omega_1 = \omega_2$ resonance is disorder-induced (be it static or dynamical) and is not related to a specific pair of states. We call such resonances collective and discuss them in detail in Sections 11 and 12.

(3) *Degenerate four-wave mixing.* In frequency domain degenerate four-wave mixing $\omega_1 \approx \omega_2$ and $\boldsymbol{k}_1 \approx \boldsymbol{k}_2$. In this region the third-order optical response is given by the $R^{(b)}$ contribution. For the homodyne detection we obtain from Eq. (2.19a)

$$S_{\mathrm{hom}}(\boldsymbol{k}_{\mathrm{s}}\,\omega_{\mathrm{s}}) \propto |R^{(b)}(-\omega_{\mathrm{s}} - \boldsymbol{k}_{\mathrm{s}}; \omega_1\boldsymbol{k}_1, -\omega_2 - \boldsymbol{k}_2, \omega_3\boldsymbol{k}_3)|^2\,. \quad (8.14)$$

For the heterodyne detection we assume $E_1 = E_2$ and take the heterodyne field in the form $E_{\mathrm{h}} = E_3\exp(\mathrm{i}\varphi)$. The heterodyne signal (Eq. (2.20a)) yields

$$S_{\mathrm{het}}(\boldsymbol{k}_{\mathrm{s}}\,\omega_{\mathrm{s}}) = |E_1|^2|E_3|^2\,\mathrm{Re}\{\exp(-\mathrm{i}\varphi)R^{(b)}(-\omega_{\mathrm{s}} - \boldsymbol{k}_{\mathrm{s}}; \omega_1\boldsymbol{k}_1, -\omega_2 - \boldsymbol{k}_2, \omega_3\boldsymbol{k}_3)\} \quad (8.15)$$

and for $\varphi = 0$ and $\varphi = \pi/2$, $S_{\mathrm{het}}(\boldsymbol{k}_{\mathrm{s}}\omega_{\mathrm{s}}) \propto \mathrm{Re}(R^{(b)})$ and $S_{\mathrm{het}}(\boldsymbol{k}_{\mathrm{s}}\omega_{\mathrm{s}}) \propto \mathrm{Im}(R^{(b)})$. Summarizing, the heterodyne and the homodyne detections allow us to measure $\mathrm{Re}(R^{(b)})$, $\mathrm{Im}(R^{(b)})$ and $|R^{(b)}|^2$. The measurement is performed by fixing ω_1 inside the single-exciton band, and scanning ω_2 in the vicinity of ω_1

$$R(-\omega_{\mathrm{s}} - \boldsymbol{k}_{\mathrm{s}}; \omega_1\boldsymbol{k}_1, -\omega_2 - \boldsymbol{k}_2, \omega_3\boldsymbol{k}_3) = R^{(b)}(-\omega_{\mathrm{s}} - \boldsymbol{k}_{\mathrm{s}}; \omega_1\boldsymbol{k}_1, -\omega_2 - \boldsymbol{k}_2, \omega_3\boldsymbol{k}_3)$$

$$= A(\omega_3)/[-\mathrm{i}\omega_{12} + \Gamma_0 + q^2D]\,. \quad (8.16a)$$

$$A(\omega_3) = \mu^4(C_0/M)\sum_{\boldsymbol{p}}\exp[-\varepsilon(\boldsymbol{p})/kT]\,\bar{\Gamma}(\varepsilon(\boldsymbol{p}) + \omega_3, \boldsymbol{p})[G^2(\omega_3, 0)]^2\,, \quad (8.16b)$$

where $\omega_{12} = \omega_1 - \omega_2$, $q = |\boldsymbol{k}_1 - \boldsymbol{k}_2|$.[5]

[5] In Eq. (8.16b) and in the rest of the section we replace $\int \mathrm{d}\boldsymbol{p}$ by $(1/M)\sum_{\boldsymbol{p}}$, since the numerical calculations are performed for a finite chain of M atoms.

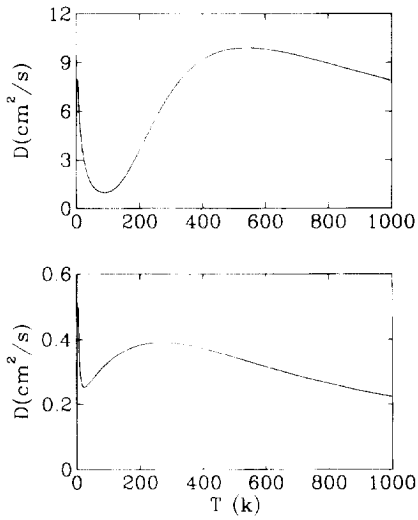

Fig. 5. Exciton diffusion coefficient (with phonons but no disorder) D as a function of temperature. The lattice constant $a = 10$ Å. Upper panel $V_{op} = 140\ \mathrm{cm}^{-1}$, $V_{ac} = 0$, lower panel $V_{ac} = 140\ \mathrm{cm}^{-1}$, $V_{op} = 0$.

$|R^{(b)}|^2$ has a Lorentzian resonance at $\omega_{12} = 0$ with width $\Gamma_0 + q^2 D$. From the dependence of this width on wave vector q, we obtain the exciton diffusion coefficient D. This can be rationalized as follows: the $\boldsymbol{k}_1$ and $\boldsymbol{k}_2$ fields interfere in the system and create a grating with wave vector $\boldsymbol{q} = \boldsymbol{k}_1 - \boldsymbol{k}_2$. The signal results from a Bragg diffraction of $\boldsymbol{k}_3$ off that grating. Exciton diffusion tends to drive the system towards a uniform excitation thus destroying the grating, and $q^2 D$ is the grating decay rate due to diffusion. We have calculated the temperature dependence of the exciton diffusion constant for our model, and the result is displayed in Fig. 5. The figure shows that D decreases with temperature at both low and high temperatures, and increases with temperature for intermediate temperatures. This can be explained using the following argument: $D \sim \langle v^2 \rangle / \langle \Gamma \rangle$, where $\langle v^2 \rangle$ is the mean square exciton velocity, and $\langle \Gamma \rangle$ is the average phonon-induced exciton dephasing rate. At low temperatures, exciton population is accumulated at the lower bandedge and $\langle v^2 \rangle$ is proportional to the exciton energy above the lower bandedge, $\langle v^2 \rangle \sim \Delta\varepsilon \sim kT$. The exciton dephasing at the lower bandedge is caused by phonon absorption (phonon emission processes do not contribute), whose rate is proportional to the phonon population $\exp[-\Omega(q)/kT]$. $\Omega(q)$ is the absorbed phonon frequency, determined by the momentum and energy conservation relations $\varepsilon_0(k_0) + \Omega(q) = \varepsilon(k_0 + q)$, and $\boldsymbol{k}_0$ is the exciton momentum at the lower bandedge. Therefore as $T \to 0$, $D \sim kT \exp[\Omega(q)/kT] \to \infty$. At high temperatures, $\langle v^2 \rangle$ approaches a constant, $\langle \Gamma \rangle$ is proportional to the phonon population which is proportional to kT, and we have $D \sim T^{-1}$. For intermediate temperatures, both $\langle v^2 \rangle$ and $\langle \Gamma \rangle$ increase with temperature, but $\langle v^2 \rangle$ increases faster, resulting in a net increase of D with temperature.

The excitation profile $A(\omega_3)$ for degenerate four-wave mixing (DFWM) is obtained by setting $\omega_1 = \omega_2$, and measuring the signal as a function of ω_3. $A(\omega_3)$ for a J-aggregate is shown in Fig. 6. Here, the exciton population is accumulated near $p = 0$ in the equilibrium distribution. When ω_3 is

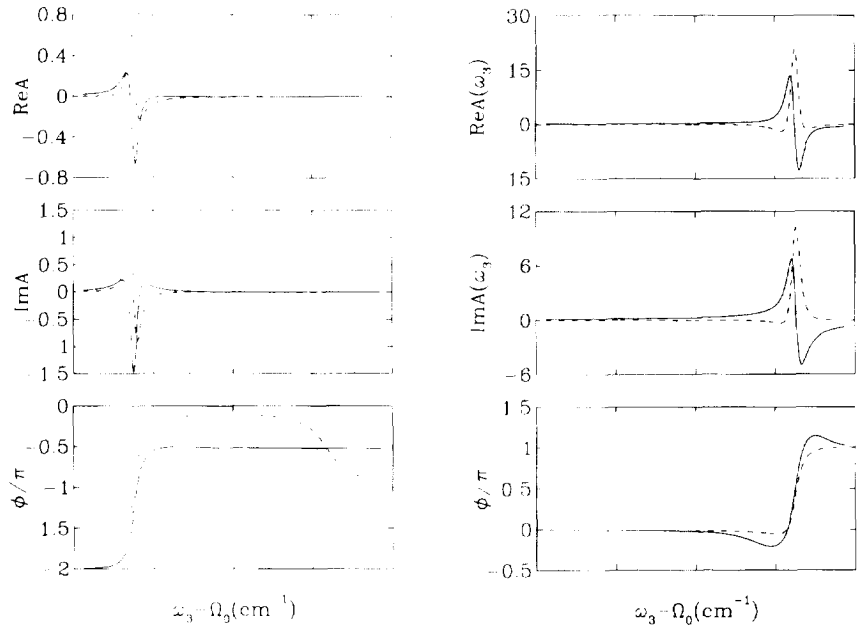

Fig. 6. Excitation profile of DFWM. $A(\omega_3)$, for 1-D J-aggregate as described in Fig. 9 and 10. $V_{ac} = 140\ cm^{-1}$, $V_{op} = 0$. Upper, middle, and lower panel corresponding to the real part, the imaginary part, and the phase of A. Solid line – GFE, dash line – LFA. $\tan\phi \equiv \mathrm{Im}\,A\ \mathrm{Re}\,A$.

Fig. 7. The same as Fig. 6 but for H-aggregate as described in Fig. 14.

far from the lower bandedge, $G(\omega_3, 0)$ is real, and the phase of A is close to the phase of $\bar{\Gamma}(\Omega_0 + 2J + \omega_3, 0)$, which is close to $-\pi/2$. This is evident from the solid line in the lowest panel of Fig. 6. This indicates that the imaginary part of A is much larger than the real part. If we measure the DFWM signal $R^{(b)}$ as a function of $\omega = \omega_1 - \omega_2$, the real part of $R^{(b)}$ is dispersive and the imaginary part is absorptive. In the LFA' (dashed line), the phase of $\bar{\Gamma}(\Omega_0 + 2J + \omega_3, 0)$ is close to 0 or $-\pi$, and thus the real part of A is much larger than the imaginary part. When the lineshape of $R^{(b)}$ with $\omega = \omega_1 - \omega_2$ is displayed we find that, the real part of $R^{(b)}$ is absorptive and the imaginary part is dispersive, which is exactly the opposite of the GFE result! For H-aggregates, as shown in Fig. 7, the exciton population is accumulated near $p = \pi/a$, and the phase of A is the same as $\bar{\Gamma}(\Omega_0 + 2J + \omega_3, \pi/a)$. From the lowest panel of Fig. 7 we note that $\bar{\Gamma}$ is real as long as ω_3 is far from the upper bandedge. The same conclusion holds in the LFA. If we measure $R^{(b)}$ as a function of $\omega = \omega_1 - \omega_2$, both the GFE and LFA' predict that the real part of $R^{(b)}$ is absorptive and the imaginary part is dispersive.

(4) *Transient grating.* This is the time-domain counterpart of the degenerate four-wave mixing [51]. In the transient grating technique, pulses 1 and 2 coincide, and come before pulse 3 (we assume that pulses 1 and 2 are centered at $t = 0$, and pulse 3 at $t = \tau'$). This technique provides a direct probe for exciton transport in real space. Taking the heterodyne pulse to have the same form as pulse 3, i.e., $E_h = E_3 \exp(i\varphi)$ we obtain for the integrated signal $S^{I}_{het}(\boldsymbol{k}_s; \tau')$ as a function of

the time delay τ':

$$S^{I}_{het}(\boldsymbol{k}_s;\tau') = \mathrm{Re}\{\alpha(E_1,E_2)\exp\{-[\Gamma_0 + D(\boldsymbol{k}_1-\boldsymbol{k}_2)^2]\tau'\}\exp(-i\varphi)$$
$$\times \int dt\, d\tau\, K(t-\tau)E_3(\tau)E_3^*(t)\}\,. \tag{8.17a}$$

where α depends on the slow envelopes of the pump pulses E_1 and E_2 (we set $\Omega_1 = \Omega_2 = \Omega$)

$$\alpha(E_1,E_2) = \mu^4 \int \frac{d\omega}{2\pi}\, d\boldsymbol{p}\, |G(\Omega+\omega)|^2 g(\boldsymbol{p},0;\Omega+\omega)E_1(\omega)E_2^*(\omega)\,, \tag{8.17b}$$

and $K(t)$ has the form

$$K(t) = \int \frac{d\omega}{2\pi}\, d\boldsymbol{p}\, C\exp[-\varepsilon(\boldsymbol{p})/kT]\bar{\Gamma}(\omega+\Omega_3+\varepsilon(\boldsymbol{p}),\boldsymbol{p})[G(\omega+\Omega_3)]^2\exp(-i\omega t)\,. \tag{8.17c}$$

Eq. (8.17a) shows the transient grating decay due to the exciton lifetime and transport in real space.

For static disorder, the signal can be obtained using Eq. (4.22) by taking into account the contribution $R^{(b)}$ in the r.h.s. of Eq. (4.22b) (Eqs. 4.14(a) and (c)). This yields for an off-resonant probe pulse Ω_3:

$$R(t\boldsymbol{k}_s;\tau_1\boldsymbol{k}_1,\tau_2-\boldsymbol{k}_2,\tau_3\boldsymbol{k}_3) = [G(\Omega_3)]^2|G(\Omega_1)|^2\mu^4\sigma^2\int d\boldsymbol{p}\, 2\pi\delta(\Omega_1-\varepsilon(\boldsymbol{p}))\bar{\Gamma}(\Omega_1+\Omega_3;\boldsymbol{p}+\boldsymbol{k}_3)$$
$$\times\delta(\tau_1-\tau_2)\delta(t-\tau_3)\theta(t-\tau_1)\exp\{-[\Gamma_0(\Omega_1)+\boldsymbol{q}^2D(\Omega_1)](\tau_3-\tau_1)\}\,, \tag{8.18a}$$

where $\theta(t) = 1$ for $t > 0$, $\theta(t) = 0$ otherwise is the Heavyside step function.

The integrated heterodyne signal $S^{I}_{het}(\boldsymbol{k}_s)$ can be easily obtained from Eq. (8.18a); it has the form of Eq. (8.17a) with

$$\alpha(E_1,E_2) = \mu^4\sigma^2|G(\Omega_1)|^2\int\frac{d\omega}{2\pi}E_1(\omega)E_2^*(\omega)\,, \tag{8.18b}$$

$$K(t) = \int d\boldsymbol{p}\, 2\pi\delta(\Omega-\varepsilon(\boldsymbol{p}))\bar{\Gamma}(\Omega_1+\Omega_3,\boldsymbol{p}+\boldsymbol{k}_3)[G(\Omega_3)]^2\delta(t)\,, \tag{8.18c}$$

and where $\Gamma_0(\Omega_1)$ and $D(\Omega_1)$ (Eq. (4.17)) should be substituted for Γ_0 and D in Eq. (8.17a). For exciton–phonon interaction the transient grating decay shows processes of exciton lifetime and transport in real space. Since exciton scattering on static disorder is elastic, the exciton energy does not change, and $\Gamma_0(\Omega)$ and $D(\Omega)$ describe the lifetime and transport of excitons with energy Ω, which is determined by the pump field frequency, as discussed in Section 4.

(5) *Nonlinear reflection.* Consider the propagation of a single beam in a medium. As its intensity is increased, its propagation is affected by the nonlinear response of the medium. We shall now calculate the lowest nonlinear correction, related to $\chi^{(3)}$. In this case we set $\boldsymbol{k}_s = \boldsymbol{k}_1 = \boldsymbol{k}_2 = \boldsymbol{k}_3$, $\omega_s = \omega_1 = \omega_2 = \omega_3$, $E_1 = E_2 = E_3$. Since $\boldsymbol{k}_s$ is the projection of the signal wave vector on the aggregate, for a 2-D system there are two possible propagation directions of the signal (the projection of the photon wave vector should be equal to $\boldsymbol{k}_s$), corresponding to the reflected and transmitted light. For a 1-D system all possible reflection directions (with projection equal to $\boldsymbol{k}_s$)

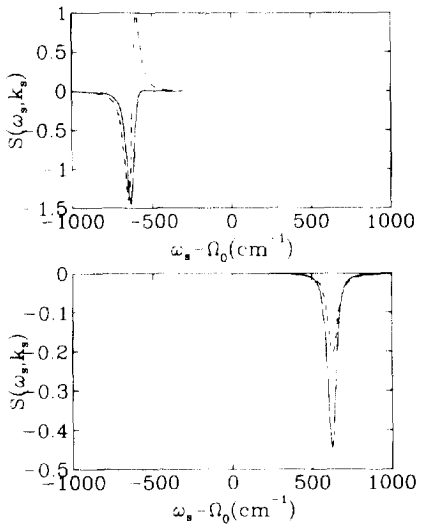

Fig. 8. Nonlinear reflection spectrum (Eq. (8.19)) for 1-D J-aggregate (upper panel) and H-aggregate (lower panel). Solid line is the GFE result, and dash line is the LFA result.

form a cone. $R^{(b)}$ is given by Eq. (8.16) with $\omega_{12} = 0, q = 0$. Since $\boldsymbol{k}_s = \boldsymbol{k}_3$, the nonlinear signal mixes with the linear signal, which has the same frequency and direction, and the configuration has a built-in heterodyne detection. The nonlinear contribution to the reflected signal is

$$S(\boldsymbol{k}_s\omega_s) = \mathrm{Re}\{R^{(1)*}(\omega_s)R^{(b)}(-\omega_s;\omega_3,-\omega_3,\omega_3)\}|E_3|^4 \propto \mathrm{Re}[G^*(\omega_3,0)A(\omega_3)]$$
$$= \mu^4|G(\omega_3,0)|^2(C/M)\sum_p \exp[-\varepsilon(\boldsymbol{p})/kT]\,\mathrm{Re}\{\bar{\Gamma}(\varepsilon(\boldsymbol{p})+\omega_3,\boldsymbol{p})G(\omega_3,0)\}\,, \tag{8.19}$$

This expression is similar to degenerate four-wave mixing. The signal is displayed in Fig. 8. For J-aggregates, the $p = 0$ state dominates the p summation, the imaginary part of $\bar{\Gamma}(\varepsilon(0)+\omega_3,0)$ is much larger than its real part, and the signal shows an absorptive dependence on ω_3 (solid line of the upper panel of Fig. 8). In the LFA′, $\bar{\Gamma}$ is real and the signal has a dispersive dependence on ω_3 (dashed line of the upper panel of Fig. 8). For H-aggregates, the $p = \pi/a$ state dominates the p summation. In the LFA′, $\bar{\Gamma}(\Omega_0+2J+\omega_3,\pi/a) \to -2[\omega_3 - 2J + \Omega_0 + \mathrm{i}(2/M)\sum_p \Gamma(p)]$, which is pure imaginary when ω_3 is at the upper bandedge. Therefore both the LFA′ and the GFE give an absorptive dependence of the signal on ω_3 near the upper bandedge (lower panel of Fig. 8). The LFA′ signal is weaker compared with the GFE. The time domain analogue of this effect is pump-probe spectroscopy which will be considered in the next section, where we shall also compare it with time and frequency resolved luminescence.

9. Exciton scattering and relaxation probed by time and frequency resolved fluorescence

In this section we consider spontaneous emission (luminescence) spectroscopy of molecular assemblies using the same models of molecular nanostructures used in the discussion of the

coherent optical response in previous sections. We first express the time and frequency resolved emission spectra in terms of the exciton Green functions (an analogue of the GFE for the coherent optical response), and then present numerical calculations for the exciton–phonon model introduced in Section 8. Applications of the present formalism to the simplest case of static disorder were made in [67, 23].

There are various formal procedures for defining the time-dependent emission spectrum [86]. We will adopt the following definition [37, 65]:

$$S_{\mathrm{fl}}(\boldsymbol{k}, t) \equiv \frac{\mathrm{d}}{\mathrm{d}t} \langle \tilde{a}_{\boldsymbol{k}}^{\dagger}(t) \tilde{a}_{\boldsymbol{k}}(t) \rangle \,, \tag{9.1}$$

where $\hat{a}_{\boldsymbol{k}}$, $\hat{a}_{\boldsymbol{k}}^{\dagger}$ are the photon annihilation and creation operators which satisfy the boson commutation rules

$$[\hat{a}_{\boldsymbol{k}}, \hat{a}_{\boldsymbol{q}}^{\dagger}] = \delta(\boldsymbol{k} - \boldsymbol{q}) \,. \tag{9.2a}$$

and $\boldsymbol{k}$ is the photon wave vector which determines the frequency of the observed signal and the direction of observation. Our definition is equivalent to the rate of change of the number of photons with a wave vector $\boldsymbol{k}$. Other definitions which take into account the detection device can all be expressed in terms of Eq. (9.1) with a proper convolution with frequency filter and time gate functions [86]. Eq. (9.1) is then the fundamental quantity that carries all microscopic information necessary for calculating the time-dependent emission spectrum. Using the field operators, the vector potential and the displacement field can be expanded as

$$\hat{A}(\boldsymbol{r}) = \int \frac{\mathrm{d}\boldsymbol{k}}{(2\pi)^3} \frac{1}{(2\pi\omega(\boldsymbol{k}))^{1/2}} [\exp(\mathrm{i}\boldsymbol{k}\boldsymbol{r}) \hat{a}_{\boldsymbol{k}} + \exp(-\mathrm{i}\boldsymbol{k}\boldsymbol{r}) \hat{a}_{\boldsymbol{k}}^{\dagger}] \,, \tag{9.2b}$$

$$\hat{D}^{\perp}(\boldsymbol{r}) = \mathrm{i} \int \frac{\mathrm{d}\boldsymbol{k}}{(2\pi)^3} (2\pi\omega(\boldsymbol{k}))^{1/2} [\exp(\mathrm{i}\boldsymbol{k}\boldsymbol{r}) \hat{a}_{\boldsymbol{k}} - \exp(-\mathrm{i}\boldsymbol{k}\boldsymbol{r}) \hat{a}_{\boldsymbol{k}}^{\dagger}] \,, \tag{9.2c}$$

and the radiation field Hamiltonian (Eq. (2.2)) is given by

$$\hat{H}_{\mathrm{rad}} = \int \frac{\mathrm{d}\boldsymbol{k}}{(2\pi^3)} \omega(\boldsymbol{k}) \hat{a}_{\boldsymbol{k}}^{\dagger} a_{\boldsymbol{k}} \,, \tag{9.2d}$$

where $\omega(\boldsymbol{k}) \equiv c|\boldsymbol{k}|$ is the photon dispersion.

We shall now show that the signal $S_{\mathrm{fl}}(\boldsymbol{k}, t)$ may be expressed in terms of the correlation function $\mathscr{C}_p$ (Eq. (2.16a)) introduced for the description of the correlated detection. To that end we first recast Eq. (9.1) in a symmetrized form, making use of the commutation relation (9.2a):

$$S_{\mathrm{fl}}(\boldsymbol{k}, t) = \tfrac{1}{2} \frac{\mathrm{d}}{\mathrm{d}t} \langle \tilde{a}_{\boldsymbol{k}}^{\dagger}(t) \tilde{a}_{\boldsymbol{k}}(t) + \tilde{a}_{\boldsymbol{k}}(t) \tilde{a}_{\boldsymbol{k}}^{\dagger}(t) \rangle \,. \tag{9.3}$$

Using the Heisenberg equations of motion for the photon operators $\tilde{a}$ and $\tilde{a}^{\dagger}$ (which are equivalent to the Maxwell equations written in terms of the photon creation and annihilation operators), we

can relate $\tilde{a}(t)$ and $\tilde{a}^{\dagger}(t)$ in terms of the polarization operator $\tilde{P}$:

$$\tilde{a}_{\boldsymbol{k}}(t) = \sqrt{2\pi\omega(\boldsymbol{k})} \int \mathrm{d}t'\, \mathscr{G}_0(\boldsymbol{k}, t-t')\tilde{P}(\boldsymbol{k}, t')\,. \tag{9.4a}$$

$$\tilde{a}^{\dagger}_{\boldsymbol{k}}(t) = \sqrt{2\pi\omega(\boldsymbol{k})} \int \mathrm{d}t'\, \mathscr{G}^{*}_0(\boldsymbol{k}, t-t')\tilde{P}(-\boldsymbol{k}, t')\,, \tag{9.4b}$$

where

$$\mathscr{G}_0(\boldsymbol{k}, t) \equiv \int \frac{\mathrm{d}\omega}{2\pi} \exp(-\mathrm{i}\omega t) \frac{1}{\omega - \omega(\boldsymbol{k}) + \mathrm{i}\eta}, \qquad \tilde{P}(\boldsymbol{k}, t) = \int \mathrm{d}\boldsymbol{r} \exp(-\mathrm{i}\boldsymbol{k}\cdot\boldsymbol{r})\tilde{P}(\boldsymbol{r}, t)\,. \tag{9.5a, b}$$

Substituting these expressions into Eq. (9.3) we obtain

$$S_{\mathrm{fl}}(\boldsymbol{k}, t) = 2\pi\omega(\boldsymbol{k}) \int \frac{\mathrm{d}\omega}{2\pi} \frac{\mathrm{d}\Omega}{2\pi}\, \mathrm{d}t_1\, \mathrm{d}t_2 \exp\left[\mathrm{i}\omega\left(\frac{t_1 + t_2}{2} - t\right) + \mathrm{i}\Omega(t_1 - t_2)\right]$$
$$\times \frac{\mathrm{i}\omega}{\Omega + (\omega/2) - \omega(\boldsymbol{k}) - \mathrm{i}0} \frac{1}{\Omega - (\omega/2) - \omega(\boldsymbol{k}) + \mathrm{i}0} \mathscr{C}_{\mathrm{p}}(\boldsymbol{k}t_1, -\boldsymbol{k}t_2)\,, \tag{9.6a}$$

where the correlation function $\mathscr{C}_{\mathrm{p}}$ in the momentum domain is given by the Fourier transform of $\mathscr{C}_{\mathrm{p}}(\boldsymbol{r}t, \boldsymbol{r}'t')$ defined in Section 2 (Eq. (2.16a))

$$\mathscr{C}_{\mathrm{p}}(\boldsymbol{k}_1 t_1, \boldsymbol{k}_2 t_2) \equiv \int \mathrm{d}\boldsymbol{r}_1\, \mathrm{d}\boldsymbol{r}_2 \exp(-\mathrm{i}\boldsymbol{k}_1\cdot\boldsymbol{r}_1 - \mathrm{i}\boldsymbol{k}_2\cdot\boldsymbol{r}_2)\mathscr{C}_{\mathrm{p}}(\boldsymbol{r}_1 t_1, \boldsymbol{r}_2 t_2)\,. \tag{9.6b}$$

When the spectrum is slowly changing in time, the important contribution for the ω integration in Eq. (9.6a) is from the region $|\omega| \ll \omega(\boldsymbol{k})$, and we can set

$$\frac{\mathrm{i}\omega}{\Omega + (\omega/2) - \omega(\boldsymbol{k}) - \mathrm{i}0} \frac{1}{\Omega - (\omega/2) - \omega(\boldsymbol{k}) + \mathrm{i}0} \approx 2\pi\delta(\Omega - \omega(\boldsymbol{k}))\,. \tag{9.7}$$

Substituting this in Eq. (9.6a) we obtain

$$S_{\mathrm{fl}}(\boldsymbol{k}, t) = 2\pi\omega(\boldsymbol{k}) \int \mathrm{d}\tau\, \mathrm{e}^{\mathrm{i}\omega(\boldsymbol{k})\tau} \mathscr{C}_{\mathrm{p}}\left(\boldsymbol{k}t + \frac{\tau}{2}, -\boldsymbol{k}t - \frac{\tau}{2}\right). \tag{9.8}$$

Eqs. (9.6a) and (9.8) express the time and frequency resolved spectrum $S_{\mathrm{fl}}(\boldsymbol{k}, t)$ introduced by Eq. (9.1) in terms of the correlation function of the polarization [72].

Expanding $\mathscr{C}_{\mathrm{p}}$ in powers of the external field (Eq. (2.24b)), retaining only the lowest (first-) order in the incoming intensity, and substituting into Eq. (9.8), we finally obtain the GFE for the luminescence spectrum

$$S_{\mathrm{fl}}(\boldsymbol{k}, t) = 2\pi\omega(\boldsymbol{k}) \int \mathrm{d}\boldsymbol{r}_1\, \mathrm{d}\tau_1\, \mathrm{d}\boldsymbol{r}_2\, \mathrm{d}\tau_2\, \mathrm{d}\boldsymbol{r}\, \mathrm{d}\boldsymbol{r}'\, \mathrm{d}\tau \exp(\mathrm{i}\omega(\boldsymbol{k})\tau)\exp(\mathrm{i}\boldsymbol{k}\cdot(\boldsymbol{r}' - \boldsymbol{r}))$$
$$\times R_{\mathrm{c}}^{(2)}\left(\boldsymbol{r}t + \frac{\tau}{2}, \boldsymbol{r}'t - \frac{\tau}{2}; \boldsymbol{r}_1\tau_1, \boldsymbol{r}_2\tau_2\right) \mathscr{E}(\boldsymbol{r}_1, \tau_1)\mathscr{E}(\boldsymbol{r}_2, \tau_2)\,. \tag{9.9}$$

Making use of the correlation function expressions for $R_c^{(2)}$ (Eq. (5.8b)) we can follow the procedure of Appendix C and express $\langle \hat{P}_+ \hat{P}_+ \hat{P}_- \hat{P}_- \rangle$ in terms of exciton Green functions. Unlike the coherent nonlinear optical response, the terms in the perturbative expansion involving exciton–exciton scattering (due to Pauli exclusion) do not affect the luminescence signal. The physical reason is obvious: only one-exciton states are involved in luminescence. Formally the difference shows up in the fact that $R^{(3)}$ is given by the $\langle \hat{P}_+ \hat{P}_- \hat{P}_- \hat{P}_- \rangle$ correlation function whereas $R_c^{(2)}$ is related to $\langle \hat{P}_+ \hat{P}_+ \hat{P}_- \hat{P}_- \rangle$. Consequently, the expression for the luminescence signal can be derived using the free-boson system ($g = 0$ in the notation of Appendix C) and the result may be expressed in terms of the two-exciton Green function $\mathscr{G}^{(2)}$. Evaluating $\langle \hat{P}_+ \hat{P}_+ \hat{P}_- P_- \rangle$ and expressing the external field in a form

$$\mathscr{E}(\boldsymbol{r}, t) = \int \frac{\mathrm{d}\Omega}{2\pi} \exp(-\mathrm{i}\Omega t + \mathrm{i}\boldsymbol{k}_1 \cdot \boldsymbol{r}) \mathscr{E}(\Omega) + \text{c.c} . \tag{9.10}$$

we obtain for the signal

$$\begin{aligned} S_{\mathrm{fl}}(\boldsymbol{k}, t) = {} & \mu^4 2\pi \omega(\boldsymbol{k}) \\ & \times \int \frac{\mathrm{d}\omega}{2\pi} \frac{\mathrm{d}\omega'}{2\pi} \sum_{mnm'n'} \left\{ \mathscr{G}^{(2)}_{mnm'n'}(\omega', \omega(\boldsymbol{k}); \omega) \exp(-\mathrm{i}\omega t) + G_{mm'}\left(\omega' + \frac{\omega}{2}\right) \right. \\ & \left. \times G^*_{n'n}\left(\omega' - \frac{\omega}{2}\right) 2\pi\delta(\omega - \omega(\boldsymbol{k})) \right\} \\ & \times \exp(-\mathrm{i}\boldsymbol{k}_1 \cdot (\boldsymbol{R}_m - \boldsymbol{R}_n) + \mathrm{i}\boldsymbol{k} \cdot (\boldsymbol{R}_{m'} - \boldsymbol{R}_{n'})) \mathscr{E}\left(\omega' + \frac{\omega}{2}\right) \mathscr{E}^*\left(\omega' - \frac{\omega}{2}\right) . \end{aligned} \tag{9.11}$$

Hereafter, we denote the luminescence signal $S_{\mathrm{fl}}(\boldsymbol{k}_s \omega_s, t)$, where ω_s is its frequency and $\boldsymbol{k}_s$ is the projection of the wave vector onto the system, i.e. this signal is observed in the direction θ with $\cos\theta = |\boldsymbol{k}_s| c/\omega_s$. Recasting Eq. (9.11), in this notation and switching to the momentum domain, we obtain for a periodic system:

$$S_{\mathrm{fl}}(\boldsymbol{k}_s \omega_s, t) = S^c_{\mathrm{fl}}(\boldsymbol{k}_s \omega_s, t) + S^i_{\mathrm{fl}}(\boldsymbol{k}_s \omega_s, t) . \tag{9.12a}$$

$$\begin{aligned} S^c_{\mathrm{fl}}(\boldsymbol{k}_s \omega_s, t) = {} & \mu^4 2\pi \omega_s \delta(\boldsymbol{k}_s - \boldsymbol{k}_0) \int \frac{\mathrm{d}\omega}{2\pi} \exp(-\mathrm{i}\omega t) \\ & \times G\left(\omega_s + \frac{\omega}{2}, \boldsymbol{k}_s\right) G^*\left(\omega_s - \frac{\omega}{2}, \boldsymbol{k}_s\right) \mathscr{E}\left(\omega_s + \frac{\omega}{2}\right) \mathscr{E}^*\left(\omega_s - \frac{\omega}{2}\right) , \end{aligned} \tag{9.12b}$$

$$S^i_{\mathrm{fl}}(\boldsymbol{k}_s \omega_s, t) = \mu^4 2\pi \omega_s \int \frac{\mathrm{d}\omega}{2\pi} \frac{\mathrm{d}\omega'}{2\pi} \mathscr{G}^{(2)}_s(\omega' \boldsymbol{k}_0, \omega_s \boldsymbol{k}_s; \omega) \mathrm{e}^{-\mathrm{i}\omega t} \mathscr{E}\left(\omega' + \frac{\omega}{2}\right) \mathscr{E}^*\left(\omega' - \frac{\omega}{2}\right) . \tag{9.12c}$$

where S^c and S^i denote coherent and incoherent components respectively, $\boldsymbol{k}_0$ is the projection of $\boldsymbol{k}_1$ on the system, and

$$\mathscr{G}_s^{(2)}(\omega' \boldsymbol{k}_0, \omega_s \boldsymbol{k}_s; \omega) \equiv \sum_{mnm'} \mathscr{G}^{(2)}_{mnm'n}(\omega', \omega_s; \omega) \exp[i\boldsymbol{k}_s \cdot (\boldsymbol{R}_{m'} - \boldsymbol{R}_n) - i\boldsymbol{k}_0 \cdot (\boldsymbol{R}_m - \boldsymbol{R}_n)] . \tag{9.12d}$$

For a frequency domain measurement we set $\mathscr{E}(\Omega) \equiv E\delta(\Omega - \omega_0)$, for $\omega_s \neq \omega_0$ we obtain from Eq. (9.12c):

$$S_{fl}^i(\boldsymbol{k}_s \omega_s) = \mu^4 2\pi \omega_s \mathscr{G}_s^{(2)}(\omega_0 \boldsymbol{k}_0, \omega_s \boldsymbol{k}_s; \omega = 0) |E|^2 . \tag{9.13}$$

In Appendix D the Green function $\mathscr{G}_s^{(2)}$ is expressed in terms of the Green function $\mathscr{D}$ of the Boltzmann equation:

$$\mathscr{G}_s^{(2)}(\omega_0 \boldsymbol{k}_0, \omega_s \boldsymbol{k}_s; \omega) = G\left(\omega_0 + \frac{\omega}{2}, \boldsymbol{k}_0\right) G^*\left(\omega_0 - \frac{\omega}{2}, \boldsymbol{k}_0\right) G\left(\omega_s + \frac{\omega}{2}, \boldsymbol{k}_s\right) G^*\left(\omega_s - \frac{\omega}{2}, \boldsymbol{k}_s\right) \times \bar{\Gamma}_s(\omega_0 \boldsymbol{k}_0, \omega_s \boldsymbol{k}_s; \omega) . \tag{9.14a}$$

here the one-exciton Green function is given by Eq. (7.2b), and the irreducible vertex $\bar{\Gamma}_s$ has the form:

$$\bar{\Gamma}_s(\omega_0 \boldsymbol{k}_0, \omega_s \boldsymbol{k}_s; \omega) = \int d\boldsymbol{p}' \, d\boldsymbol{p} \, g(\boldsymbol{p}', \boldsymbol{k}_0; \omega_0) \mathscr{D}(\boldsymbol{p}, \boldsymbol{p}; \boldsymbol{q} = 0, \omega) g_s(\boldsymbol{k}_s, \boldsymbol{p}; \omega_s) , \tag{9.14b}$$

g_s is defined in Appendix D and evaluated in Appendix E.

The first contribution in Eq. (9.12a) gives the coherent signal S_{fl}^c, which has the same frequency and wave vector as the incident light, and is related to the modulus squared of the electric field in the coherent linear signal:

$$S_{fl}^c(\boldsymbol{k}_s \omega_s, t) = 2\pi \omega_s \delta(\boldsymbol{k}_s - \boldsymbol{k}_0) \int d\tau \, P\left(\boldsymbol{k}_s, t + \frac{\tau}{2}\right) P^*\left(\boldsymbol{k}_s, t - \frac{\tau}{2}\right) \exp(i\omega_s \tau) , \tag{9.15a}$$

with

$$P(\boldsymbol{k}_s, t) \equiv \int dt' \, R^{(1)}(\boldsymbol{k}_s, t - t') \mathscr{E}(\boldsymbol{k}_s, t') , \tag{9.15b}$$

being the linear coherent polarization. The second contribution S_{fl}^i is the incoherent signal which may have frequencies and wave vectors different from the incident beam.

Expanding the Green function $\mathscr{D}$ using the eigenmodes of the transport equation, we obtain the following representation for $\bar{\Gamma}_s$

$$\bar{\Gamma}_s = \bar{\Gamma}_{ss} + \bar{\Gamma}_{sf} , \tag{9.16a}$$

with

$$\bar{\Gamma}_{ss}(\omega_0 \boldsymbol{k}_0, \omega_s \boldsymbol{k}_s; \omega) = \frac{iC}{\omega + i\Gamma_0} \int d\boldsymbol{p}' \, g(\boldsymbol{p}', \boldsymbol{k}_0; \omega_0) \int d\boldsymbol{p} \, g_s(\boldsymbol{k}_s, \boldsymbol{p}; \omega_s) \exp[-\varepsilon(\boldsymbol{p})/kT] , \tag{9.16b}$$

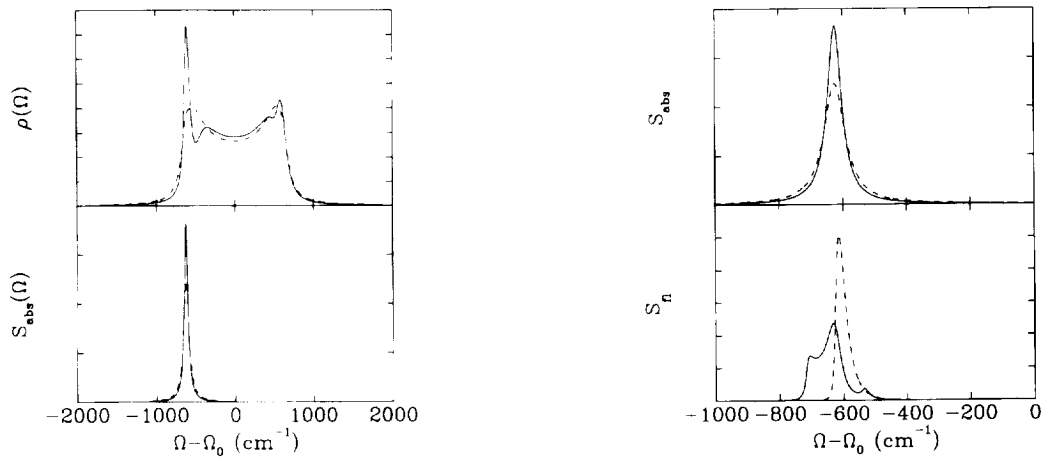

Fig. 9. Single exciton density of states, linear absorption coefficient, for a 1-D molecular lattice (J-aggregate) with exciton–phonon interaction as described in Section 8. $|J| = 312.5\ \mathrm{cm}^{-1}$, $T = 100$ K. Solid line is the contribution from optical phonon, $V_{op} = 140\ \mathrm{cm}^{-1}$, $V_{ac} = 0$, and dash line is the contribution from acoustical phonon, $V_{ac} = 140\ \mathrm{cm}^{-1}$, $V_{op} = 0$.

Fig. 10. Linear absorption coefficient and long time fluorescence spectrum for the same system. Solid line is the contribution from optical phonons $V_{op} = 140\ \mathrm{cm}^{-1}$, $V_{ac} = 0$, and dash line is the contribution from acoustical phonon, $V_{ac} = 140\ \mathrm{cm}^{-1}$, $V_{op} = 0$.

and

$$\bar{\Gamma}_{sf}(\omega_0 \boldsymbol{k}_0, \omega_s \boldsymbol{k}_s; \omega) = \sum_{\alpha \neq 0} \frac{i}{\omega + i\lambda_\alpha} \int d\boldsymbol{p}'\, \bar{\varphi}_\alpha(\boldsymbol{p}')\, g(\boldsymbol{p}', \boldsymbol{k}_0; \omega_0) \int d\boldsymbol{p}\, g_s(\boldsymbol{k}_s, \boldsymbol{p}; \omega_s)\, \varphi_\alpha(\boldsymbol{p}) \,. \tag{9.16c}$$

where $\bar{\Gamma}_{ss}$ and $\bar{\Gamma}_{sf}$ are the "slow" and the "fast" contributions which are related to the zero mode φ_0 and all other φ_α, $\alpha \neq 0$ modes respectively. For frequencies ω much smaller than the dephasing rate, (which corresponds to a continuous wave setup $\omega = 0$, or to the long-time limit in a time-domain measurement) we can simply set

$$\bar{\Gamma}_s = \bar{\Gamma}_{ss} \,. \tag{9.16d}$$

The luminescence signal is given by Eqs. (9.12a)–(9.12c) with $\mathscr{G}_s^{(2)}$ determined by Eq. (9.14a) with $\bar{\Gamma}_s$ calculated using Eq. (9.16).

The following numerical calculations performed on the same model systems introduced in Section 8 show the time and frequency resolved luminescence spectrum. To set the stage, the single-exciton density of states $\rho(\Omega) \equiv -(1/\pi) \int d\boldsymbol{k}\, \mathrm{Im}\, G(\Omega, \boldsymbol{k})$ and the linear absorption coefficient $S_{abs}(\Omega) \equiv -\mathrm{Im}\, G(\Omega, 0)$ are displayed in Fig. 9. The relaxed fluorescence spectrum in the long-time limit where the exciton distribution reaches the Boltzmann form is shown in Fig. 10 (lower panel). In the figure, Ω_0 is the isolated molecular resonance frequency which is the same for all molecules.

The time-resolved fluorescence spectrum $S_{fl}(\boldsymbol{k}_s = 0, \Omega', t)$ for $t = 0$ (instantaneous spectrum) and with incident frequency $\Omega = \Omega_0$ is displayed in Fig. 11. The upper panel shows the effects of optical

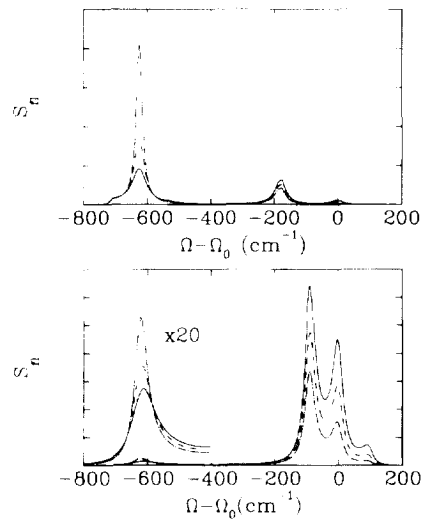

Fig. 11. The instantaneous fluorescence spectrum $S_{fl}(k' = 0, \Omega', t = 0)$ for a J-aggregate at various temperature T. Incident frequency $\Omega = \Omega_0$, $T = 100, 80, 60$ K, for solid, dashed, and dash dotted curves. Upper panel is the contribution of optical phonons, $V_{op} = 140\,\text{cm}^{-1}$, $V_{ac} = 0$. Lower is the contribution of acoustical phonons, $V_{op} = 0$, $V_{ac} = 140\,\text{cm}^{-1}$, and the peak around $-625\,\text{cm}^{-1}$ enlarged by 20 times is also shown.

phonons; the spectrum has three peaks located at $\Omega_0, \Omega_0 - 2\Omega_{op}$ and the exciton bandedge $\varepsilon(\boldsymbol{k} = 0)$. The $\Omega - 2\Omega_{op}$ resonance is generated through the following process: the excitation pulse creates an exciton with momentum $\boldsymbol{k}$. Since the exciton energy $\varepsilon(\boldsymbol{k})$ is not equal to the excitation frequency Ω_0, energy is not conserved and this is a virtual excitation. To conserve energy as well as momentum, the exciton emits an optical phonon with momentum $-\boldsymbol{q}$ and ends up in the final state with momentum $\boldsymbol{k} + \boldsymbol{q}$ and energy $\varepsilon(\boldsymbol{k} + \boldsymbol{q})$. $\boldsymbol{q}$ is determined by the requirement of energy conservation $\varepsilon(\boldsymbol{k} + \boldsymbol{q}) = \Omega - \Omega_{op}$. After that, the exciton emits another phonon with momentum $\boldsymbol{k} + \boldsymbol{q} - \boldsymbol{k}'$, and ends up in the virtual state with momentum $\boldsymbol{k}'$. It then emits a photon with energy Ω', and with the projection of wave vector in the lattice line $\boldsymbol{k}'$. Energy conservation requires $\Omega' = \Omega_0 - 2\Omega_{op}$. Therefore, the $\Omega' - \Omega_0 = -180\,\text{cm}^{-1}$ peak results from the emission of two phonons. For the same reason, the peak at $\Omega' - \Omega_0 = 0$ results from the emission and absorption of a phonon respectively. For the present parameters, the optical phonon population $N(\Omega_{op}) \equiv [\exp(\Omega_{op}/kT) - 1]^{-1}$ is small compared with 1 since the optical phonon frequency is larger than the temperature. Therefore, the probability of absorbing a phonon, $\propto N$, is small compared to the probability of emitting a phonon, $\propto (1 + N)$, and the peak at $\Omega' - \Omega_0 = 0$ is much weaker than the $\Omega' - \Omega_0 = -180\,\text{cm}^{-1}$ peak. An additional peak at $\Omega' - \Omega_0 = 180\,\text{cm}^{-1}$ resulting from the absorption of two phonons, is too weak to be seen in the figure. As the temperature T decreases, the phonon population N decreases and the peak magnitudes decrease, since the probability of both phonon emission and absorption decreases. In the low temperature limit, $N \to 0$, the probability of phonon absorption vanishes, but the probability of phonon emission approaches a finite value. Therefore the peaks at $\Omega' - \Omega_0 = 0$ and $\Omega' - \Omega_0 = 180\,\text{cm}^{-1}$ vanish while the peak at $\Omega' - \Omega_0 = -180\,\text{cm}^{-1}$ remains finite at zero temperature. Similar

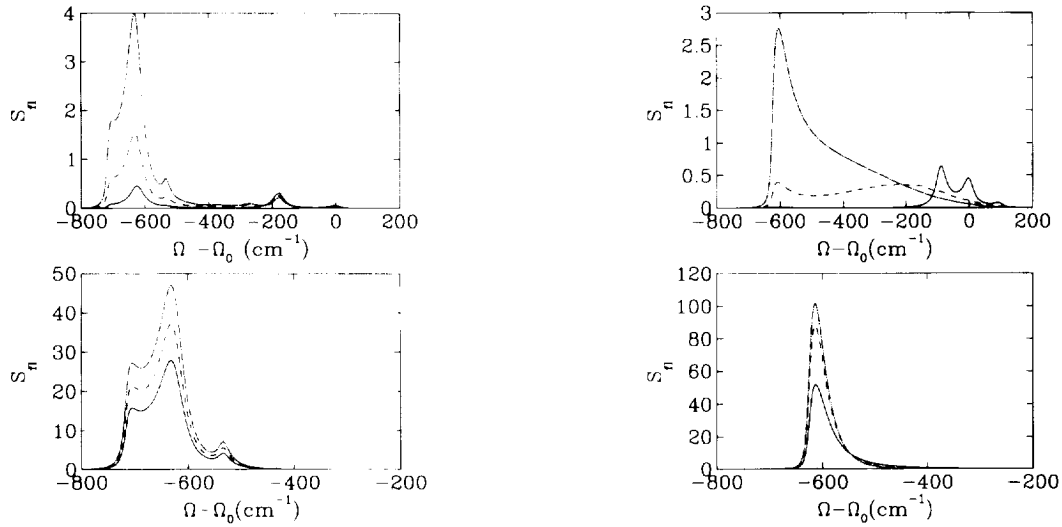

Fig. 12. Time-dependent fluorescence spectrum $S_{fl}(k' = 0, \Omega'; t)$ for a J-aggregate with optical phonon, and with incident frequency $\Omega = \Omega_0$. $V_{op} = 140\ \text{cm}^{-1}$, $V_{ac} = 0$, $T = 100$ K. Upper panel, $t = 0$, 0.265, 0.531 ps for solid, dashed, and dash-dotted curves. Lower panel, $t = 2.65$, 5.31, 159 ps for solid, dashed, and dash-dotted curves.

Fig. 13. The same as Fig. 12 but with acoustic phonons. $V_{ac} = 140\ \text{cm}^{-1}$, $V_{op} = 0$, $T = 100$ K. Upper panel $t = 0$, 0.265, 0.531 ps for solid, dashed, and dash-dotted curves. Lower panel, $t = 1.6$, 2.65, 5.31 ps for solid, dashed, dash-dotted curves.

arguments apply also to the contribution of acoustic phonons. Since acoustic phonon frequencies are low compared with optical phonons, their populations are relatively high, and acoustic phonon absorption processes are more important. This explains why in the lower panel, the two high-frequency peaks (involving phonon absorption) are relatively large compared to those in the upper panel.

The lowest frequency peak in Fig. 11 can be understood as follows. The exciton created by the incident light (through phonon emission) has a Lorentzian energy distribution centered at $\Omega - \Omega_{op}$ with width η. It has a tail at the bandedge, i.e., there is a small but finite exciton population with momentum $\boldsymbol{k}'$ at the lower bandedge. Although this population is small, this exciton can directly emit a photon with the projection of the wave vector in the lattice line $\boldsymbol{k}'$, and frequency $\varepsilon(0)$, without emitting or absorbing a phonon (since the momentum and the energy are conserved without the assistance of phonon scattering). The rate of direct photon emission is much larger than indirect photon emission, which is accompanied by phonon scattering. This is the origin of the peak at the lower bandedge. This can be easily seen from the expression of $S_{fl}(\boldsymbol{k}', \Omega', t)$, since the factor $|G(\Omega', \boldsymbol{k}')|^2 = \{[\Omega' - \varepsilon(0)]^2 + \Sigma^2(0)\}^{-1}$ produces the resonance at the bandedge with width $\Sigma(\boldsymbol{k} = 0)$ which is the phonon-induced dephasing rate of the lower bandedge exciton. This is the rate of phonon-assisted exciton scattering into a higher energy state. As the temperature decreases, the phonon population N (and thus the phonon absorption probability) decreases. Therefore, $\Sigma(\boldsymbol{k} = 0)$ decreases and the peak at the lower bandedge increases and becomes narrower.

In Figs. 12 and 13 we show the time resolved emission spectra. Let us consider first the contribution of optical phonons. In Fig. 12, the initial exciton population produces the peaks at

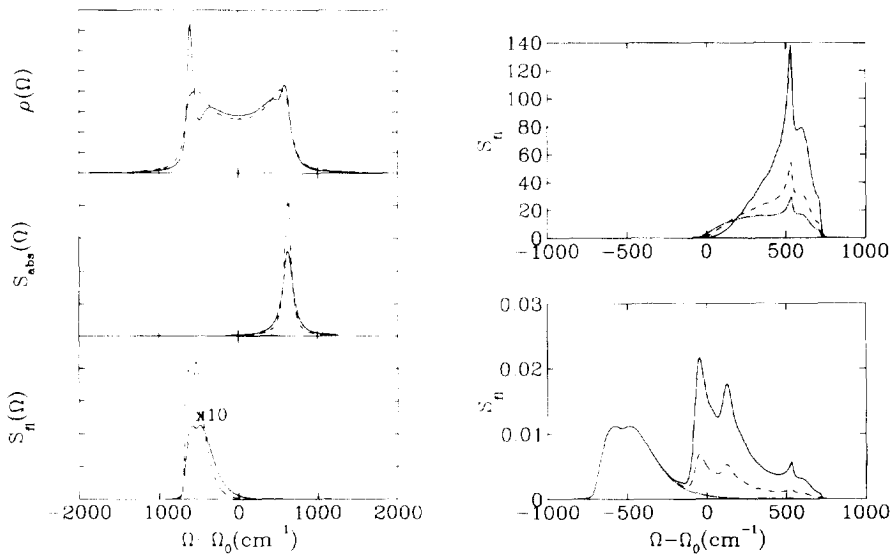

Fig. 14. Same as Figs. 9 and 10, except the nearest neighbor interaction change sign (H-aggregate), $J = 312.5\,\mathrm{cm}^{-1}$. Consequently, the absorption peak is at the upper bandedge. The solid line in the lowerest panel (long time fluorescence with only optical phonon contribution) has been amplified by 10 times.

Fig. 15. Time-dependent fluorescence spectrum $S_{\mathrm{fl}}(k' = 0, \Omega'; t)$ for H-aggregate with optical phonon, incident frequency at the upper bandedge $\Omega = \Omega_0 + 2J$. $T = 100$ K. Upper panel, $t = 0.53$, 1.06, 1.6 ps for solid, dashed, and dash-dotted curves. Lower panel, $t = 265$, 318, 531 ps for solid, dashed, and dash-dotted curves.

$\Omega' - \Omega_0 = -180\,\mathrm{cm}^{-1}$ and 0. As time evolves, the initial exciton population relaxes to lower energy states by exciton–phonon scattering. Therefore, as time evolves, the peaks at $-180\,\mathrm{cm}^{-1}$ and 0 decrease and the lower bandedge resonance increases. At long times ($t > 160$ ps), the exciton population reaches the equilibrium Boltzmann distribution and does not evolve any longer (see the lower panel), and the exciton population is accumulated at the lower bandedge. The exciton at the bandedge with momentum $\boldsymbol{k}'$ can emit a photon with frequency $\varepsilon(0)$ directly, and this results in the middle peak. Bandedge excitons with momenta close, but not equal to $\boldsymbol{k}'$ can emit photons by either emitting or absorbing a phonon, and this results in the left and right peaks in the lower panel respectively. For acoustic phonons (Fig. 13), the equilibrium distribution is obtained at $t = 5.3$ ps, which is much shorter than for optical phonons. This is because the acoustic phonon frequencies form a much broader band than optical phonons, which makes the exciton spectral diffusion faster. There is only one peak corresponding to direct emission of an exciton with momentum $\boldsymbol{k}'$. The left and right peaks in Fig. 12 disappear because acoustic phonon scattering vanishes when the initial and final exciton momenta are close, i.e., $V_{\mathrm{ac}}(\boldsymbol{k}, \boldsymbol{q}) \to 0$ for small q (see Eq. (8.1c)).

In the above numerical calculation, we used Eq. (8.1a) for $J < 0$. This is the J-aggregate model since the $\boldsymbol{k} = 0$ exciton state is at the lower bandedge. We now consider the H-aggregate ($J > 0$) model where the $\boldsymbol{k} = 0$ exciton state is at the upper bandedge. We took $4J = 1250\,\mathrm{cm}^{-1}$ in the numerical calculations. The density of states, linear absorption lineshape, and the long time fluorescence spectrum are displayed in Fig. 14. The time-dependent fluorescence spectrum $S_{\mathrm{fl}}(\Omega', \Omega, t)$, where Ω' is the emitted and Ω is the excitation frequency for the case of optical phonons is shown in Fig. 15. The excitation frequency is tuned to the upper bandedge $\Omega = \Omega_0 + 2J$ where

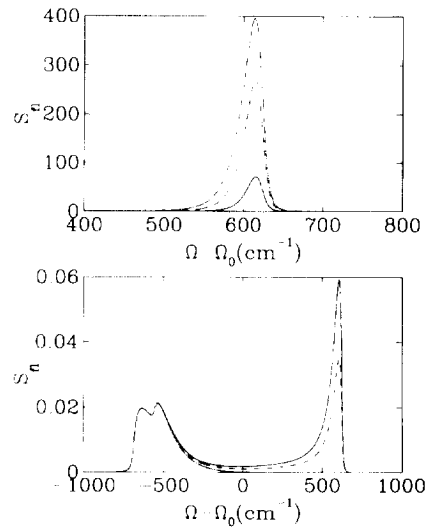

Fig. 16. The same as Fig. 15 but with acoustic phonons. $\Gamma_{ac} = 140\ \text{cm}^{-1}$, $V_{op} = 0$, $T = 100$ K. Upper panel, $t = 5.3, 26.5, 53$ fs for solid, dashed, and dash-dotted curves. Lower panel, $t = 8.5, 9, 15.9$ ps for solid, dashed, and dash-dotted curves.

the absorption is maximum. It creates an exciton with momentum $\boldsymbol{k}$ that is at the upper bandedge. For optical phonons, the signal shows up immediately following the excitation. Fig. 15 shows that at short times (upper panel), the signal is peaked at the upper bandedge. As time increases, the peak becomes broader and extends to lower frequencies. For $t > 531$ ps, the exciton population reaches thermal equilibrium and is accumulated at the lower bandedge (lower panel).

For acoustic phonons, there is no signal immediately after excitation, since the created exciton has momentum $\boldsymbol{k}$, which must be scattered to $\boldsymbol{k}'$, emitting a phonon. As stated earlier, this scattering probability is zero for the exciton-acoustic phonon coupling since both, $\boldsymbol{k}$ and $\boldsymbol{k}'$ are very close. At short times the signal is peaked at the upper bandedge and increases with time (Fig. 16 upper panel). Later, the peak decreases and broadens and extends to the lower energy side. At long times ($t > 15.9$ ps), the exciton population reaches thermal equilibrium and is accumulated at the lower bandedge (see lower panel). Again we see that the excitons equilibrate much faster through coupling to acoustic phonons than through optical phonons.

We shall now compare the time-resolved luminescence with pump probe spectroscopy [37] which is a time-domain four-wave mixing technique that is sensitive to exciton relaxation. In a pump probe experiment the system interacts with two pulses: the pump and the probe, and the signal is defined as the difference between the probe absorption with and without the pump. Since the signal is linear in the probe field and quadratic in the pump amplitude, and it can be viewed as a four-wave mixing process with pulses 1 and 2 identical and represent the pump, and pulse 3 is the probe: $\boldsymbol{k}_1 = \boldsymbol{k}_2 \equiv \boldsymbol{k}, \boldsymbol{k}_3 = \boldsymbol{k}_s \equiv \boldsymbol{k}'$; we will also introduce the notation $\Omega_1 = \Omega_2 \equiv \Omega, \Omega_3 \equiv \Omega'$. Since the nonlinear signal comes in the same direction as the linear signal induced by the probe, the latter acts as a heterodyne field. We assume that the probe is peaked with a time delay τ after the pump. The signal is given by

$$S_{pp}(\Omega', \Omega; \tau) = \text{Im} \int dt\, P(t) \mathcal{E}_3^*(t)\,. \tag{9.17a}$$

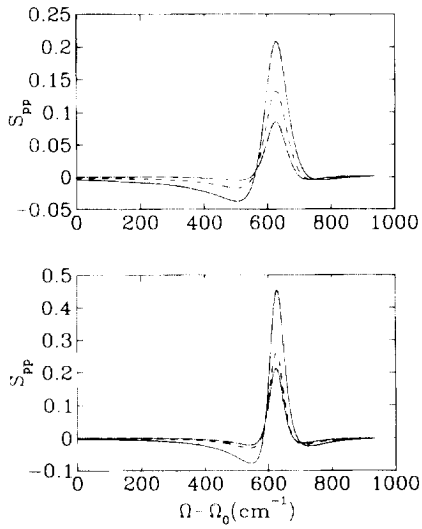

Fig. 17. Pump probe signal for an H-aggregate $S(\Omega', \Omega, \tau)$ as a function of probe frequency Ω' for various delay time τ. $\Omega = \Omega_0 + 2J$ is at the upper bandedge. Upper panel is the contribution of optical phonon. $V_{op} = 140\,cm^{-1}$, $V_{ac} = 0$, $t = 5.3$, 53, 265 ps for solid, dash, and dash-dot lines. The spectrum does not change for $t > 265$ ps. Lower panel is the contribution of acoustic phonon. $V_{ac} = 140\,cm^{-1}$, $V_{op} = 0$, $t = 2.65$, 5.3, 8.5 ps for solid, dash, and dash-dot lines. The spectrum does not change for $t > 8.5$ ps.

Expressing the polarization amplitude $P(t)$ in terms of the incoming fields using the optical response function we obtain

$$S_{pp}(\Omega', \Omega, \tau) \propto \int d\boldsymbol{p}\, d\boldsymbol{p}'\, \bar{\Gamma}[\Omega' + \varepsilon(\boldsymbol{p}), \boldsymbol{k}' + \boldsymbol{p}]\, \mathscr{Y}(\boldsymbol{p}, \boldsymbol{p}', \boldsymbol{q} = 0, \tau') \times g(\boldsymbol{p}', \boldsymbol{k}, \Omega)\, |G(\Omega, \boldsymbol{k})|^2 G^2(\Omega', \boldsymbol{k}') \,. \tag{9.17b}$$

$S_{pp}(\Omega', \Omega, \tau)$ is similar to the time-dependent fluorescence spectrum except for changing the window function $g_s(\boldsymbol{k}', \boldsymbol{p}, \Omega')$ to $\bar{\Gamma}[\Omega' + \varepsilon(\boldsymbol{p}), \boldsymbol{k}' + \boldsymbol{p}]$ and replacing $|G(\Omega', \boldsymbol{k}')|^2$ by $G^2(\Omega', \boldsymbol{k}')$. The pump-pulse creates an exciton wave packet which evolves during the time period τ. The second pulse creates a virtual exciton which is scattered by the first exciton and then emits a photon. The new window function is related to the scattering strength of the first and the second excitons. In pump-probe spectroscopy the pump pulse creates an exciton population which affects the probe absorption. The absorption spectrum dependence on the time delay τ reflects the population relaxation of excitons.

Calculations of $S_{pp}(\Omega', \Omega, \tau)$ for an H-aggregate with Ω tuned to the upper bandedge as a function of probe frequency Ω' for various delay times τ are displayed in Fig. 17.

We shall now compare time- and frequency-resolved luminescence with the pump-probe spectrum. The expressions for both signals contain $\mathscr{Y}$, which is related to the exciton population relaxation. However, $\mathscr{Y}$ is convoluted with $\bar{\Gamma}$ (describing exciton–exciton scattering) in the pump-probe spectrum, and with g_s (describing the probability of emission of a photon) in the luminescence spectrum. Physically this means that both experiments probe the exciton population relaxation but in a different manner: looking for exciton annihilation with photon creation in

the case of the luminescence, and for the scattering of an exciton on a virtual exciton created by the probe pulse in the case of the pump-probe measurement. The upper panel of Fig. 17 shows that the pump-probe spectrum does not change for $t > 265$ ps, while Fig. 15 shows that the time dependent fluorescence spectrum continues to evolve up to $t > 530$ ps. During the time $265 < t < 530$ ps, the exciton population distribution continues to change, which is manifested in the time-dependent fluorescence, but not in the pump probe spectrum. The same is true for acoustic phonons (compare the lower panel of Fig. 17 with Fig. 16). This is because the window function of the time-dependent fluorescence, $g_s(\boldsymbol{k}', \boldsymbol{p}, \Omega')$, is strongly peaked at Ω' which is close to the exciton energy $\varepsilon(\boldsymbol{p})$ (but differs by a phonon frequency); this is not the case for $\bar{\Gamma}(\Omega' + \varepsilon(\boldsymbol{p}), \boldsymbol{k}' + \boldsymbol{p}]$, the window function of pump probe. Therefore, unlike the pump probe signal, the fluorescence frequency reflects the exciton energy distribution.

10. Combined phonon and static disorder effects on the optical response

In the previous sections we have studied the third-order nonlinear optical response of molecular nanostructures with additional static or dynamical degrees of freedom. The response function has four contributions $R^{(i)}$, $i = a, b, c, d$. $R^{(a)}$ is nonzero without additional degrees of freedom. Disorder (static or dynamical) leads to a minor renormalization of $R^{(a)}$. The situation with $R^{(b)}$ and $R^{(c)}$ is different: these contributions are disorder-induced. $R^{(b)}$ is finite for both static and dynamical disorder, and $R^{(c)}$ is nonzero for static disorder only. $R^{(b)}$ was obtained in the LFA′ (which is justified when ω_3 is off-resonant) for some models of exciton-phonon interaction [5]. The same contribution but for static disorder has been obtained in [56]. Our expressions generalize these results to the case of resonant values of ω_3. $R^{(d)}$ is not considered here.

In this section we consider the situation when we have both static disorder and exciton–phonon interactions. The excitons now undergo two scattering mechanisms: elastic scattering induced by disorder and inelastic scattering by phonons. We denote the corresponding dephasing rates Γ_e and Γ_i respectively. When $\Gamma_e \ll \Gamma_i$, disorder makes minor corrections to the scattering amplitudes and to exciton transport, and the nonlinear response can be described using the results of Section 7. Even when the two dephasing rates are comparable, the results do not change qualitatively, and can be obtained from the results of Section 7 by simply adding elastic scattering contributions to the scattering amplitudes (the functions f, g, g_s and g_d).

A more dramatic effect on exciton transport is when $\Gamma_e \gg \Gamma_i$. Under these circumstances we have two distinct frequency (or time) scales related to elastic and inelastic processes. For times much shorter than $1/\Gamma_i$ (i.e., short-time behavior) we can neglect the inelastic processes altogether, and the nonlinear response is given by the expressions of Section 4. For longer times, of the order of $1/\Gamma_i$, inelastic scattering becomes important; however, exciton transport can no longer be described in the framework of Section 7, since it is strongly affected by elastic scattering. The only range of parameters not explored so far is when the frequencies are much smaller than the elastic scattering rate. This will be discussed below. We adopt a model that includes both the exciton–phonon interaction given by Eq. (7.1) and static disorder described by Eq. (4.5). The one-exciton Green function contains the self-energy $\Sigma_t(\boldsymbol{k}, \omega)$:

$$\Sigma_t(\boldsymbol{k}, \omega) \equiv \Sigma(\omega) + \Sigma_{ph}(\boldsymbol{k}, \omega) . \tag{10.1}$$

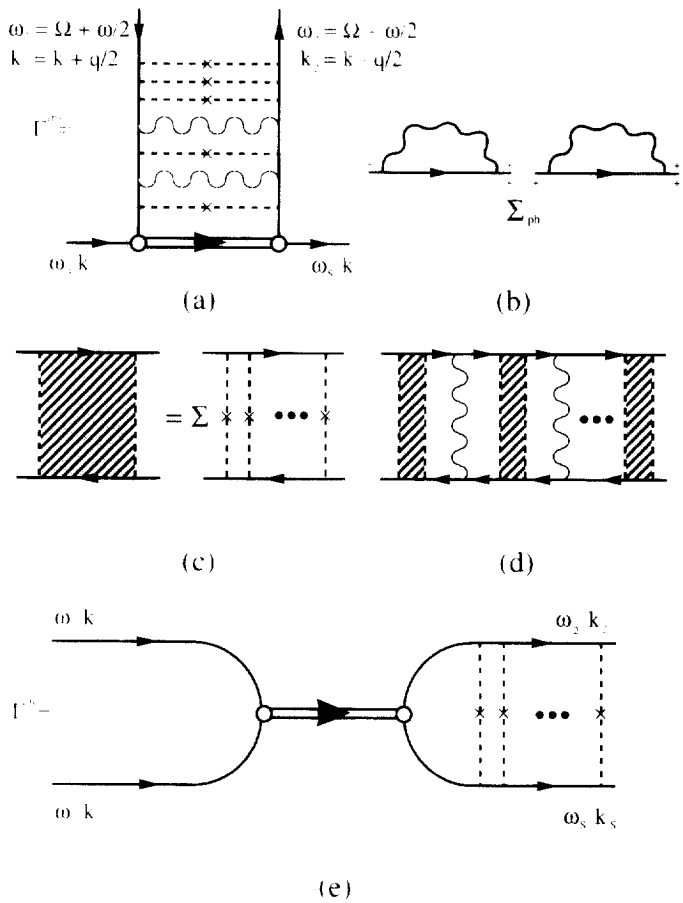

Fig. 18. (a) The diagrams contributing to $\bar{\Gamma}^{(b)}$. (b) Diagrams for the phonon-induced self-energy Σ_{ph}. (c) Summation over disorder (dashed lines). (d) Summation over the phonon (wavy) lines. (e) Diagrams contributing to $\bar{\Gamma}^{(c)}$.

where $\Sigma(\omega)$ is the elastic self-energy (see Eq. (4.12)), and Σ_{ph} is the correction due to the exciton–phonon interaction. This contribution is given by the diagrams shown in Fig. 18b (note that the exciton Green function in these diagrams contains the self-energy $\Sigma(\omega)$, this corresponds to a disordered system without exciton–phonon interaction). In the present case we can neglect $\Sigma_{ph}(\boldsymbol{k}, \omega)$ in Eq. (10.1) if we are interested in the linear response, which is therefore given by Eqs. (4.11) and (4.12). The nonlinear response has the form of Eqs. (7.3a) and (4.14a), and we will concentrate on the calculation of $\bar{\Gamma}^{(b)}$ and $\bar{\Gamma}^{(c)}$.

$\bar{\Gamma}^{(b)}$ is given by the diagrams shown in Fig. 18a. The exciton Green functions in Fig. 18a contain the total self-energy $\Sigma_t(\boldsymbol{k}, \omega)$. Details of the calculations are presented in Appendix F; here we only outline them schematically. We first perform the summation over ladder diagrams containing disorder lines only (see Fig. 18c), and then perform the sum over ladder diagrams with all possible numbers of phonon lines (see Fig. 18d). This summation is equivalent to inverting a linear operator.

$\bar{\Gamma}^{(b)}$ is given by

$$\bar{\Gamma}^{(b)}(-\omega_s - \boldsymbol{k}_s, \omega_1 \boldsymbol{k}_1, -\omega_2 - \boldsymbol{k}_2, \omega_3 \boldsymbol{k}_3)$$
$$= \rho(\tfrac{1}{2}(\omega_1 + \omega_2))\sigma^4 \int \frac{d\Omega'}{2\pi} \rho(\Omega')\, d\boldsymbol{p}\, \mathscr{D}(\Omega', \tfrac{1}{2}(\omega_1 + \omega_2); \boldsymbol{q}\omega) |G(\Omega', \boldsymbol{p})|^2 \bar{\Gamma}(\omega_3 + \Omega', \boldsymbol{p} + \boldsymbol{k}_3) . \tag{10.2}$$

In Eq. (10.2) $\omega = \omega_1 - \omega_2$, $\boldsymbol{q} \equiv \boldsymbol{k}_1 - \boldsymbol{k}_2$, $\rho(\Omega)$ is the density of states in the disordered system:

$$\rho(\Omega) = -2 \operatorname{Im} \int d\boldsymbol{p}\, G(\Omega, \boldsymbol{p}) , \tag{10.3}$$

and $\mathscr{D}$ is the Green function of the spectral transport equation defined as a matrix element

$$\mathscr{D}(\Omega, \Omega'; \boldsymbol{q}\omega) \equiv \langle \Omega | (-i\omega + L(\boldsymbol{q}))^{-1} | \Omega' \rangle . \tag{10.4a}$$

Here $|\Omega\rangle$ denotes a "state" (vector) in the space of functions $n(\varepsilon)$ depending on energy which has the form $n(\varepsilon) = 2\pi\delta(\varepsilon - \Omega)$ (see also the comment following Eq. (D.6) in Appendix D). The "state" $|\Omega\rangle$ can be also expressed in terms of the "states" $|\boldsymbol{p}\rangle$ introduced in Appendix D: $|\Omega\rangle = 2\pi \int d\boldsymbol{p}\, \delta(\Omega - \varepsilon(\boldsymbol{p}))|\boldsymbol{p}\rangle$.

The operator L acts on the space of functions of energy $n(\varepsilon)$, and has the form

$$L = L_0 + L_1 + L_2 , \tag{10.4b}$$

with

$$(L_0 n)(\varepsilon) \equiv -\int \frac{d\varepsilon'}{2\pi} \rho(\varepsilon') [F(\varepsilon, \varepsilon') n(\varepsilon') - F(\varepsilon', \varepsilon) n(\varepsilon)] , \tag{10.4c}$$

$$(L_1 n)(\varepsilon) = \Gamma_0(\varepsilon) n(\varepsilon) , \tag{10.4d}$$

$$(L_2 n)(\varepsilon) = \boldsymbol{q}^2 D(\varepsilon) n(\varepsilon) . \tag{10.4e}$$

The function F is given by

$$F(\varepsilon, \varepsilon') = 2\pi\sigma^4 \int d\boldsymbol{k}\, d\boldsymbol{k}' |G(\varepsilon, \boldsymbol{k})|^2 |G(\varepsilon', \boldsymbol{k}')|^2$$
$$\times \{ |V(\boldsymbol{k}', \boldsymbol{k}' - \boldsymbol{k})|^2 (1 + N(\varepsilon' - \varepsilon)) \delta(\varepsilon - \varepsilon' + \Omega(\boldsymbol{k}' - \boldsymbol{k})) + |V(\boldsymbol{k}, \boldsymbol{k} - \boldsymbol{k}')|^2$$
$$\times N(\varepsilon - \varepsilon') \delta(\varepsilon - \varepsilon' - \Omega(\boldsymbol{k} - \boldsymbol{k}')) \} , \tag{10.5}$$

where N are the boson occupation numbers and $\Omega(\boldsymbol{k})$ is the phonon spectrum (see Appendix E).

$\bar{\Gamma}^{(c)}$ is given by the diagrams shown in Fig. 18e. The resonant contributions do not contain the phonon lines; and, therefore, $\bar{\Gamma}^{(c)}$ is given by Eq. (4.14d) with the only difference that we should add the imaginary part of the phonon self-energy to the damping; physically this implies that inelastic scattering destroys the phase memory and, therefore, provides a damping mechanism

$$\bar{\Gamma}^{(c)}(-\omega_s - \boldsymbol{k}_s, \omega_1 \boldsymbol{k}_1, -\omega_2 - \boldsymbol{k}_2, \omega_3 \boldsymbol{k}_3)$$
$$= \frac{|2 \operatorname{Im} \Sigma(\omega_2)| i}{\omega_1 + \omega_3 - 2\omega_2 + i\Gamma_0(\omega_2) + i\Gamma_{ph}(\omega_2) + i(\boldsymbol{k}_1 + \boldsymbol{k}_3)^2 D(\omega_2)}$$
$$\times \bar{\Gamma}(\omega_1 + \omega_3, \boldsymbol{k}_1 + \boldsymbol{k}_3) , \tag{10.6a}$$

where $\Gamma_{ph}(\omega)$ has the form

$$\Gamma_{ph}(\omega) = \int \frac{d\varepsilon}{2\pi} \rho(\varepsilon) F(\varepsilon, \omega) \tag{10.6b}$$

The nonlinear response function $R(-\omega_s - \boldsymbol{k}_s; \omega_1 \boldsymbol{k}_1, -\omega_2 - \boldsymbol{k}_2, \omega_3 \boldsymbol{k}_3)$ is given by Eqs. (4.8a) and (4.14a) with the one-exciton Green function $G(\omega, \boldsymbol{k})$ (Eq. (4.12a)) and $\bar{\Gamma}^{(i)}(\omega_s \boldsymbol{k}_s, \omega_1 \boldsymbol{k}_1, -\omega_2 - \boldsymbol{k}_2, \omega_3 \boldsymbol{k}_3)$ given by Eqs. (4.14b), (10.2) and (10.6a), with $\bar{\Gamma}(\omega, \boldsymbol{k})$ given by Eq. (4.14e). From Eq. (10.6) we see that the width of the resonance of $\bar{\Gamma}^{(c)}$ is given by the sum of the inverse lifetime and inelastic exciton scattering rate. The situation with the resonances of $\bar{\Gamma}^{(b)}$ is different, however, and their widths are determined by the decay rate. To see this we derive an asymptotic form of Eq. (10.2) for $\omega = \omega_1 - \omega_2$ and $D\boldsymbol{q}^2$ much smaller than the inelastic dephasing rate (in the opposite limit, the result is simply given by Eq. (4.14c)). Expanding the operator L_0 using its eigenmodes, taking into account only the zero mode, we obtain in the resonance approximation

$$\begin{aligned}
&\bar{\Gamma}^{(b)}(\omega_s \boldsymbol{k}_s, \omega_1 \boldsymbol{k}_1, -\omega_2 - \boldsymbol{k}_2, \omega_3 \boldsymbol{k}_3) \\
&\quad = \frac{\sigma^4 C_0 \rho(\Omega) i}{\omega_1 - \omega_2 + i\Gamma_0 + i(\boldsymbol{k}_1 - \boldsymbol{k}_2)^2 D_0} \int d\boldsymbol{p} \frac{d\Omega'}{2\pi} \rho(\Omega') |G(\boldsymbol{p}, \Omega')|^2 \exp[-\Omega'/kT] \\
&\qquad \times \bar{\Gamma}(\Omega' + \omega_3, \boldsymbol{p} + \boldsymbol{k}_3) .
\end{aligned} \tag{10.7a}$$

with

$$\Gamma_0 \equiv C_0 \int \frac{d\omega}{2\pi} \rho(\omega) \exp[-\omega/kT] \Gamma_0(\omega) , \tag{10.7b}$$

$$D_0 \equiv C_0 \int \frac{d\omega}{2\pi} \rho(\omega) \exp[-\omega/kT] D(\omega) . \tag{10.7c}$$

and

$$C_0 \equiv \left\{ \int \frac{d\omega}{2\pi} \rho(\omega) \exp[-\omega/kT] \right\}^{-1} . \tag{10.7d}$$

From Eq. (10.7) we see that the width Γ_0 of this resonance is proportional to the decay rate.

The luminescence signal is given by Eqs. (9.12) and (9.14a), where the one-exciton Green function $G(\omega, \boldsymbol{k})$ is given by Eq. (4.12) and $\Gamma_s(\omega_0 \boldsymbol{k}_0, \omega_s \boldsymbol{k}_s; \omega)$ can be expressed as a sum of two contributions, corresponding to transport and weak localization (the diagrams contributing to $\bar{\Gamma}_s$ are presented in Fig. 19):

$$\bar{\Gamma}_s = \bar{\Gamma}_s^{(b)} + \bar{\Gamma}_s^{(c)} . \tag{10.8a}$$

where

$$\bar{\Gamma}_s^{(b)}(\omega_0 \boldsymbol{k}_0, \omega_s \boldsymbol{k}_s; \omega) = \sigma^4 \rho(\omega_s) \mathcal{I}(\omega_s, \omega_0; \omega) , \tag{10.8b}$$

$$\Gamma_s^{(c)}(\omega_0 \boldsymbol{k}_0, \omega_s \boldsymbol{k}_s; \omega) = \frac{2\sigma^2 |\operatorname{Im} \Sigma(\omega_0)| i}{\omega + i\Gamma_0(\omega_0) + i\Gamma_{ph}(\omega_0) + i(\boldsymbol{k}_0 + \boldsymbol{k}_s)^2 D(\omega_0)} 2\pi\delta(\omega_s - \omega_0) . \tag{10.8c}$$

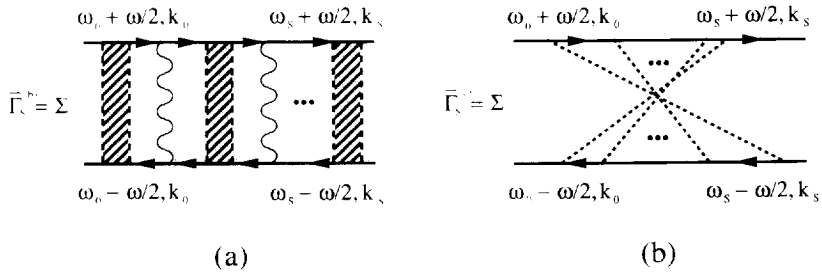

Fig. 19. Diagrams contributing to the incoherent luminescence signal in the presence of phonons and disorder. (a) $\bar{\Gamma}_s^{(b)}$ contribution of transport. (b) $\bar{\Gamma}_s^{(c)}$ contribution of weak localization.

For ω much smaller than the inelastic dephasing rate, we can represent $\Gamma_s^{(b)}$ in a similar form (the contribution $\bar{\Gamma}_s^{(c)}$ is much smaller in this region):

$$\bar{\Gamma}_s = \bar{\Gamma}_s^{(b)} = \frac{\sigma^+ \rho(\omega_s) C_0 i}{\omega + i\Gamma_0} \exp(-\omega_s/kT) . \tag{10.8d}$$

We shall now summarize the results obtained in this section. The first important observation is that exciton population-relaxation which affects the nonlinear response and the luminescence takes place in the energy space. This means that the transport is described by the Green function $\mathscr{D}(\Omega, \Omega'; \omega)$ of a transport equation for $n(\Omega)$ which is the total exciton population at energy Ω. Physically, due to elastic scattering, the exciton distribution becomes uniform among the states of a given energy on a very short timescale. However, elastic scattering cannot change the exciton energy, the only way for an exciton to change its energy is to scatter on a phonon, and these processes are much slower. In other words, fast elastic scattering makes sure that the exciton distribution depends on the exciton energy alone, and the exciton–phonon scattering is responsible for slower transport processes in energy space. Note that in this case the equation for the Green function $\mathscr{G}^{(2)}$ is reduced to an equation for the function $\mathscr{D}$. The only requirement for obtaining a rather simple equation for the function $\mathscr{D}$ is for elastic processes to be much faster than inelastic scattering.

Another important point is that the widths of the $\omega_1 = \omega_2$ and the $\omega_1 + \omega_3 = 2\omega_2$ resonances in the nonlinear response, which were of the same magnitude for disordered aggregates become quite different when inelastic scattering is incorporated. The width of the $\omega_1 = \omega_2$ resonance is determined by processes which change the number of excitons. Consequently, it has only lifetime broadening and exciton–phonon scattering which conserves the number of excitons does not contribute to the width. The $\omega_1 + \omega_3 = 2\omega_2$ resonance reflects the phase memory of excitons which is lost if the exciton energy is changed. Therefore, finite lifetime as well as inelastic scattering contribute to its width. In the case of luminescence, in addition to the contribution of Eq. (10.8b) which is related to exciton diffusion, we have a contribution of Eq. (10.8c) which is resonant at $\boldsymbol{k}_s = -\boldsymbol{k}_0$, and is, therefore, related to the backscattering peak [23, 68], which is due to the long exciton phase memory. Since phase memory is lost in inelastic processes, the backscattering peak must have the same frequency of the incident light and the inelastic dephasing rate in addition to finite lifetime contributes to the resonance width.

11. Collective versus simple resonances in the nonlinear optical response; the sum over states representation

In the previous sections we analyzed the third-order nonlinear optical response of molecular nanostructures $R(-\omega_s - \boldsymbol{k}_s, \omega_1\boldsymbol{k}_1, -\omega_2 - \boldsymbol{k}_2, \omega_3\boldsymbol{k}_3)$ in the presence of dynamical (phonon) or static (disorder) dephasing mechanisms. We have studied the resonances at $\omega_1 \approx \omega_2$ and $\omega_1 + \omega_3 \approx 2\omega_2$. The width of the former resonance reflects exciton lifetime. The latter resonance exists only if the inelastic dephasing rate is much slower than the elastic rate, and its width is determined by the sum of the inverse lifetime and the elastic scattering rates.

In this section we analyze the origin of these resonances, and discuss some general properties of the optical response using the standard expressions for the susceptibilities in terms of the eigenstates of the material system. The nonlinear response functions can be expanded either using the global eigenstates of the system containing all degrees of freedom, or using the eigenstates of a reduced system containing the electronic degrees of freedom alone. For the first description one can either start with the time-dependent Schrodinger equation for the wave function or with the Liouville equation for the density matrix. Both formulations give exact expressions for the response functions. However, these expressions contain a large number of terms, and there is no simple correspondence between individual terms obtained using both approaches. If we adopt a reduced description, we must use the density matrix expression, since a "reduced wave function" is not a useful concept. Other degrees of freedom show up in the reduced description in the form a relaxation superoperator in the equations of motion for the reduced density matrix. The main advantage of the reduced description is the simplicity of the equations of motion for the reduced density matrix, since they contain relatively few variables. A limitation of this approach is that one can close the equations of motion for a reduced density matrix only by invoking certain approximations. The reduced description is advantageous when the number of reduced degrees of freedom is finite and small. For some applications for many-body systems it may, therefore, be more appropriate to start with the first approach, which is based on the global eigenstates of the system.

Let E_i be the eigenvalues of the Hamiltonian of the entire system and μ_{ij} the matrix elements of the polarization operator. For clarity we assume that the system size is small compared with the optical wavelength, and set all wave vectors $\boldsymbol{k}_j = 0$. The wave function expression for the third-order nonlinear optical response function is [37]

$$
\begin{aligned}
R(-\omega_s;\omega_1, -\omega_2, \omega_3) = \sum_{\text{perm}} \sum_{abcd} \mu_{ac}\mu_{cd}\mu_{db}\mu_{ba}\rho_{aa} \\
\times \left\{ \frac{1}{(\omega_1 - (E_b - E_a) + i\eta} \frac{1}{\omega_1 + \omega_3 - (E_d - E_a) + i\eta} \right. \\
\times \frac{1}{\omega_s - (E_c - E_a) + i\eta} + \frac{1}{\omega_1 - (E_b - E_a) + i\eta} \\
\left. \times \frac{1}{\omega_1 + \omega_3 - (E_d - E_a) + i\eta} \frac{1}{\omega_2 - (E_c - E_a) - i\eta} \right\} + \text{c'.c'.} \quad (11.1)
\end{aligned}
$$

where $\omega_s = \omega_1 - \omega_2 + \omega_3$, η is a small positive parameter which is sent to zero at the end of the calculation, and ρ_{aa} are the matrix elements of the equilibrium density matrix, and $\sum_{\text{perm}}$ denotes the sum over six permutations of the frequencies ω_1, $-\omega_2$ and ω_3.

The response function R has many resonances related to the vanishing of the denominators in the r.h.s. of Eq. (11.1), when certain combinations of frequencies coincide with a specific molecular transition energy. These are the only possible resonances in a small system, and will be denoted "simple resonances". However, systems with a very large number of degrees of freedom can show resonances of a very different origin; the infinite sum in the r.h.s. of Eq. (11.1) can diverge for certain combinations of the frequencies ω_1, ω_2 and ω_3. We will denote resonances of this type, which cannot be attributed to a specific pair of levels as collective. The resonances at $\omega_1 = \omega_2$ and $\omega_1 + \omega_3 = 2\omega_2$ discussed in previous sections are clear examples of collective resonances. They can be obtained starting with Eq. (11.1) by taking into account specific diverging terms in the sum. Unlike the simple resonances, these collective resonances can be most adequately treated using the many-body Green function procedure, and the many-body nature of the problem is essential for predicting and understanding these resonances. This is in contrast to the simple resonances which can be adequately understood by inspection of the sum over state expression. This is why we focused our previous analysis on these unusual resonances.

To reproduce the collective $\omega_1 = \omega_2$ resonance we start with the second term in the r.h.s. of Eq. (11.1) and set $b = c$ in the sum:

$$R^{(b)}(-\omega_s; \omega_1, -\omega_2, \omega_3) = \sum_{abd} |\mu_{ab}|^2 |\mu_{bd}|^2 \rho_{aa} \frac{1}{\omega_1 + \omega_3 - (E_d - E_a) + i\eta} \frac{1}{\omega_1 - (E_b - E_a) + i\eta} \times \frac{1}{\omega_2 - (E_b - E_a) - i\eta} . \tag{11.2}$$

When $\omega_1 \approx \omega_2$, Eq. (11.2) contains two close poles in different complex half planes (the last two factors). To see how this leads to the collective resonance, we represent Eq. (11.2) in the form

$$R^{(b)}(-\omega_s; \omega_1, -\omega_2, \omega_3) = \int \frac{d\varepsilon}{2\pi} \mathcal{J}(\varepsilon, \omega_1 + \omega_3) \frac{1}{\omega_1 - \varepsilon + i\eta} \frac{1}{\omega_2 - \varepsilon - i\eta} , \tag{11.3a}$$

where

$$\mathcal{J}(\varepsilon, \varepsilon') \equiv \sum_{abd} 2\pi\delta(\varepsilon - E_b + E_a) |\mu_{ab}|^2 |\mu_{bd}|^2 \rho_{aa} \frac{1}{\varepsilon' - (E_d - E_a) + i\eta} . \tag{11.3b}$$

The large contribution to the integral in Eq. (11.3a) for $\omega_1 \approx \omega_2$ is from the region $\varepsilon \approx \omega_1 \approx \omega_2$. Putting $\mathcal{J}(\varepsilon, \omega_1 + \omega_3) \approx \mathcal{J}(\omega_1, \omega_1 + \omega_3)$ in this region we obtain the following resonant contribution to the response function

$$R(-\omega_s; \omega_1, -\omega_2, \omega_3) \approx (i\mathcal{J}(\omega_1, \omega_1 + \omega_3))/[\omega_1 - \omega_2 + i\eta] . \tag{11.4}$$

All we need to generate this resonance is a continuous distribution of energy levels in the vicinity of $\varepsilon \approx \omega_1 \approx \omega_2$, regardless of the origin of this distribution: be it dynamical or static. In both cases we obtain a sharp resonance since the only broadening mechanism is due to lifetime; pure dephasing and the broad distribution of energy levels does not affect the line width.

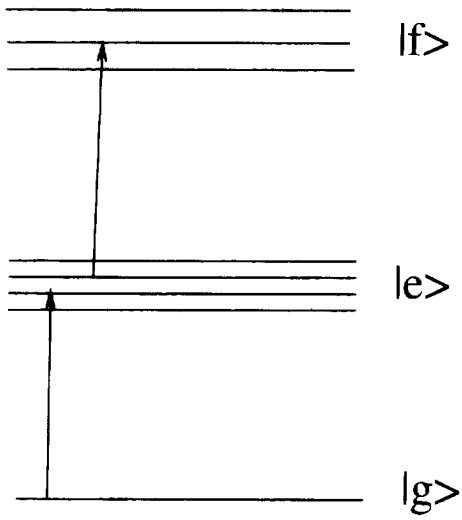

Fig. 20. Level scheme of a system showing resonances in the nonlinear response at $\omega_1 + \omega_3 = 2\omega_2$; the ground state $|g\rangle$, the group of levels $|e\rangle$, the group of levels $|f\rangle$. The matrix elements of the polarization are nonzero between successive levels only.

The collective four photon resonance at $2\omega_2 = \omega_1 + \omega_3$ is less universal and requires a specific material level structure. Consider the following three level scheme (Fig. 20): a ground level g, and two groups of levels denoted e and f. We assume that the polarization operator has nonzero matrix elements only between successive levels μ_{ge} and μ_{ef}. For molecular aggregates g is the ground state, e represents one-exciton states, and f stands for two-exciton states. We will assume that for each pair of e-levels b and b' there is a f-level d with energy (this is justified for molecular aggregates)

$$E_d \approx E_b + E_{b'} \tag{11.5a}$$

In particular when $b = b'$ we will denote this level $d(b)$:

$$E_{d(b)} \approx 2E_b \tag{11.5b}$$

Note that the difference $E_{d(b)} - 2E_b$ tends to zero when the number of molecules in the aggregate is increased, since exciton interactions are weaker and they behave more as bosons.

Taking the second term in the r.h.s. of Eq. (11.1) into account, substituting $d = d(c)$ in the sum, and permuting ω_1 and ω_3, we obtain the following sum of resonant terms:

$$R^{(c)}(-\omega_s; \omega_1, -\omega_2, \omega_3) = \sum_{b \neq c} \mu_{gc}\mu_{cd(c)}\mu_{d(c)b}\mu_{bg} \frac{1}{\omega_1 - E_b + i\eta} \frac{1}{\omega_3 - E_b + i\eta}$$

$$\times \frac{\omega_1 + \omega_3 - 2E_b}{(\omega_1 + \omega_3 - 2E_c + i\eta)(\omega_2 - E_c - i\eta)}. \tag{11.6}$$

We have further assumed that the temperature is much lower than the exciton frequency, setting $a = g$ and $\rho_{gg} = 1$. The collective resonance is in this case due to poles in the denominator of the last factors in the r.h.s. of Eq. (11.6), which are close when $\omega_1 + \omega_3 \approx 2\omega_2$. We put $b \neq c$ in the sum since for $b = c$, one of the poles in the denominator is cancelled by the numerator. We also assume that ω_1 and ω_3 are off-resonant (i.e., outside the e-band), whereas $\omega_1 + \omega_3$ is inside the f-band.

Proceeding in the same manner as in the derivation of Eq. (11.4), we obtain the resonant expressions for R in the vicinity of $\omega_1 + \omega_3 \approx 2\omega_2$:

$$R(-\omega_s; \omega_1, -\omega_2, \omega_3) \approx \frac{ig(\omega_1, \omega_3; \omega_2)}{\omega_1 + \omega_3 - 2\omega_2 + i\eta}, \tag{11.7a}$$

with

$$g(\omega_1, \omega_3; \varepsilon) \equiv \sum_{b \neq c} \mu_{gc}\mu_{cd(c)}\mu_{d(c)b}\mu_{bg} 2\pi\delta(\varepsilon - E_c) \frac{2(\varepsilon - E_b)}{(\omega_1 - E_b + i\eta)(\omega_3 - E_b + i\eta)}. \tag{11.7b}$$

This resonance is induced in assemblies of two-level systems only due to the combined influence of disorder and aggregation. In the absence of disorder we do not have a continuous distribution of energies of e-levels interacting with the field. For noninteracting two-level systems with disorder (inhomogeneous broadening), the e-levels are localized on individual molecules and the f-states with energy $E_d = 2E_b$ do not contribute to the third-order response.

When dynamical disorder due to phonons is incorporated, Eq. (11.5b) no longer holds, since the exciton states mix with phonons. This implies that the resonance width is determined by the inelastic dephasing rate, and the resonance exists only provided the elastic dephasing rate connected with static disorder is larger than the inelastic dephasing rate due to dynamical disorder. This result for molecular aggregates was obtained in Section 10. To illustrate this point we introduce a simple four-level model with inhomogeneous broadening. The four-levels are denoted g, e, e' and f with the energies $E_g = 0$, $E_e = \Omega$, $E_{e'} = \Omega_0$, $E_f = \Omega + \Omega'$. We denote the distribution of Ω and Ω' by $n(\Omega, \Omega')$, which has the form

$$n(\Omega, \Omega') = n_0(\Omega) n_c(\Omega - \Omega'), \quad n_c(\omega) \equiv \frac{\delta}{\omega^2 + \delta^2}, \tag{11.8a,b}$$

and the width of the $n_0(\omega)$ distribution is much larger than δ. $n_c(\omega)$ describes the correlation between the e and f energy levels. For $\delta = 0$ we have $E_f = 2E_e$, so that for small δ, condition (11.5b) holds. Applying Eq. (11.6) to this four-level model and integrating over Ω and Ω' with the weight function $n(\Omega, \Omega')$ given by Eq. (11.8), we obtain the following resonant expression for the nonlinear response function:

$$R(\omega_s; \omega_1, -\omega_2, \omega_3) = i\mu_{ge}\mu_{ef}\mu_{fe'}\mu_{e'g} \frac{2(\omega_2 - \Omega_0)n_0(\omega_2)}{(\omega_1 - \Omega_0)(\omega_3 - \omega_0)} \frac{1}{\omega_1 + \omega_3 - 2\omega_2 + i\delta}. \tag{11.9}$$

The correlation width of the energies of the e- and f-levels is determined by the homogeneous broadening which controls the resonance width in Eq. (11.9).

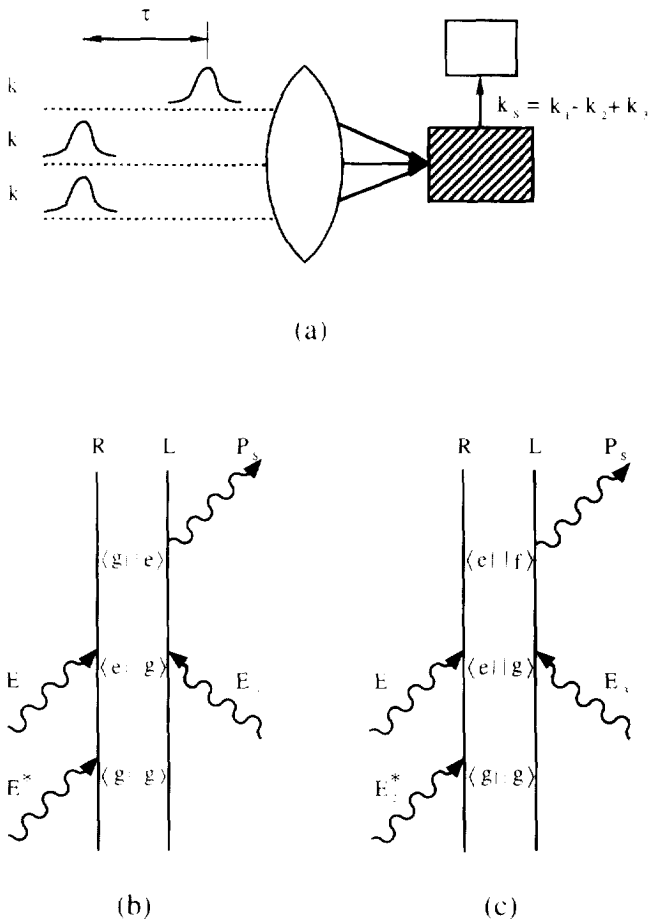

Fig. 21. Pathways in the Liouville space of the system density matrix contributing to different types of photon echoes. (a) Pulse-configuration. For ordinary echo the pulses 1 and 3 are the same. (b) Ordinary echo. (c) Two-exciton echo.

It has been shown in Section 4 that the resonance (Eq. (11.9)) leads to a two-exciton photon echo in time-domain spectroscopy. In this section we have shown that the resonance in Eq. (11.9) is a consequence of a certain correlation between one- and two-exciton states. At this point we show directly using time-domain arguments how this level-correlation leads to the two-exciton echo (these arguments explain the term "two-exciton" echo).

In a usual echo setup [43] one comes first with a short resonant pulse with frequency and wave vector $\omega_2, \boldsymbol{k}_2$ and time $t = -\tau_1$, and after a time delay τ_1 with a short resonant pulse with the same frequency and wave vector $\boldsymbol{k}_1$ and $t = 0$, the signal is measured in the direction $2\boldsymbol{k}_1 - \boldsymbol{k}_2$ at time $t = \tau_2$ (see Fig. 21a). The photon echo signal is described by the following pathway in the Liouville space, shown in Fig. 21b: starting with the density matrix $|g\rangle\langle g|$, after interaction with the first pulse the density matrix is $|g\rangle\langle e|$, and after the second pulse it becomes $|e\rangle\langle g|$. The contribution of this pathway to the signal is

$$P_s = \alpha \exp[\mathrm{i}\, E_e(\tau_2 - \tau_1)] \tag{11.10}$$

When inhomogeneous broadening is incorporated, the contributions from the different levels E_e have different phases for $\tau_1 \neq \tau_2$ and therefore cancel. When $\tau_1 = \tau_2$ all the contributions have the same phase (i.e., rephase), which generates the echo.

We will now change the setup using instead of the second pulse two short overlapping pulses with frequencies ω_1 and ω_3. We assume that ω_1 and ω_3 are off-resonant with

$$\omega_1 + \omega_3 = 2\omega_2 \,, \tag{11.11}$$

which means that $\omega_1 + \omega_3$ is on-resonance with the f continuum. The Liouville-space pathway contributing to the signal in this case is presented in Fig. 21c. We start with the density matrix $|g\rangle\langle g|$, from $t = -\tau_1$ to $t = 0$ the density matrix is $|g\rangle\langle e|$; since ω_1 and ω_3 are off-resonant, the ω_1 and ω_3 pulses cannot induce a transition between $|g>$ and $|e>$, however, $\omega_1 + \omega_3$ is on resonance with the f states, and when the pulses overlap they can induce the $|g\rangle \rightarrow |f\rangle$ transition. We will choose $f = d(e)$ (i.e., $E_f = 2E_e$), the density matrix from $t = 0$ and $t = \tau_2$ is $|d(e)\rangle\langle e|$. The signal in this case

$$P_s = \alpha \exp[-i2E_e\tau_2 + iE_e(\tau_2 + \tau_1)] \tag{11.12}$$

and we again have an echo at $\tau_1 = \tau_2$. Although this echo shows up at $\tau_1 = \tau_2$, which coincides with the ordinary echo, the mechanism is quite different; it is induced by the strong correlation between levels in the e and f continua. When $\omega_1 = \omega_3$ both the ordinary and the new echo contribute, and are indistinguishable. However, when ω_1 and ω_3 are off-resonant, only the second pathway contributes, and there will be no echo for an assembly of noninteracting two-level systems with inhomogeneous broadening! To summarize, the ordinary photon echo exists in systems of two-level molecules and molecular aggregates, whereas the new photon echo shows up only in molecular aggregates.

We have shown that systems with a certain correlation between e and f levels show specific resonances in the frequency domain (Eq. (11.7a)) and a photon echo signal in the time domain. We now show that the resonance of Eq. (11.7a) is related to the new photon echo. Since the g function in Eq. (11.7a) changes weakly on the scale of the inelastic dephasing rate, we can represent Eq. (11.7a) as

$$R(-\omega_s; \omega_1, -\omega_2, \omega_3) = \int \frac{d\Omega}{2\pi} \frac{ig(\omega_1, \omega_3; \Omega)}{(\omega_1 + \omega_3 - 2\Omega + i\eta)(\omega_2 - \Omega - i\eta)} \,. \tag{11.13}$$

Introducing the pulse envelopes

$$\mathscr{E}_1(t) = E_1(t)\, e^{-i\omega_1 t} + \text{c.c.} \,, \qquad \mathscr{E}_2(t) = E_2(t + \tau_1)\, e^{-i\omega_2(t+\tau_1)} + \text{c.c.} \,,$$

$$\mathscr{E}_3(t) = E_3(t)\, e^{-i\omega_3 t} + \text{c.c.} \,, \tag{11.14}$$

and switching to the time domain, we obtain the following expression for the signal amplitude, provided the pulses are short:

$$P_s(t) = \int \frac{d\Omega}{2\pi} g(\omega_1, \omega_3; \Omega) e^{-i\Omega(t-\tau_1)} \int E_1(\tau') E_3(\tau')\, d\tau' \int E_2^*(\tau'')\, d\tau'' \,. \tag{11.15}$$

We thus get an echo at $t = \tau_1$. In conclusion, we have shown that both the $\omega_1 + \omega_3 = 2\omega_2$ resonance (see Eq. (11.7a)) and the two-exciton photon echo contain the signature of the same property of a system: a specific correlation between the e- and f-levels.

12. The multidimensional spectral density and the Kramers–Kronig representation of the optical response

Linear response functions are commonly calculated using the spectral density

$$J(\varepsilon) = 2\pi \mathrm{Tr}[\hat{\rho}\hat{\mu}\delta(\varepsilon - \hat{H})\hat{\mu}] = 2\pi \sum_{a,b}' \rho_{aa}|\mu_{ab}|^2 \delta(\varepsilon - E_b) . \tag{12.1}$$

The linear susceptibility is then given by

$$R(-\omega;\omega) = \int \frac{\mathrm{d}\varepsilon}{2\pi} J(\varepsilon)\left[\frac{1}{\omega - \varepsilon + \mathrm{i}\eta} - \frac{1}{\omega + \varepsilon + \mathrm{i}\eta}\right] . \tag{12.2}$$

The integral relationship between the spectral density and the response function is known as the Kramers–Kronig relation [87]. This representation of the linear response has several advantages. First, $J(\omega)$ is positive definite and allows us to consider the system as a collection of oscillators. In theoretical modelling it is common to calculate J rather than R. By calculating R via Eq. (12.2) we guarantee that it satisfies all the necessary symmetries, such as time reversal, and analytical properties. The connection between the real and the imaginary parts of the response function can also be tested experimentally and can be used to calculate the index of refraction from a knowledge of the absorption spectrum.

In this section we explore the possible generalization of this representation to the nonlinear response. To that end we introduce the multidimensional spectral density $\kappa(\varepsilon', \varepsilon, \varepsilon'')$ which depends on three energy variables [23]

$$\kappa(\varepsilon', \varepsilon, \varepsilon'') = (2\pi)^3 \sum_{a,b,c,d}' \rho_{dd}\mu_{da}\mu_{ac}\mu_{cb}\mu_{bd}\delta(\varepsilon' - E_b)\delta(\varepsilon - E_c)\delta(\varepsilon'' - E_a) , \tag{12.3a}$$

Eq. (12.3a) can also be expressed in an operator form:

$$\kappa(\varepsilon', \varepsilon, \varepsilon'') = (2\pi)^3 \mathrm{Tr}\{\hat{\rho}\hat{\mu}\delta(\varepsilon'' - \hat{H})\hat{\mu}\delta(\varepsilon - \hat{H})\hat{\mu}\delta(\varepsilon' - \hat{H})\hat{\mu}\} . \tag{12.3b}$$

Using this quantity we can express Eq. (11.1) as

$$\begin{aligned} R(-\omega_s;\omega_1, -\omega_2, \omega_3) = \sum_{\mathrm{perm}} \int \frac{\mathrm{d}\varepsilon'}{2\pi}\frac{\mathrm{d}\varepsilon''}{2\pi}\frac{\mathrm{d}\varepsilon}{2\pi} \kappa(\varepsilon', \varepsilon, \varepsilon'') \\ \times \left\{ \frac{1}{\omega_1 - \varepsilon' + \mathrm{i}\eta}\frac{1}{\omega_1 + \omega_3 - \varepsilon + \mathrm{i}\eta}\frac{1}{\omega_s - \varepsilon'' + \mathrm{i}\eta} \right. \\ \left. + \frac{1}{\omega_1 - \varepsilon' + \mathrm{i}\eta}\frac{1}{\omega_1 + \omega_3 - \varepsilon + \mathrm{i}\eta}\frac{1}{\omega_2 - \varepsilon'' - \mathrm{i}\eta} + \mathrm{c'.c'.} \right\} . \end{aligned} \tag{12.4}$$

For the sake of simplicity, we consider a system whose size is much smaller than the wavelength, and in this case we need only to follow the dynamics of the total polarization[6]

$$\hat{\mu} = \int \mathrm{d}\boldsymbol{r}\, \hat{P}(\boldsymbol{r}) .$$

Eq. (12.4) is the Kramers–Kronig representation for the third-order response function. The nonlinear response function in the time domain which is necessary for the analysis of time-resolved spectroscopy can also be expressed in terms of κ. We define

$$\kappa(\varepsilon', \varepsilon, \varepsilon'') = \int_{-\infty}^{+\infty} \int_{-\infty}^{+\infty} \int_{-\infty}^{+\infty} \mathrm{d}\tau_1\, \mathrm{d}\tau_2\, \mathrm{d}\tau_3 \langle (\hat{P}(\tau_1 + \tau_2 + \tau_3)\hat{P}(\tau_1 + \tau_2)\hat{P}(\tau_1)\hat{P}(0)\rangle$$
$$\times \exp(\mathrm{i}\varepsilon'\tau_1 + \mathrm{i}\varepsilon\tau_2 + \mathrm{i}\varepsilon''\tau_3) . \tag{12.5}$$

and the reverse transform

$$\langle \hat{P}(t_4)\hat{P}(t_3)\hat{P}(t_2)\hat{P}(t_1)\rangle$$
$$= \int \frac{\mathrm{d}\omega_1}{2\pi} \cdots \int \frac{\mathrm{d}\omega_4}{2\pi}\, 2\pi\delta(\omega_1 + \omega_2 - \omega_3 - \omega_4)\exp(-\omega_4 t_4 - \mathrm{i}\omega_3 t_3 + \mathrm{i}\omega_2 t_2 + \mathrm{i}\omega_1 t_1)$$
$$\times \kappa(\omega_1, \omega_1 + \omega_2, \omega_1 + \omega_2 - \omega_3) , \tag{12.6}$$

The derivation of Green function expressions for the multidimensional spectral density function in molecular aggregates is outlined in Appendix G. The result is[6,7]

$$\kappa = \kappa^{(a)} + \kappa^{(b)} + \kappa^{(c)} + \kappa^{(d)} , \tag{12.7a}$$

with

$$\kappa^{(b)} = \kappa_{\mathrm{s}}^{(b)} + \kappa_{\mathrm{f}}^{(b)} , \tag{12.7b}$$

$$\kappa^{(d)} = \kappa_{\mathrm{s}}^{(d)} + \kappa_{\mathrm{f}}^{(d)} . \tag{12.7c}$$

For the exciton–phonon model of Section 7, we obtain [10]

$$\kappa^{(a)}(\varepsilon', \varepsilon, \varepsilon'') = 4\pi\mu^4 \operatorname{Im} G(\varepsilon') \operatorname{Im} G(\varepsilon'')$$
$$\times \{ G(\varepsilon - \varepsilon') G(\varepsilon - \varepsilon'') \bar{\Gamma}(\varepsilon) - G^*(\varepsilon - \varepsilon') G^*(\varepsilon - \varepsilon'') \bar{\Gamma}^*(\varepsilon) \} , \tag{12.8a}$$

[6] All the expressions derived below can be easily extended for the general case; the spectral density κ will then be also a function of four coordinates (or four momenta).

[7] An additional term $\kappa^{(0)}$ which does not contribute to the nonlinear response function when substituted into the Kramers–Kronig relation (Eq. (12.4)), was omitted here.

$$\kappa_s^{(b)}(\varepsilon', \varepsilon, \varepsilon'') = 4\pi\mu^4 C \int d\boldsymbol{p}\, g(\boldsymbol{p}, 0; \varepsilon') \frac{\Gamma_0}{(\varepsilon'' - \varepsilon')^2 + \Gamma_0^2}$$
$$\times \{ G(\varepsilon') G^*(\varepsilon'') G(\varepsilon - \varepsilon') G(\varepsilon - \varepsilon'') \int d\boldsymbol{q} \exp[-\varepsilon(\boldsymbol{q})/kT]\, \bar{\Gamma}(\varepsilon - \varepsilon' + \varepsilon(\boldsymbol{q}), \boldsymbol{q})$$
$$- G^*(\varepsilon') G(\varepsilon'') G^*(\varepsilon - \varepsilon') G(\varepsilon - \varepsilon'') \int d\boldsymbol{q} \exp[-\varepsilon(\boldsymbol{q})/kT]\, \bar{\Gamma}^*(\varepsilon - \varepsilon' + \varepsilon(\boldsymbol{q}), \boldsymbol{q}) \} , \tag{12.8b}$$

$$\kappa_f^{(b)}(\varepsilon', \varepsilon, \varepsilon'') = 4\pi\mu^4 \sum_{\alpha \neq 0} \int d\boldsymbol{p}\, \bar{\varphi}_\alpha(\boldsymbol{p}) g(\boldsymbol{p}, 0; \varepsilon') \frac{\lambda_\alpha}{(\varepsilon'' - \varepsilon')^2 + \lambda_\alpha^2}$$
$$\times \{ G(\varepsilon') G^*(\varepsilon'') G(\varepsilon - \varepsilon') G(\varepsilon - \varepsilon'') \int d\boldsymbol{q}\, \varphi_\alpha(\boldsymbol{q})\, \bar{\Gamma}(\varepsilon - \varepsilon' + \varepsilon(\boldsymbol{q}), \boldsymbol{q})$$
$$- G^*(\varepsilon') G(\varepsilon'') G^*(\varepsilon - \varepsilon') G^*(\varepsilon - \varepsilon'') \int d\boldsymbol{q}\, \varphi_\alpha(\boldsymbol{q})\, \bar{\Gamma}^*(\varepsilon - \varepsilon' + \varepsilon(\boldsymbol{q}), \boldsymbol{q}) \} , \tag{12.8c}$$

$$\kappa^{(c)}(\varepsilon', \varepsilon, \varepsilon'') = 0 , \tag{12.8d}$$

$$\kappa_s^{(d)}(\varepsilon', \varepsilon, \varepsilon'') = 2\pi\mu^4 \frac{\Gamma_0}{(\varepsilon'' - \varepsilon')^2 + \Gamma_0^2} C \int d\boldsymbol{p}\, g(\boldsymbol{p}, 0; \varepsilon') \int d\boldsymbol{q} \exp[-\varepsilon(\boldsymbol{q})/kT]$$
$$\times \{ g_s(0, \boldsymbol{q}; \varepsilon' - \varepsilon) [G(\varepsilon') G(\varepsilon' - \varepsilon) G^*(\varepsilon'') G^*(\varepsilon'' - \varepsilon) + \text{c.c.}]$$
$$+ g_s(0, \boldsymbol{q}; \varepsilon - \varepsilon'') [G(\varepsilon') G(\varepsilon - \varepsilon'') G^*(\varepsilon'') G^*(\varepsilon - \varepsilon') + \text{c.c.}] \} , \tag{12.8e}$$

$$\kappa_f^{(d)}(\varepsilon', \varepsilon, \varepsilon'') = 2\pi\mu^4 \sum_{\alpha \neq 0} \frac{\lambda_\alpha}{(\varepsilon'' - \varepsilon')^2 + \lambda_\alpha^2} \int d\boldsymbol{p}\, \bar{\varphi}_\alpha(\boldsymbol{p}) g(\boldsymbol{p}, 0; \varepsilon') \int d\boldsymbol{q}\, \varphi_\alpha(\boldsymbol{q})$$
$$\times \{ g_s(0, \boldsymbol{q}; \varepsilon' - \varepsilon) [G(\varepsilon') G(\varepsilon' - \varepsilon) G^*(\varepsilon'') G^*(\varepsilon'' - \varepsilon) + \text{c.c.}]$$
$$+ g_s(0, \boldsymbol{q}; \varepsilon - \varepsilon'') [G(\varepsilon') G(\varepsilon - \varepsilon'') G^*(\varepsilon'') G^*(\varepsilon - \varepsilon') + \text{c.c.}] \} , \tag{12.8f}$$

G, $\bar{\Gamma}$, and φ_α were defined in Sections 7 and 8.

Expressions for $\kappa^{(a)}$, $\kappa^{(b)}$ and $\kappa^{(c)}$ for the model of a disordered molecular assembly with exciton–phonon interaction considered in Section 10 are also derived in Appendix G. The contribution $\kappa^{(a)}$ is given by Eq. (12.8a) with G and $\bar{\Gamma}$ from Section 4. The contributions $\kappa^{(b)}$ and $\kappa^{(c)}$ have the form:

$$\kappa_s^{(b)}(\varepsilon', \varepsilon, \varepsilon'') = 4\pi\mu^4 C_0 \sigma^4 \frac{\Gamma_0}{(\varepsilon'' - \varepsilon')^2 + \Gamma_0^2}$$
$$\times \{ G(\varepsilon') G^*(\varepsilon'') G(\varepsilon - \varepsilon') G(\varepsilon - \varepsilon'') \int d\boldsymbol{p} \frac{d\Omega}{2\pi} \rho(\Omega) |G(\Omega, \boldsymbol{p})|^2 \exp[-\Omega/kT]$$
$$\times \bar{\Gamma}(\varepsilon - \varepsilon' + \Omega; \boldsymbol{p}) - G^*(\varepsilon') G(\varepsilon'') G^*(\varepsilon - \varepsilon') G^*(\varepsilon - \varepsilon'')$$
$$\times \int d\boldsymbol{p} \frac{d\Omega}{2\pi} \rho(\Omega) |G(\Omega, \boldsymbol{p})|^2 \exp[-\Omega/kT]\, \bar{\Gamma}^*(\varepsilon - \varepsilon' + \Omega; \boldsymbol{p}) \} , \tag{12.9a}$$

$$\kappa_{\mathrm{f}}^{(b)}(\varepsilon', \varepsilon, \varepsilon'') = 4\pi\mu^4\sigma^4 \sum_{\alpha} \bar{\varphi}_{\alpha}(\varepsilon') \frac{\lambda_{\alpha}}{(\varepsilon'' - \varepsilon')^2 + \lambda_{\alpha}^2}$$

$$\times \{G(\varepsilon')G^*(\varepsilon'')G(\varepsilon - \varepsilon')G(\varepsilon - \varepsilon'') \int \mathrm{d}\boldsymbol{p} \frac{\mathrm{d}\Omega}{2\pi} \rho(\Omega)|G(\Omega, \boldsymbol{p})|^2 \varphi_{\alpha}(\Omega)$$

$$\times \bar{\Gamma}(\varepsilon - \varepsilon' + \Omega, \boldsymbol{p}) - G^*(\varepsilon')G(\varepsilon'')G^*(\varepsilon - \varepsilon')G^*(\varepsilon - \varepsilon'')$$

$$\times \int \mathrm{d}\boldsymbol{p} \frac{\mathrm{d}\Omega}{2\pi} \rho(\Omega)|G(\Omega, \boldsymbol{p})|^2 \varphi_{\alpha}(\Omega) \bar{\Gamma}^*(\varepsilon - \varepsilon' + \Omega; \boldsymbol{p})\} , \tag{12.9b}$$

$$\kappa^{(c)}(\varepsilon', \varepsilon, \varepsilon'') = 4\pi\mu^4 \operatorname{Im} G(\varepsilon') \frac{2|\operatorname{Im}\Sigma(\varepsilon'')|[\Gamma_0(\varepsilon'') + \Gamma_{\mathrm{ph}}(\varepsilon'')]^2}{(\varepsilon - 2\varepsilon'')^2 + [\Gamma_0(\varepsilon'') + \Gamma_{\mathrm{ph}}(\varepsilon'')]^2}$$

$$\times \{G(\varepsilon - \varepsilon')G(\varepsilon - \varepsilon'')G^*(\varepsilon'')\bar{\Gamma}(\varepsilon) - G^*(\varepsilon - \varepsilon')G^*(\varepsilon - \varepsilon'')G(\varepsilon'')\bar{\Gamma}^*(\varepsilon)\}$$

$$+ 4\pi\mu^2 \operatorname{Im} G(\varepsilon'') \frac{2|\operatorname{Im}\Sigma(\varepsilon')|[\Gamma_0(\varepsilon') + \Gamma_{\mathrm{ph}}(\varepsilon')]}{(\varepsilon - 2\varepsilon')^2 + [\Gamma_0(\varepsilon') + \Gamma_{\mathrm{ph}}(\varepsilon')]^2}$$

$$\times \{G(\varepsilon - \varepsilon')G(\varepsilon - \varepsilon'')G^*(\varepsilon')\bar{\Gamma}(\varepsilon) - G^*(\varepsilon - \varepsilon')G^*(\varepsilon - \varepsilon'')G(\varepsilon')\bar{\Gamma}^*(\varepsilon)\} . \tag{12.9c}$$

Each of the $\kappa^{(j)}$ terms is responsible for the contribution $R^{(j)}$ to the nonlinear response function $j = a, b, c, d$. The spectral density representation provides a direct way for incorporating effects of level statistics in the nonlinear response function. It further guarantees the correct analytical properties of the function $R(-\omega_s; \omega_1, -\omega_2, \omega_3)$ for all possible spectral density functions $\kappa(\varepsilon', \varepsilon, \varepsilon'')$.

In the previous section we have shown that systems with a large number of degrees of freedom can show resonances which come from divergencies of the sum over states at certain combinations of frequencies. These collective resonances originate from specific correlations among energy levels, i.e., energy levels statistics. $\kappa^{(b)}$ is important for $\omega_1 \approx \omega_2$. The function $\kappa_{\mathrm{f}}^{(b)}$ shows the correlation between one-exciton levels ε' and ε'' with the width given by the dephasing rate. $\kappa_{\mathrm{s}}^{(b)}$ comes from terms in which one takes the same one-exciton level in the ε' and ε'' groups, and the width of the resonance in $\kappa_{\mathrm{s}}^{(b)}$ with respect to $\varepsilon'' - \varepsilon'$ is given by the inverse lifetime only. The contribution $\kappa^{(c)}$ is nonzero in disordered aggregates only, shows a strong correlation between one-exciton states with the energies ε', ε'' and two-exciton states with the energies $\varepsilon = 2\varepsilon'$ and $\varepsilon = 2\varepsilon''$ respectively. This allows us to attribute the origin of the resonances $\omega_1 + \omega_3 \approx 2\omega_2$ to certain correlations among levels. Leegwater and Mukamel have shown by numerical simulations [88] that photon echoes in neat clusters and liquids can be analyzed using a four-point spectral density, which is a special case of the one considered here.

13. Summary

In this paper we have calculated luminescence and four-wave mixing spectra of confined Frenkel exciton systems, taking into account exciton–phonon interactions and static disorder. We have discussed optical techniques which can probe various aspects of exciton dynamics in these systems.

Luminescence experiments provide information on properties of one-exciton states, which become rather complicated in the presence of phonons and static disorder. The following simple physical picture applies to time and frequency resolved luminescence: a short excitation pump pulse creates an initial exciton distribution (the doorway wave packet), the exciton distribution then evolves due to scattering on phonons and impurities, as described by transport equations. The time-dependent luminescence spectrum is given by a convolution of the exciton distribution with a window wave packet. Calculations of the time and frequency luminescence spectra in J- and H-aggregates, including interactions with acoustic and optical phonons were presented in Section 9. In Section 10 we discussed the combined effect of phonons and static disorder in luminescence. The situation is particularly interesting when $\Gamma_e \gg \Gamma_1$ (Γ_e is the elastic scattering rate due to static disorder, Γ_1 is the inelastic scattering rate due to phonons). In this case there are two distinct relevant time scales. On the Γ_e^{-1} time scale one can neglect phonon effects, the scattering is elastic and affects the angular distribution of the signal which has a form a homogeneous background which conserves the exciton frequency. On the top of the homogeneous background there appear backscattering components reflecting the long exciton phase memory in elastic scattering. The evolution of the spectrum takes place on the $\sim \Gamma_1^{-1}$ time scale due to inelastic exciton–phonon scattering processes which change the exciton energy. The spectrum variation on the $\sim \Gamma_1^{-1}$ time scale is, however, strongly affected by elastic scattering: exciton transport takes place in energy (not momentum) space, since fast elastic scattering keeps the exciton distribution homogeneous within a given energy. Exciton–phonon scattering leads then to transport in energy space. Inelastic scattering also destroys the backscattering through the loss of phase memory.

Properties of two-exciton states, which do not contribute to luminescence, can be probed by applying various nonlinear four-wave mixing techniques. We have considered four-wave mixing techniques in the frequency and time domain which show an interplay of two-exciton coherent motion, exciton diffusive motion due to inelastic scattering on phonons, and exciton phase memory due to elastic exciton-scattering on static disorder. Special attention was paid to the breakdown of the local field approximation. This can be clearly seen in phase-controlled measurements (using heterodyne detection) in the vicinity of two-photon resonances. To see the signatures of these effects we considered four-wave mixing techniques in which the signal is observed in the $\boldsymbol{k}_s = \boldsymbol{k}_1 - \boldsymbol{k}_2 + \boldsymbol{k}_3$ direction, and $\omega_1 + \omega_3$ is tuned on resonance with two-exciton states. Observing the same physical phenomena by applying frequency-domain or time-domain measurements was discussed.

Properties of two-exciton coherent motion can be studied by tuning all frequencies off-resonance, with $\omega_1 + \omega_3$ tuned to the two-exciton band, scanning ω_3 and making a phase-sensitive measurement. The appearance of the imaginary part in the polarization when $\omega_1 + \omega_3$ in inside the two-exciton band is a clear signature of two-exciton coherent motion, which is completely missed by the local field approximation. The time-domain analogue of this technique is the interaction-induced two-exciton spectroscopy discussed in Section 8. In this technique two-exciton states are excited by two short time-coincident off-resonant pulses, with the sum of their frequencies $\omega_1 + \omega_3$ tuned to the two-exciton band, and the two-exciton dynamics is monitored with an off-resonant ω_2 probe pulse which comes after a time delay τ'. The decay of the time-integrated signal as a function of the time delay, which has the time scale of the inverse exciton band width W^{-1}, is a clear measure of the two-exciton coherent motion.

The interplay of exciton transport and two-exciton coherent motion shows up in degenerate four-wave mixing by an additional collective narrow resonance at $\omega_1 = \omega_2$, provided ω_1 is inside the exciton band, which can be observed by scanning ω_2. This resonance reflects effects of exciton transport. Two-exciton coherent motion affects the excitation profile, i.e., the dependence of the peak value of the signal at $\omega_1 = \omega_2$ on ω_3. The phase of the excitation profile changes drastically as $\omega_1 + \omega_3$ is tuned inside the two-exciton band. The time-domain counterpart of degenerate four-wave mixing, which probes exciton transport directly in the time domain is the transient grating technique.

An additional resonance is predicted in disordered aggregates at $\omega_1 + \omega_3 = 2\omega_2$, provided ω_2 is tuned inside the exciton band and ω_1 and ω_3 are off-resonant. This resonance depends on the combined effort of inhomogeneous broadening (due to static disorder) and aggregation (it does not exist for a set of noninteracting molecules). This resonance, which shows up when $\Gamma_e \gg \Gamma_1$, is due to the strong correlation between one and two-exciton states. It is destroyed by phonon scattering which makes the resonance width to have an order of magnitude of Γ_1. Since the absorption line width is of the order of Γ_e, it eliminates inhomogeneous broadening, and we can denote this technique four-photon hole burning. Note, that the width of the degenerate four-wave mixing resonance is given by the inverse exciton lifetime Γ_0 since it is due to self-correlations of levels. This means that when $\Gamma_0 \ll \Gamma_1 \ll \Gamma_e$ we have three distinct resonance widths which correspond to different physical phenomena. The absorption line width is given by the elastic scattering rate Γ_e, the four-photon hole-burning resonance width is determined by the inelastic scattering rate Γ_1, and finally the degenerate four-wave mixing resonance line width is related to the inverse lifetime. Two-exciton coherent motion shows up in this technique in a form of the ω_2-dependence of the phase of the peak value of the signal at $\omega_1 + \omega_3 = 2\omega_2$. We have shown that the time-domain counterpart of the four-photon hole-burning is the two-exciton photon echo (see Section 4) which reflects the strong correlation between one-exciton and two-exciton states. The time-integrated signal as a function of the time-delay decays on a time scale of Γ_1^{-1} since that correlation is destroyed by inelastic processes. The decay of the echo on the Γ_1^{-1} time scale implies that this time-domain technique eliminates the $\sim \Gamma_e$ inhomogeneous broadening.

Acknowledgements

The support of the National Science Foundation, the Air Force Office of Scientific Research, and the NSF Center for Photoninduced Charge Transfer is gratefully acknowledged.

Appendix A. Optical response of disordered molecular nanostructures

In this appendix we develop a perturbation theory which allows us to calculate the average optical response of molecular nanostructures with Gaussian diagonal disorder. We can then justify the factorization used to obtain Eq. (4.8) by invoking the ladder approximation (Eqs. (4.13)–(4.17)).

We start with the expressions for the optical response of a molecular assembly of arbitrary geometry given by Eqs. (3.8)–(3.10). Eqs. (3.8)–(3.10), together with Eq. (3.13), which express the linear and third-order nonlinear optical response in terms of the one-exciton Green $G_{mn}(\omega)$.

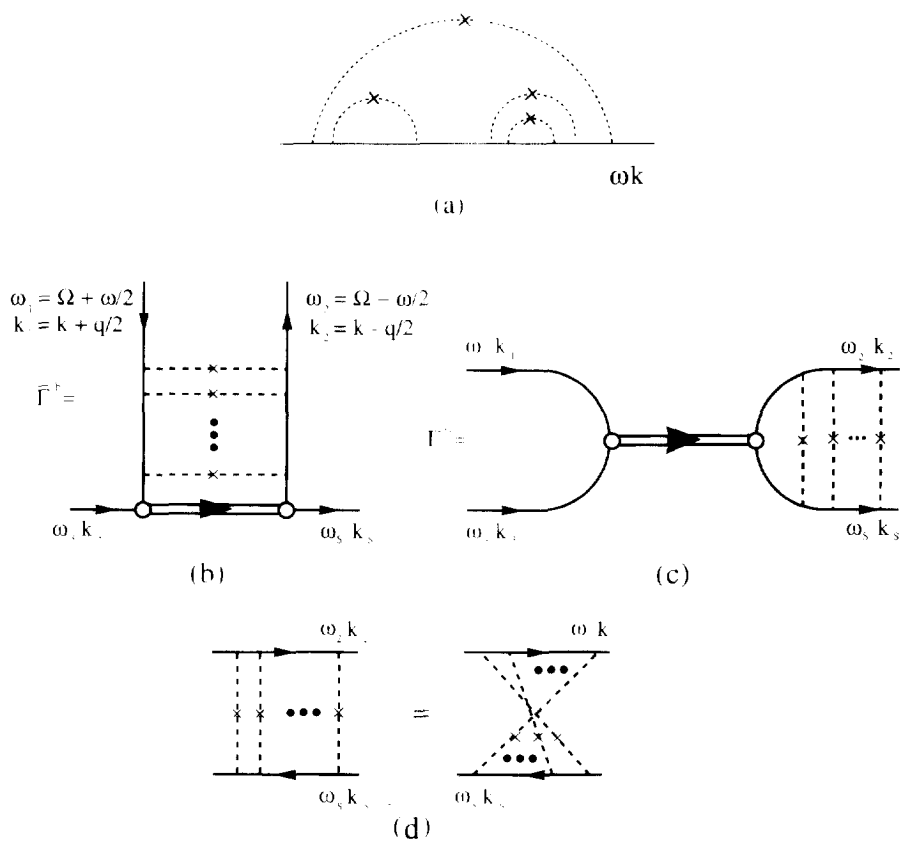

Fig. 22. Diagrammatic representation of the third-order nonlinear optical response of disordered molecular nanostructures. (a) Diagrams for to the Green function $G(\omega, \boldsymbol{k})$. (b) Diagrams for function $\bar{\Gamma}^{(b)}$. (c) Diagrams for $\bar{\Gamma}^{(c)}$. (d) Diagrammatic representation of an equality showing that diagrams in (c) which look like ladder diagrams are maximally crossed diagrams in the conventional sense (see Eq. (A.4)).

To formulate a perturbation theory in disorder we substitute Ω_n from Eq. (4.5a) into Eq. (3.9) and expand the one-exciton Green function $G_{mn}(\omega; U_j)$ in powers of the random variable U_j. The expansion has the form

$$G_{mn}(\omega; U_j) = G^{(0)}_{mn}(\omega) + \sum_{N=1}^{\infty} \sum_{j_1, j_2, \ldots, j_N}^{\infty} G^{(0)}_{j_N n}(\omega) \prod_{s=1}^{N} G^{(0)}_{j_s, j_{s-1}}(\omega) U_{j_s}, \tag{A.1}$$

where we define $j_0 \equiv m$ and $G^{(0)}_{mn}(\omega)$ is the nonperturbed one-exciton Green function, given by Eq. (3.9) with $\Omega_n \equiv \Omega$ (i.e., $U_n \equiv 0$, which implies no disorder).

Substituting the expansion (A.1) to the GFE given by Eqs. (3.8), (3.10) and (3.13), we can obtain the linear and nonlinear optical response order by order in U_j. To average these expansions over realizations of disorder we make use of Eq. (4.5c) and the factorization of a correlation function $\langle U_{j_1} \cdots U_{j_N} \rangle_F$ into a sum of products of pair correlation functions $\langle U_{j_a} U_{j_b} \rangle_F$. All of these contributions can be presented diagrammatically (see Fig. 22), using the following rules: the solid line stands for the Green function $G^{(0)}_{mn}$, the double line for $\bar{\Gamma}^{(0)}_{mn}$, given by Eq. (3.13). If we put $G^{(0)}$

instead of G, the dashed line denotes the disorder correlation function $\langle U_m U_n \rangle_F$. Evaluating the one-exciton Green function averaged over disorder $\langle G_{mn}(\omega) \rangle_F$ we take into account only diagrams without intersection of dashed lines (see Fig. 22a). The Green function in this approximation can be found from Eq. (4.7) (see [64, 76]). Eq. (4.7) together with Eq. (4.6) provide a closed system of equations for the linear optical response.

To obtain a closed system of equations for the third-order nonlinear optical response we will use the following procedure: we take into account higher-order corrections of the perturbation theory only if the small parameter related to weak disorder is compensated by a large resonant factor. When we insert an additional dashed line which connects two solid lines we gain an additional small factor σ^2 (we assume, that disorder is weak and hence σ is small), according to Eq. (4.5c). A large resonant factor can occur only if the dashed line connects two solid lines related to a retarded Green function $G(\omega')$ and an advanced Green function $G^*(\omega'')$ with close frequencies ($\omega'' \approx \omega'$). Since there is only one advanced Green function $G^*(\omega_2)$, and the Green functions $G(\omega)$ related to internal Green functions in the diagrams are integrated over frequencies, resonant factors occur for each dashed line only if the dashed lines connect the solid lines related to $G(\omega_1)$ and $G^*(\omega_2)$ for $\omega_1 \approx \omega_2$ or $G(\omega_s)$ and $G^*(\omega_2)$ for $\omega_s \approx \omega_2$ (or, equivalently $\omega_1 + \omega_3 \approx 2\omega_2$). If we put all possible dashed lines between $G(\omega_1)$ and $G^*(\omega_2)$ (with at least one line) we obtain $\langle\langle G(\omega_1) G^*(\omega_2) \rangle\rangle$. Inserting all dashed lines between $G(\omega_s)$ and $G^*(\omega_2)$ we obtain $\langle\langle G(\omega_s) G^*(\omega_2) \rangle\rangle$. Putting all possible lines between each one-exciton Green function and itself, and summing over all contributions described above we obtain Eq. (4.8).

Finally we derive Eq. (4.13), which lead immediately to the expressions for the nonlinear optical response (Eqs. (4.14)–(4.17)). Eq. (4.13b) means that L_0 is a one-particle irreducible two-exciton Green function in the momentum domain (the term "one-particle irreducible" means that it does not contain contributions from diagrams which have subdiagrams connected to the rest of a diagram with one solid line only). L_0 can be expressed in terms of the two-particle irreducible vertex $\bar{U}$ (which does not include contributions from diagrams with subdiagrams connected to the rest of the diagrams with two solid lines only) by means of a Bethe–Salpeter equation [89]:

$$L_0(\boldsymbol{p}, \boldsymbol{p}'; \boldsymbol{q}, \omega, \Omega) = \bar{U}(\boldsymbol{p}, \boldsymbol{p}'; \boldsymbol{q}, \omega, \Omega) + \int \mathrm{d}\boldsymbol{p}''\, \bar{U}(\boldsymbol{p}, \boldsymbol{p}''; \boldsymbol{q}, \omega, \Omega) L_0(\boldsymbol{p}'', \boldsymbol{p}'; \boldsymbol{q}, \omega, \Omega) \times G\left(\boldsymbol{p}'' + \frac{\boldsymbol{q}}{2}, \Omega + \frac{\omega}{2}\right) G^*\left(\boldsymbol{p}'' - \frac{\boldsymbol{q}}{2}, \Omega - \frac{\omega}{2}\right). \tag{A.2}$$

In the first nonvanishing order of perturbation theory we have for $\bar{U}$:

$$\bar{U}(\boldsymbol{p}, \boldsymbol{p}'; \boldsymbol{q}, \omega, \Omega) \equiv \sigma^2 \tag{A.3}$$

Substituting Eq. (A.3) into Eq. (A.2) we obtain L_0 in the ladder approximation (see [74, 85]), L_0 has the form of Eq. (4.13c) for small ω and $\boldsymbol{q}$. Eq. (4.13d) which gives L_0 for small $(\boldsymbol{p} + \boldsymbol{p}')$ can be immediately obtained for Eq. (4.13c) by making use of the time-reversal symmetry [76, 89]:

$$L_0(\boldsymbol{p}, \boldsymbol{p}', \boldsymbol{q}, \omega, \Omega) = L_0([(\boldsymbol{p} - \boldsymbol{p}')/2] + \boldsymbol{q}, [(\boldsymbol{p}' - \boldsymbol{p})/2] + \boldsymbol{q}; \boldsymbol{p} + \boldsymbol{p}', \omega, \Omega) \tag{A.4}$$

$\bar{\Gamma}^{(b)}$ and $\bar{\Gamma}^{(c)}$ in the ladder approximation are given by diagrams presented in Fig. 22b and 22c respectively. The diagrammatic expansion of Eq. (A.4) in the same approximation is given in Fig. 22d.

Appendix B. Correlation function expressions for the scattered field

In this appendix we derive relations connecting the correlation functions in a system with external polarization described by the Hamiltonian $\hat{H}_T(t)$ (Eq. (2.5)) to the correlation function in the isolated system without external polarization, described by the Hamiltonian $\hat{H}$ (Eq. (2.1)). These relations are given by Eq. (5.6). To that end, following [46] we introduce the path-integral representation [79] of the correlation functions on the Keldysh time loop [81, 82].

Let Q be the complete set of classical variables of our quantum system. We define $Q^{(k)}(t)$ as

$$Q^{(k)}(t) \equiv (Q_L(t), Q_R(t)) \quad Q_L(t = +\infty) = Q_R(t = +\infty) . \tag{B.1a, b}$$

Let $S[Q(t)]$ be the classical action of the system. We define the action on the Keldysh time loop [81, 82] as [46]

$$S^{(k)}[Q^{(k)}(t)] \equiv S[Q_L(t)] - S[Q_R(t)] . \tag{B.2}$$

Hereafter we use brackets for listing functional variables. We will also omit the superscript (k) in $Q^{(k)}$ and $S^{(k)}$ where possible. Let $Q^{(1)}, \ldots, Q^{(n)}$ be the classical variables corresponding to the operators $\hat{Q}^{(1)}, \ldots, \hat{Q}^{(n)}$. The path-integral representation then has the following form

$$\langle \hat{Q}^{(1)}_{\alpha_1}(t_1) \cdots \hat{Q}^{(n)}_{\alpha_n}(t_n) \rangle = \int \mathcal{D}[Q(t)] Q^{(1)}_{\alpha_1}(t_1) \cdots Q^{(n)}_{\alpha_n}(t_n) \times \exp\{iS^{(k)}[Q(t)]\} \equiv \langle Q^{(1)}_{\alpha_1}(t_1) \cdots Q^{(n)}_{\alpha_n}(t_n) \rangle_{S[Q(t)]} . \tag{B.3}$$

Let S_T and S be the classical actions corresponding to the Hamiltonians $\hat{H}_T$ and $\hat{H}$ respectively. The relation between these actions which follows from Eq. (2.5) has the form

$$S_T = S + \int d\boldsymbol{r}\, dt\, P_{ext}(\boldsymbol{r}, t) \dot{A}(\boldsymbol{r}, t) . \tag{B.4a}$$

It has been shown in [23] that instead of the action S_T from Eq. (B.4a) one can use the following action:

$$S_T = S + \int d\boldsymbol{r}\, dt\, P(\boldsymbol{r}, t) \mathcal{E}(\boldsymbol{r}, t) , \tag{B.4b}$$

where $P(\boldsymbol{r}, t)$ is the classical version of the polarization operator, and $\mathcal{E}(\boldsymbol{r}, t)$ is the external field which is related to the external polarization $P_{ext}(\boldsymbol{r}, t)$ by Eq. (2.23).

We will use for the classical variables Q the same convention as Eq. (5.2) for the operators. Making use of Eqs. (B.2) and (B.4b) we obtain

$$S_T^{(k)} = S^{(k)} + \int d\boldsymbol{r}\, dt\, P \quad (\boldsymbol{r}, t) \mathcal{E}(\boldsymbol{r}, t) \tag{B.5}$$

Substituting Eq. (B.5) in the path-integral representation Eq. (B.3) we obtain the following relation

$$\langle Q_{\alpha_1}^{(1)}(t_1)\cdots Q_{\alpha_n}^{(n)}(t_n)\rangle_{S_1} = \left\langle Q_{\alpha_1}^{(1)}(t_1)\cdots Q_{\alpha_n}^{(n)}(t_n)\exp\left\{\mathrm{i}\int \mathrm{d}\boldsymbol{r}\,\mathrm{d}t\; P_-(\boldsymbol{r},t)\mathscr{E}(\boldsymbol{r},t)\right\}\right\rangle_S . \tag{B.6}$$

Combining Eq. (B.6) with the path-integral representations

$$\langle \tilde{Q}_{\alpha_1}^{(1)}(t_1)\cdots \tilde{Q}_{\alpha_n}^{(n)}(t_n)\rangle = \langle Q_{\alpha_1}^{(1)}(t_1)\cdots Q_{\alpha_n}^{(n)}(t_n)\rangle_{S_1} , \tag{B.7a}$$

$$\langle \hat{Q}_{\alpha_1}^{(1)}(t_1)\cdots \hat{Q}_{\alpha_n}^{(n)}(t_n)\rangle = \langle Q_{\alpha_1}^{(1)}(t_1)\cdots Q_{\alpha_n}^{(n)}(t_n)\rangle_{S} , \tag{B.7b}$$

we obtain the relations of Eq. (5.6).

The path-integral representations of Eqs. 5.7(a) and (b) assume the form

$$R^{(n)}(\boldsymbol{r}t;\boldsymbol{r}_1t_1,\ldots,\boldsymbol{r}_nt_n) = \mathrm{i}^n\langle P_+(\boldsymbol{r},t)P_-(\boldsymbol{r}_1,t_1)\cdots P_-(\boldsymbol{r}_n,t_n)\rangle_S , \tag{B.8a}$$

$$R^{(n)}(\boldsymbol{r}t,\boldsymbol{r}'t';\boldsymbol{r}_1t_1,\ldots,\boldsymbol{r}_nt_n) = \mathrm{i}^n\langle P_-(\boldsymbol{r},t)P_+(\boldsymbol{r}',t')P_-(\boldsymbol{r}_1,t_1)\cdots P_-(\boldsymbol{r}_n,t_n)\rangle_S . \tag{B.8b}$$

Appendix C. Perturbation theory for correlation functions, and the Green function expressions in real space

In this appendix we develop a perturbative expansion in the exciton–phonon interaction and static disorder, and derive the Green function expressions (Eqs. (6.4) and (9.11)) for the third-order nonlinear response function and for the luminescence signal of a molecular nanostructure in real space.

We will work with a general material Hamiltonian given by Eq. (4.1) which describes Frenkel excitons interacting with phonons (dynamical disorder) in the presence of static disorder. We also adopt the averaging scheme over static disorder given by Eq. (4.2).

The path-integral representation for the correlation functions in the presence of static disorder can be written in the form:

$$\langle \hat{Q}_{\alpha_1}^{(1)}(t_1,q)\cdots \hat{Q}_{\alpha_n}^{(n)}(t_n,q)\rangle_q = \int \mathscr{D}[Q(t)]\,Q_{\alpha_1}^{(1)}(t_1)\cdots Q_{\alpha_n}^{(n)}(t_n) \times \exp\{\mathrm{i}S[Q(t),q]\} \equiv \langle Q_{\alpha_1}^{(1)}(t_1)\cdots Q_{\alpha_n}^{(n)}(t_n)\rangle_{S[Q(t),q]} , \tag{C.1a}$$

$$\langle Q_{\alpha_1}^{(1)}(t_1)\cdots \hat{Q}_{\alpha_n}^{(n)}(t_n)\rangle = Z^{-1}\int \mathrm{d}q\,\mathscr{D}[Q(t)]\,Q_{\alpha_1}(t_1)\cdots Q_{\alpha_n}^{(n)}(t_n) \times \exp\{\mathrm{i}S[Q(t),q]\}\exp\{-F(q)\} . \tag{C.1b}$$

Eq. (C.1a) gives a correlation function for a given realization of static disorder, and Eq. (C.1b) gives the correlation function averaged over all possible realizations of the disorder.

As indicated in Section 6, we will work with the interacting boson Hamiltonian (Eq. (6.1)) instead of the Hamiltonian (4.1) setting $g \to \infty$ in the end. For our case

$$Q = (C, \bar{C}, b, \bar{b}, A) \tag{C.2}$$

where the classical variables in Eq. (C.2) correspond to operators, $\hat{C}$, $\hat{C}^{\dagger}$, $\hat{b}$, $\hat{b}^{\dagger}$, and the action has the form (see [46] for details):

$$S^{(k)} = S^{(k)}_{\mathrm{rad}}[A(t)] + S^{(k)}_{\mathrm{m}}[C(t), \bar{C}(t), b(t), \bar{b}(t); q] + \int \mathrm{d}\boldsymbol{r}\, \mathrm{d}t \{P_-(\boldsymbol{r}, t)\dot{A}_-(\boldsymbol{r}, t) + P_-(\boldsymbol{r}, t)\dot{A}_+(\boldsymbol{r}, t)\} . \tag{C.3}$$

Note, that here we distinguish between dynamical disorder described by means of quantum mechanical operators $\hat{b}$, $\hat{b}^{\dagger}$ and static disorder described by means of its general coordinates q on which the quantum Hamiltonian depends parametrically. In Eq. (C.3) S_{rad} is a free action of the transverse electromagnetic field

$$S_{\mathrm{rad}}[A(t)] = \frac{1}{8\pi}\int \mathrm{d}\boldsymbol{r}\, \mathrm{d}t\, [(\dot{A}(\boldsymbol{r}, t))^2 - (\nabla \times A(\boldsymbol{r}, t))^2] . \tag{C.4a}$$

S_{m} is the material action corresponding to the Hamiltonian $\hat{H}_{\mathrm{m}}$ from Eq. (6.1)

$$S_{\mathrm{m}} = S^{(0)}_{\mathrm{m}} + S^{\mathrm{int}}_{\mathrm{m}} , \tag{C.4b}$$

$$S^{(0)}_{\mathrm{m}} = \int \mathrm{d}t \left\{ \mathrm{i}\sum_n \bar{C}_n \frac{\mathrm{d}C_n}{\mathrm{d}t} + \mathrm{i}\sum_s \bar{b}_s \frac{\mathrm{d}b_s}{\mathrm{d}t} - \sum_n \Omega^{(0)}_n \bar{C}_n C_n - \sum_{m \neq n} J^{(0)}_{mn} \bar{C}_m C_n - \sum_{r,s} A_{rs} \bar{b}_r b_s \right\} , \tag{C.4c}$$

$$S^{\mathrm{int}}_{\mathrm{m}} = -\int \mathrm{d}t \left\{ \frac{g}{2}\sum_n \bar{C}^2_n C^2_n + \sum_n \Omega^{(\mathrm{int})}_n(b, \bar{b}; q)\bar{C}_n C_n + \sum_{m \neq n} J^{(\mathrm{int})}_{mn}(b, \bar{b}; q)\bar{C}_m C_n + h_{\mathrm{ph}}(\bar{b}, b) \right. . \tag{C.4d}$$

The path-integral representation for the correlation functions in Eq. (5.6a) is

$$\langle \tilde{Q}_{\alpha_1}(t_1) \cdots \tilde{Q}_{\alpha_n}(t_n) \rangle = Z^{-1} \int \mathrm{d}q\, \mathscr{D}[A(t)]\, \mathscr{D}[C(t), \bar{C}(t)]\, \mathscr{D}[b(t), \bar{b}(t)] \times Q_{\alpha_1}(t_1) \cdots Q_{\alpha_n}(t_n) \exp\left\{ \mathrm{i}\int \mathrm{d}\boldsymbol{r}\, \mathrm{d}t\, \mathscr{E}(\boldsymbol{r}, t) P_-(\boldsymbol{r}, t) \right\} \times \exp\{\mathrm{i}S^{(k)}[A(t), C(t), \bar{C}(t), b(t), \bar{b}(t); q] - F(q)\} \tag{C.5}$$

In Eq. (C.4b) we present the material action as a sum of terms quadratic in material variables ($S^{(0)}_{\mathrm{m}}$), and higher-order terms ($S^{\mathrm{int}}_{\mathrm{m}}$). In Eqs. (C.4c) and (C.4d) we have used the following notation

$$\Omega_n(b, \bar{b}; q) = \Omega^{(0)}_n + \Omega^{(\mathrm{int})}_n(b, \bar{b}; q) , \tag{C.6a}$$

$$J_{mn}(b, \bar{b}; q) = J^{(0)}_{mn} + J^{(\mathrm{int})}_{mn}(b, \bar{b}; q) , \tag{C.6b}$$

$$\Omega^{(0)}_n = \Omega_n|_{b=\bar{b}=q=0}; \quad J^{(0)}_{mn} = J_{mn}|_{b=\bar{b}=q=0} , \tag{C.6c}$$

$$H_{\mathrm{ph}}(b, \bar{b}) = \sum_{r,s} A_{rs}\bar{b}_r b_s + h_{\mathrm{ph}}(\bar{b}, b) , \tag{C.6d}$$

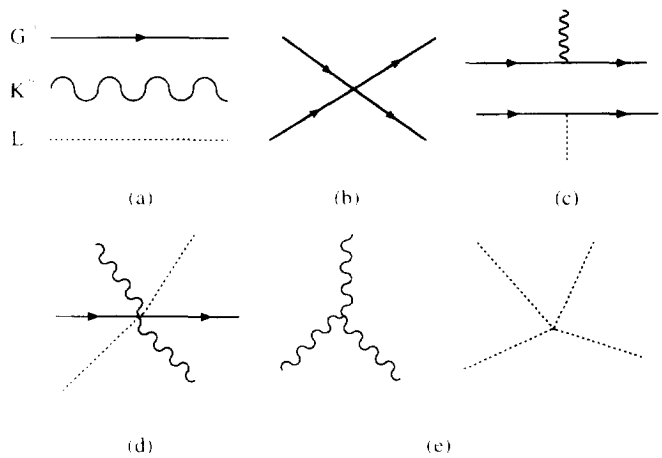

Fig. 23. Elements of the diagram technique. (a) The bare Green functions. (b) The vertex describing the exciton–exciton interaction. (c) The vertices related to the exciton phonon coupling and interaction with the disorder in the linear approximation. (d) An example of a higher order vertex related to the interaction of excitons with the phonons and disorder. (e) The vertices describing the anharmonicity of the phonon system and the non-Gaussian corrections to the disorder statistics.

where in Eq. (C.6d) $h_{\rm ph}(\bar{b}, b)$ is a sum of terms higher order in b and $\bar{b}$. Finally we represent the action S in the form

$$S = S^{(0)} + S^{\rm int}\,, \quad S^{(0)} \equiv S_{\rm rad} + S_{\rm m}^{(0)} + \int {\rm d}\boldsymbol{r}\,{\rm d}t\, P(\boldsymbol{r}, t)\,\dot{A}(\boldsymbol{r}, t)\,, \quad S^{\rm int} \equiv S_{\rm m}^{\rm int}\,. \tag{C.7a, b, c}$$

The action $S^{(0)}$ describes a system of free bosons interacting with the quantum electromagnetic field and with phonons. The action $S^{\rm int} \equiv S_{\rm m}^{\rm int}$ describes interactions in the system. The first term in Eq. (C.4d) is the boson–boson interaction which transforms into exciton–exciton interaction (Pauli exclusion) in the $g \to \infty$ limit. The second and the third terms present the exciton–phonon coupling and interaction with disorder (diagonal and off-diagonal terms). The fourth term is the self-interaction in the phonon system. To construct the perturbation theory we substitute Eq. (C.7a) into Eq. (C.5) and present $F(q)$ in Eq. (C.5) in a form

$$F(q) = \sum_{r,s} B_{rs} q_r q_s + F_{\rm int}(q)\,. \tag{C.8}$$

Note that for a Gaussian disorder $F_{\rm int}(q) \equiv 0$. Expanding the quantity $\exp\{{\rm i}S^{\rm int} - F_{\rm int}(q)\}$ in the r.h.s. of Eq. (C.5) in powers of C, $\bar{C}$, b, $\bar{b}$ and q, and using the Wick theorem for the correlation functions with respect to the quadratic action $S^{(0)}$ and for correlation functions of disorder with respect to its Gaussian part $\sum_{r,s} B_{rs} q_r q_s$, we obtain a diagrammatic perturbation theory (see [64, 79, 82]) whose elements are the bare Green functions and the vertices.

The bare Green functions corresponding to excitons, phonons and disorder are denoted $G^{(0)}$, $K^{(0)}$ and L. They are presented in the diagrams by a solid wavy and a dashed line (see Fig. 23a) and

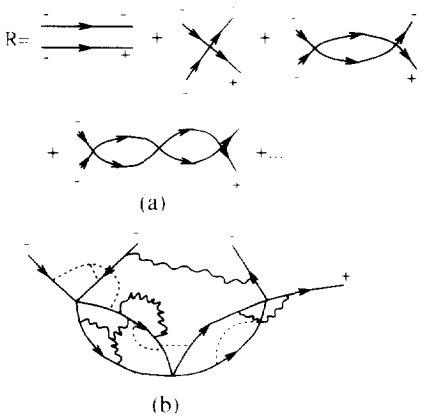

Fig. 24. Diagrams contributing to the third-order nonlinear optical response R. (a) Ladder skeleton diagrams. (b) Example of a diagram which belongs to the skeleton class of the last diagram in Fig. 24a.

have the form

$$G^{(0)}_{mn\alpha\beta}(t,t') \equiv \langle C_{m\alpha}(t)\bar{C}_{n\beta}(t')\rangle_{S^{(0)}}, \tag{C.9a}$$

$$K^{(0)}_{rs\alpha\beta}(t,t') \equiv \langle b_{r\alpha}(t)\bar{b}_{s\beta}(t')\rangle_{S^{(0)}}, \tag{C.9b}$$

$$L_{ab}(t,t') = Z^{-1}\int \mathrm{d}q\, q_a q_b \exp\left\{-\sum_{cd} B_{cd} q_c q_d\right\}. \tag{C.9c}$$

Note that radiative decay is fully incorporated since in Eq. (C.9a) the expectation values are taken with respect to $S^{(0)}$ which due to Eq. (C.7b) contains all the terms with the transverse electromagnetic field. The vertices are related to the expansion of $S^{\mathrm{int}}_{\mathrm{m}}$ from Eq. (C.4d) in powers of b, $\bar{b}$ and q and are presented in Fig. 23(b)–(e).

We will now describe the diagrams contributing to the third order nonlinear optical response function $R^{(3)}$. Making use of Eq. (3.2) we obtain for $R^{(3)}$

$$R_{nm_1m_2m_3}(t;t_1,t_2,t_3) =$$
$$\mathrm{i}^3\mu^4\langle (C_{n\cdot}(t) + \bar{C}_{n\cdot}(t))(C_{m_1\cdot}(t_1)\bar{C}_{m_1\cdot}(t_1))(C_{m_2\cdot}(t_2) + (\bar{C}_{m_2\cdot}(t_2))(C_{m_3\cdot}(t_3)$$
$$+ \bar{C}_{m_3\cdot}(t_3))\rangle_S. \tag{C.10}$$

First we describe a skeleton structure of diagrams contributing to $R_{nm_1m_2m_3}$ according with Eq. (C.10). The skeleton structure of a diagram is the topological structure of the solid lines and the vertices related to the exciton–exciton interactions. Since our Hamiltonian conserves the number of excitons, the skeleton diagrams cannot contain loops and they are, therefore, simply ladder diagrams ([46]). The skeleton diagrams are presented in Fig. 24a. Each diagram should be "decorated" in all possible ways with wavy and dashed lines and vertices as shown in Fig. 23(c)–(e). An example of such a diagram is presented in Fig. 24b.

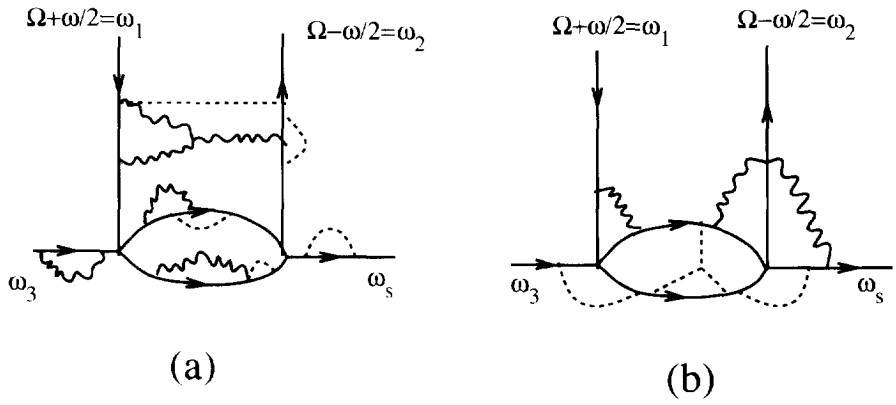

Fig. 25. (a) A typical diagram for the subclass. (b) A diagram which does not belong to this subclass. For this diagram to belong to this class one should remove all the wavy and dashed lines.

Switching to the frequency domain we define:

$$R(t;t_1,t_2,t_3)=\int\frac{d\omega_s}{2\pi}\frac{d\omega_1}{2\pi}\frac{d\omega_2}{2\pi}\frac{d\omega_3}{2\pi}\,2\pi\delta(\omega_1-\omega_2+\omega_3-\omega_s)$$

$$\times R(-\omega_s;\omega_1,-\omega_2,\omega_3)\exp(-i\omega_s t+i\omega_1 t_1-i\omega_2 t_2+i\omega_3 t_3)\,, \quad \text{(C.11a)}$$

$$\omega_s=\omega_1+\omega_3-\omega_2\,. \quad \text{(C.11b)}$$

We consider degenerate four-wave mixing, i.e., $\omega_2\approx\omega_1$ and use the following notation

$$\omega_1\equiv\Omega+\omega/2\,,\qquad \omega_2\equiv\Omega-\omega/2\,. \quad \text{(C.12)}$$

For small ω we will take into account contributions from a class of diagrams defined by "decorating" the skeleton diagrams. To obtain a diagram from the subclass we take a skeleton diagram, dress each exciton line individually and then dress together the pair of external lines with the frequencies ω_1 and ω_2 (see Fig. 25). The choice of diagrams has the following rationale: dressing lines individually gives the exciton self-energy which is important near resonances even for weak interactions; dressing the pair of lines together leads to enhancement of pairs of exciton Green functions in the diagram with close poles, each pair after integration over the internal frequency gives a factor $\sim\omega^{-1}$, which compensates the small factor of exciton–phonon and exciton–disorder interaction which arises in the procedure of dressing.

In the case of static disorder there is another source of resonant factors which comes from dressing together exciton lines carrying the frequencies ω_2 and ω_s when $\omega_s\approx\omega_2$ (see Fig. 27d). We will discuss this contribution in Section 10.

In this approximation we can express the nonlinear response function in terms of one-exciton and two-exciton Green functions G and $\mathscr{G}^{(2)}$ in the system without exciton–exciton interaction. These expressions reduce the problem of calculating the nonlinear response function to finding the exciton Green functions for a system of free bosons interacting with phonons and disorder. To define the Green functions G and $\mathscr{G}^{(2)}$, we introduce the action for the free boson system $S_f\equiv S|_{g=0}$

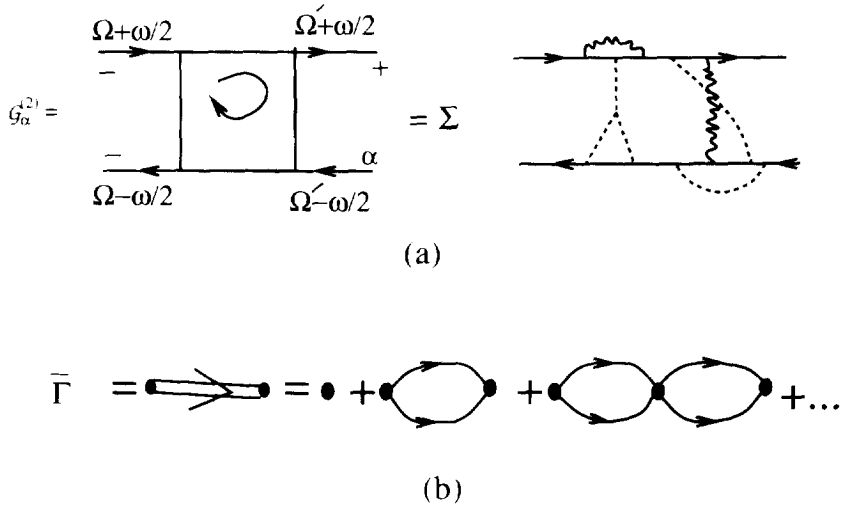

Fig. 26. Diagrammatic representation of the two exciton Green function $\mathcal{G}_\alpha^{(2)}$ (a), and the two-exciton scattering matrix $\bar{\Gamma}$ (b). A solid line stands for the one-exciton Green function G.

with the exciton–exciton interaction constant g to zero. The exciton Green functions can be presented as follows

$$G_{mn\alpha\beta}(\omega) = -\mathrm{i}\int \mathrm{d}t\, \exp(\mathrm{i}\omega(t-t'))\langle C_{m\alpha}(t)\bar{C}_{n\beta}(t')\rangle_{S_t} \tag{C.13a}$$

$$\mathcal{G}^{(2)}_{mnm'n'\alpha}(\Omega,\Omega';\omega) = \int \mathrm{d}t_1\,\mathrm{d}t_2\,\mathrm{d}t_3 \mathcal{G}^{(2)}_{mnm'n'\alpha}(t_1,t_2,t_3,t_4) \times \exp\left\{\mathrm{i}\Omega(t_1-t_2) - \mathrm{i}\Omega'(t_3-t_4) - \frac{\mathrm{i}\omega}{2}(t_1+t_2-t_3-t_4)\right\} \tag{C.13b}$$

where

$$\mathcal{G}^{(2)}_{mnm'n'\alpha}(t_1,t_2,t_3,t_4) \equiv \langle \bar{C}_{m-}(t_1)C_{n-}(t_2)C_{m'+}(t_3)\bar{C}_{n'\alpha}(t_4)\rangle_{S_t} - \langle \bar{C}_{m-}(t_1)C_{m'+}(t_3)\rangle_{S_t}\langle C_{n-}(t_2)\bar{C}_{n'\alpha}(t_4)\rangle_{S_t}\,. \tag{C.13c}$$

We will also write $G_{mn}(\omega)$ instead of $G_{mn+-}(\omega)$. The two-exciton Green function $\mathcal{G}^{(2)}$ has a diagrammatic expansion presented in Fig. 26a. We also introduce the two-exciton scattering matrix $\bar{\Gamma}_{mn}(\omega)$ as (see Fig. 26b for its diagrammatic representation):

$$\bar{\Gamma}_{mn}(\omega) = 2g\{[1-g\bar{F}(\omega)]^{-1}\}_{mn}\,, \qquad \bar{F}_{mn}(\omega) \equiv \int \frac{\mathrm{d}\omega'}{2\pi\mathrm{i}}\, G_{mn}(\omega')G_{mn}(\omega-\omega')\,. \tag{C.14a,b}$$

The Green function expression for the third-order nonlinear response function has the form of Eq. (6.4) (see Fig. 27(a)–(d) for its diagrammatic form).

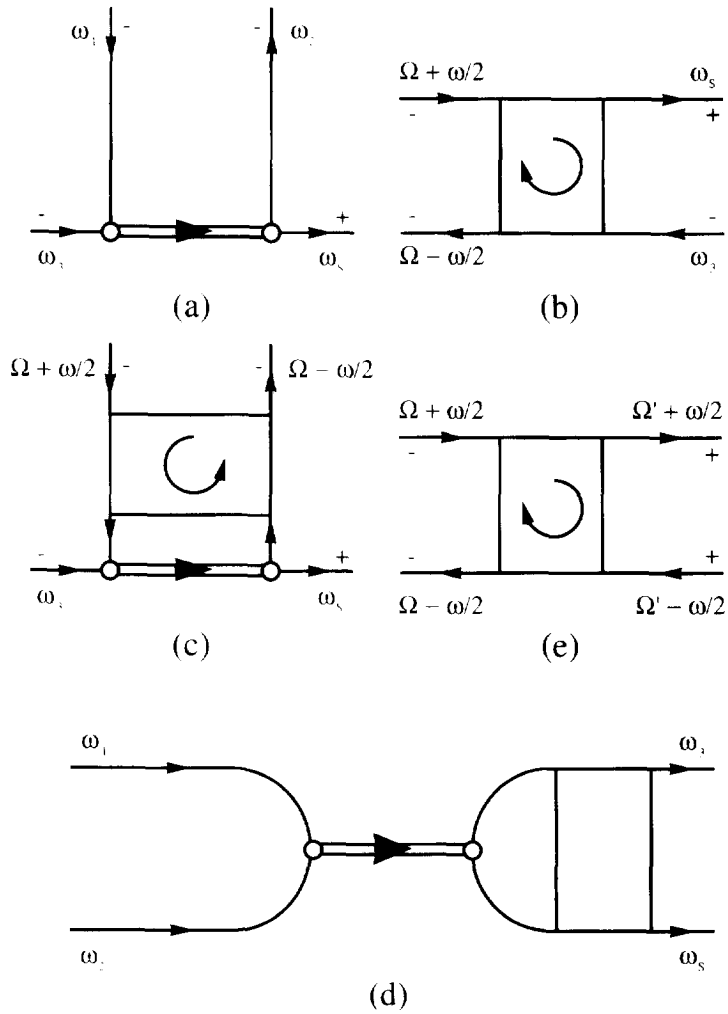

Fig. 27. (a)–(d) Diagrammatic representations of the contributions to the nonlinear response function $R^{(a)}$, $R^{(d)}$, $R^{(b)}$, and $R^{(c)}$ respectively. (e) Diagrammatic form of the luminescence signal.

The Green function expression for luminescence can be obtained starting with the correlation function (5.8b) and making use of the perturbation theory developed in this section. In the rotating wave approximation, the two-exciton states do not contribute, and the signal can be expressed in terms of the function $\mathscr{G}^{(2)}$, which leads to Eq. (9.11) (see Fig. 27e for its diagrammatic form).

Appendix D. Optical properties of periodic nanostructures with exciton–phonon interaction

In this appendix we derive expressions for the third order nonlinear optical response and the luminescence signal of a periodic molecules nanostructure with the exciton–phonon interaction, in

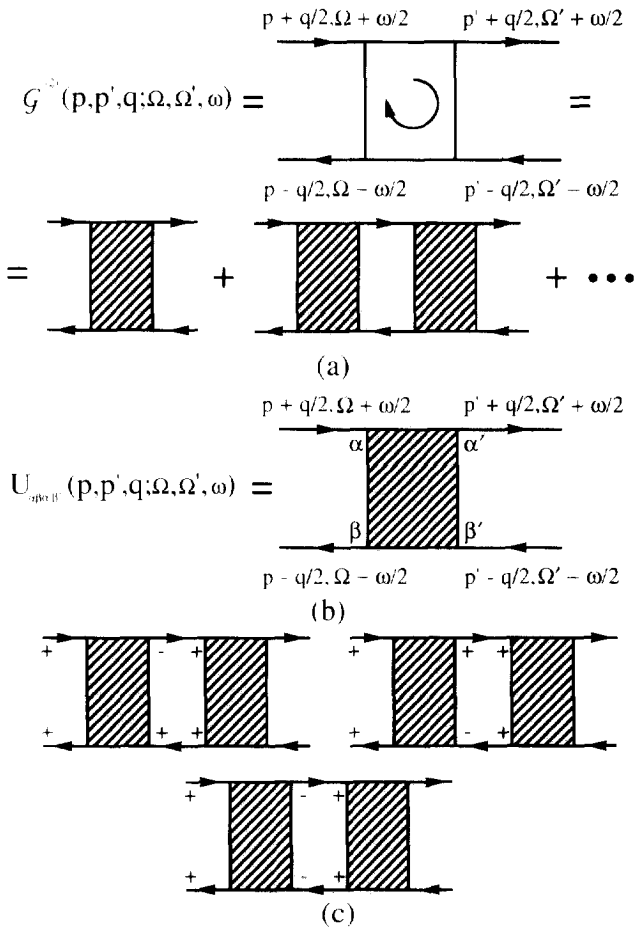

Fig. 28. (a) Expansion of the two-exciton Green function $\mathcal{G}^{(2)}$ in terms of its irreducible part U. (b) Diagrammatic representation for U. (c) Three possible sets of values of the Greek indices α in internal lines if the expansion from (a) to obtain large resonant factors.

terms of the Green function of the Boltzmann equation (Eqs. (7.3) and (9.12), together with (9.14)). We will also express the signals in terms of the eigenmodes of the collision operator of the Boltzmann equation (Eqs. (8.11) and (9.16)).

The one-exciton Green function in the momentum domain in the Markov approximation is given by Eq. (7.2).

The two-exciton Green function $\mathcal{G}^{(2)}$ can be expressed in terms of its two-particle irreducible part $U_{\alpha\beta\alpha'\beta'}(\boldsymbol{p}, \boldsymbol{p}', \boldsymbol{q}; \Omega, \Omega', \omega)$ as shown in Fig. 28. The function U is defined as the sum of all diagrams contributing to $\mathcal{G}^{(2)}$ which cannot be cut into two parts along two lines related to one-exciton Green functions which have poles in both half planes of the complex frequency space. Possible values of indices $\alpha = +, -$ which satisfy the latter conditions are presented in Fig. 28c. The summation of diagrams presented in Fig. 28c can be reduced to solving a linear integral equation. However, for Markovian transport one can obtain a much simpler equation. In the resonant

approximation ($\omega, \boldsymbol{q} \approx 0$) we take into account the poles of the one-exciton Green function only when integrating over internal frequencies in the expansion presented in Fig. 28a. Substituting the expansion of Fig. 28c into Eq. (6.4) and performing the integrations over internal frequencies using the above approximation, we can express the nonlinear response functions in terms of a function

$$\mathscr{L}(\boldsymbol{p}, \boldsymbol{p}', \omega) \equiv \int \frac{\mathrm{d}\Omega}{2\pi} \frac{\mathrm{d}\Omega'}{2\pi} \mathscr{G}_{+}^{(2)}(\Omega \boldsymbol{p}, \Omega' \boldsymbol{p}'; \boldsymbol{q}\omega) , \tag{D.1}$$

where $\mathscr{G}^{(2)}$ in Eq. (D.1) is the two-exciton Green function $\mathscr{G}^{(2)}_{mnm'n'}(\Omega, \Omega'; \omega)$ in the momentum domain.

To obtain $\bar{\Gamma}^{(b)}$ we switch to the momentum domain in Eq. (6.4c) and expand the Green function $\mathscr{G}^{(2)}$ in powers of the irreducible vertex U making use of the Bethe–Salpeter equation (Eq. (6.7)). Substituting this expansion into Eq. (6.4c) we get

$$\begin{aligned}
&\bar{\Gamma}^{(c)}(-\omega_s - \boldsymbol{k}_s; \omega_1 \boldsymbol{k}_1, -\omega_2 - \boldsymbol{k}_2, \omega_3 \boldsymbol{k}_3) \\
&= \sum_{n=1}^{\infty} \int \frac{\mathrm{d}\Omega}{2\pi} \cdots \frac{\mathrm{d}\Omega_n}{2\pi} \mathrm{d}\boldsymbol{p}_1 \cdots \mathrm{d}\boldsymbol{p}_j \prod_{j=1}^{n} U(\Omega_{j-1} \boldsymbol{p}_{j-1}, \Omega_j \boldsymbol{p}_j; \omega \boldsymbol{q}) \\
&\quad \times G\left(\Omega_j + \frac{\omega}{2}, \boldsymbol{p}_j + \frac{\boldsymbol{q}}{2}\right) G^*\left(\Omega_j - \frac{\omega}{2}, \boldsymbol{p}_j - \frac{\boldsymbol{q}}{2}\right) \bar{\Gamma}(\omega_3 + \Omega_n, \boldsymbol{k}_3 + \boldsymbol{p}_n) ,
\end{aligned} \tag{D.2a}$$

where we use the notation of Eq. (5.4) and set

$$\Omega_0 \equiv \tfrac{1}{2}(\omega_1 + \omega_2) , \qquad \boldsymbol{p}_0 \equiv \tfrac{1}{2}(\boldsymbol{k}_1 + \boldsymbol{k}_2) . \tag{D.2b}$$

Carrying out the integrations over $\Omega_j, j = 1, \ldots, n$ in Eq. (D.2a), and taking into account the poles of the Green functions G and G^* to obtain large resonant factors we get

$$\begin{aligned}
&\bar{\Gamma}^{(b)}(-\omega_s - \boldsymbol{k}_s; \omega_1 \boldsymbol{k}_1, -\omega_2 - \boldsymbol{k}_2, \omega_3 \boldsymbol{k}_3) \\
&= \sum_{n=1}^{\infty} \int \mathrm{d}\boldsymbol{p}_1 \cdots \mathrm{d}\boldsymbol{p}_n g(\boldsymbol{p}_1, \boldsymbol{k}; \Omega) \\
&\quad \times \prod_{j=2}^{n} \mathscr{f}(\boldsymbol{p}_j, \boldsymbol{p}_{j-1}) \prod_{j=1}^{n} \frac{1}{\omega - \varepsilon\left(\boldsymbol{p}_j + \frac{\boldsymbol{q}}{2}\right) + \varepsilon\left(\boldsymbol{p}_j - \frac{\boldsymbol{q}}{2}\right) + \mathrm{i}\Gamma(\boldsymbol{p}_j)} \bar{\Gamma}(\omega_3 + \varepsilon(\boldsymbol{p}_n), \boldsymbol{k}_3 + \boldsymbol{p}_n) ,
\end{aligned} \tag{D.3a}$$

where we have used the notation

$$\begin{aligned}
&\mathscr{f}(\boldsymbol{p}, \boldsymbol{p}') \equiv U(\boldsymbol{p}\varepsilon(\boldsymbol{p}), \boldsymbol{p}'\varepsilon(\boldsymbol{p}'); \boldsymbol{q} = 0, \omega = 0) , \\
&g(\boldsymbol{p}, \boldsymbol{p}'; \Omega) \equiv U(\boldsymbol{p}\varepsilon(\boldsymbol{p}), \boldsymbol{p}'\Omega; \boldsymbol{q} = 0, \omega = 0) .
\end{aligned} \tag{D.3b}$$

Performing the summation over n in Eq. (D.3a), applying the same procedure to the contribution $\bar{\Gamma}^{(d)}$ we finally obtain Eqs. 7.3(e) and (f).

The function $\mathscr{S}$ is a sum of an infinite number of terms through the expansion of $\mathscr{G}^{(2)}$. The summation is equivalent to solving the linear equation Eq. (7.5a) which is an equation for the Green function of the Boltzmann equation. The nonlinear optical response is given by Eqs. 7.3(e) and (f). The functions $\not{f}$, g, g_s, g_d and g_0 are expressed in terms of the function U in the following manner:

$$\not{f}(\boldsymbol{p},\boldsymbol{p}') \equiv U(\boldsymbol{p}',\boldsymbol{p},\boldsymbol{q}=0;\varepsilon(\boldsymbol{p}'),\varepsilon(\boldsymbol{p}),\omega=0)\,, \tag{D.4a}$$

$$U \equiv \tfrac{1}{2}(U_{+++\cdots} - U_{-+++\cdots}) + U_{++\cdots}\,, \tag{D.4b}$$

$$g(\boldsymbol{p},\boldsymbol{p}';\Omega) \equiv U(\boldsymbol{p}',\boldsymbol{p},\boldsymbol{q}=0;\Omega,\varepsilon(\boldsymbol{p}),\omega=0)\,, \tag{D.4c}$$

$$g_s(\boldsymbol{p},\boldsymbol{p}';\Omega) \equiv U(\boldsymbol{p}',\boldsymbol{p},\boldsymbol{q}=0;\varepsilon(\boldsymbol{p}'),\Omega,\omega=0)\,, \tag{D.4d}$$

$$g_d(\boldsymbol{p},\boldsymbol{p}';\Omega) \equiv U_{-+++\cdots}(\boldsymbol{p}',\boldsymbol{p},\boldsymbol{q}=0;\varepsilon(\boldsymbol{p}'),\Omega,\omega=0)\,, \tag{D.4e}$$

$$g_0(\boldsymbol{p}_s,\boldsymbol{p};\omega_s,\Omega) \equiv U_{-+++\cdots}(\boldsymbol{p},\boldsymbol{p}_s,\boldsymbol{q}=0;\Omega,\omega_s,\omega=0)\,. \tag{D.4f}$$

These functions are evaluated in Appendix E to the first nonvanishing order in the exciton–phonon coupling.

The phonon-induced self-energy Σ is presented in Fig. 18b, and can be related to the function $\not{f}$ by means of Eq. (7.2d). Note that Eq. (7.2d) reflects the exciton number conservation in the exciton–phonon interaction. The luminescence signal (Eq. (9.14)) is obtained by starting with Eq. (9.12) and then expressing the two-exciton Green function $\mathscr{G}^{(2)}$ in terms of the Green function $\mathscr{S}$.

We now express the signals in terms of the eigenmodes of the collision operator (Eqs. (8.11) and (9.16)). To that end we introduce an operator L acting in the space–exciton distributions $n(\boldsymbol{p})$

$$L = L_0 + L_d + L_1\,. \tag{D.5a}$$

where

$$(L_0)n(\boldsymbol{p}) \equiv -\left\{\int d\boldsymbol{p}'\, \not{f}(\boldsymbol{p},\boldsymbol{p}')n(\boldsymbol{p}') - n(\boldsymbol{p})\int d\boldsymbol{p}'\, \not{f}(\boldsymbol{p}',\boldsymbol{p})\right\}, \tag{D.5b}$$

$$(L_d)n(\boldsymbol{p}) \equiv \Gamma(\boldsymbol{p})n(\boldsymbol{p})\,, \tag{D.5c}$$

$$(L_1)n(\boldsymbol{p}) = i[\varepsilon(\boldsymbol{p}+\boldsymbol{q}/2) - \varepsilon(\boldsymbol{p}-\boldsymbol{q}/2)]n(\boldsymbol{p})\,. \tag{D.5d}$$

The operator L depends on $\boldsymbol{q}$ parametrically. In the notation of Eq. (D.5) the Green function $\mathscr{S}$ can be written making use of Eq. (7.5a) in the operator form:

$$\mathscr{S}(\boldsymbol{p},\boldsymbol{p}';\boldsymbol{q}\omega) = \langle \boldsymbol{p}|(-i\omega + L(\boldsymbol{q}))^{-1}|\boldsymbol{p}'\rangle\,. \tag{D.6}$$

$|\boldsymbol{p}_0\rangle$ in Eq. (D.6) is not related to one-exciton Green functions $B^{\dagger}_{p_0}|0\rangle$; rather it denotes a "state" in the space of functions $n(\boldsymbol{p})$ which has the form $n(\boldsymbol{p}) = \delta(\boldsymbol{p}-\boldsymbol{p}_0)$ and is related to the $\tilde{B}^{\dagger}_{p_0}\tilde{B}_{p_0}$ variable. The symbol $\langle \boldsymbol{p}|\cdots|\boldsymbol{p}'\rangle$ stands for a matrix element of an operator between two such states. It follows from (Eq. (D.6)) that the Green function $\mathscr{S}$ may be found by diagonalizing the operator $(-i\omega + L)$ numerically. However, when the relaxation rate is much smaller than the dephasing rate and when the time of diffusion at distances of the order of q^{-1} is much larger than

the time scale of the spectral diffusion, which is valid for sufficiently small q, this problem reduces to the diagonalization of the operator L_0. Let $\varphi_\alpha(\boldsymbol{p})$ be the eigenfunctions of the operator L_0 with the eigenvalue λ_α:

$$(L_0\varphi_\alpha)(\boldsymbol{p}) = \lambda_\alpha \varphi_\alpha(\boldsymbol{p}) \tag{D.7a}$$

and let $\bar{\varphi}_a(\boldsymbol{p})$ be the comodes:

$$\int \bar{\varphi}_\alpha(\boldsymbol{p})\varphi_\beta(\boldsymbol{p})\,\mathrm{d}\boldsymbol{p} = \delta_{\alpha\beta} \qquad \sum_\alpha \varphi_\alpha(\boldsymbol{p})\bar{\varphi}_\alpha(\boldsymbol{p}') = \delta(\boldsymbol{p}-\boldsymbol{p}') \tag{D.7b,c}$$

The comodes $\bar{\varphi}_\alpha(\boldsymbol{p})$ have the following meaning: $\varphi_a(\boldsymbol{p})$ are the matrix elements of the transformation from the $|\boldsymbol{p}\rangle$ basis set to the $|\alpha\rangle$ basis set, then $\bar{\varphi}_a(\boldsymbol{p})$ are the matrix elements of the inverse transformation. $|\lambda_\alpha - \lambda_\beta|$ are of the order of the dephasing rate. The zero mode with $\alpha = 0$, $\lambda_0 = 0$ is the equilibrium distribution

$$\varphi_0(\boldsymbol{p}) = \exp[-\varepsilon(\boldsymbol{p})/(kT)] \tag{D.8a}$$

regardless the form of the exciton–phonon interaction. Due to the exciton number conservation in the exciton–phonon interaction we have

$$\int \mathrm{d}\boldsymbol{p}\,\varphi_\alpha(\boldsymbol{p}) = 0\,, \quad \text{for } \alpha \neq 0\,. \tag{D.8b}$$

making use of Eqs. (D.7), D.8(a) and (b) we obtain

$$\bar{\varphi}_0(\boldsymbol{p}) = C \equiv \left\{\int \mathrm{d}\boldsymbol{p}\exp[-\varepsilon(\boldsymbol{p})/(kT)]\right\}^{-1} \tag{D.8c}$$

To invert the operator $(-\mathrm{i}\omega + L)$ for small ω and $\boldsymbol{q}$, one needs to evaluate the correction to the eigenvalue of the zero mode φ_0 of the operator L_0 to first-order in L_d and to second order in L_1. This procedure leads to Eq. (8.10). Eqs. (8.11) and (9.16) are obtained by substituting the representation (8.10) into Eqs. (7.3) and (9.14). Note that numerical diagonalization of the operator L is not very convenient since it is asymmetric (since $\mathcal{J}(\boldsymbol{p},\boldsymbol{p}')$ is not symmetric). To overcome this problem [85], we note that

$$\mathcal{J}(\boldsymbol{p},\boldsymbol{p}')\exp[-\varepsilon(\boldsymbol{p}')/(kT)] = \mathcal{J}(\boldsymbol{p}',\boldsymbol{p})\exp[-\varepsilon(\boldsymbol{p})/(kT)]\,, \tag{D.9}$$

and introduce a new quantity $\mathcal{L}'$

$$\mathcal{L}'(\boldsymbol{p},\boldsymbol{p}';\boldsymbol{q},\omega) = \exp\{[\varepsilon(\boldsymbol{p}) - \varepsilon(\boldsymbol{p}')]/(2kT)\}\mathcal{L}(\boldsymbol{p},\boldsymbol{p}';\boldsymbol{q},\omega)\,. \tag{D.10}$$

$\mathcal{L}'$ satisfy the equation

$$-\mathrm{i}\omega\mathcal{L}'(\boldsymbol{p},\boldsymbol{p}') + \int \mathrm{d}\boldsymbol{p}''\,L'(\boldsymbol{p},\boldsymbol{p}'')\mathcal{L}'(\boldsymbol{p}'',\boldsymbol{p}') = \delta(\boldsymbol{p}-\boldsymbol{p}')\,, \tag{D.11}$$

where $L' = L_0' + L_d + L_1$, and

$$L_0'(\boldsymbol{p},\boldsymbol{p}') = 2\Sigma(\boldsymbol{p})\delta(\boldsymbol{p}-\boldsymbol{p}') - \exp\{[\varepsilon(\boldsymbol{p}) - \varepsilon(\boldsymbol{p}')]/(2kT)\}\,\mathcal{J}(\boldsymbol{p},\boldsymbol{p}')\,. \tag{D.12}$$

Eq. (D.9) gaurantees that L' is a symmetric matrix. It is much easier to calculate $\mathscr{D}'$ than to calculate $\mathscr{D}$ since one need to diagonalize a symmetric matrix. We finally have

$$\mathscr{D}(\boldsymbol{p},\boldsymbol{p}';\boldsymbol{q},\omega)=\exp\{[\varepsilon(\boldsymbol{p}')-\varepsilon(\boldsymbol{p})]/(2kT)\}\left\langle \boldsymbol{p}\left|\frac{1}{-i\omega+L'}\right|\boldsymbol{p}'\right\rangle , \tag{D.13}$$

and matrix L' can also be viewed as an operator, $\langle \boldsymbol{p}|L'|\boldsymbol{p}'\rangle = L'(\boldsymbol{p},\boldsymbol{p}')$. The matrix L'_0 can be diagonalized numerically. However, when the damping rate is much smaller than the dephasing rate and when the diffusion time at distances of the order q^{-1} is much longer than the time scale of the spectral diffusion (which is the case for sufficiently small q), this problem can be reduced to the diagonalization of the matrix L'_0.

Appendix E. Perturbative expressions for the functions γ, g, g_s and g_d

In this appendix we calculate the functions γ, g, g_s and g_d, which enter the Green function expressions for four-wave mixing and the luminescence. We will do so for several models of exciton–phonon interaction in the weak coupling limit, applying perturbation theory to lowest non-vanishing order.

All of these functions are expressed in terms of the irreducible two-exciton Green function $U_{\alpha\beta\alpha'\beta'}$ (Eq. (D.4)), which is presented to first-order by a diagram shown in Fig. 29a. To evaluate these functions we need to specify the phonon part of the material Hamiltonian in which we set the exciton–exciton coupling g to zero ($g=0$).

We start with a model of harmonic phonons ($h_{\rm ph}=0$), with exciton–phonon interaction linear in the phonon operators. The Hamiltonian $\hat{H}_{\rm m}$ with $g=0$ can be written in the momentum domain in the following form:

$$\hat{H}_{\rm m}=\int d\boldsymbol{q}\{\varepsilon(\boldsymbol{q})\hat{C}_q^{\dagger}\hat{C}_q+\Omega(\boldsymbol{q})\hat{b}_q^{\dagger}\hat{b}_q\}$$
$$+\int d\boldsymbol{p}\,d\boldsymbol{q}\{V(\boldsymbol{q},\boldsymbol{q}-\boldsymbol{p})\hat{C}_p^{\dagger}\hat{C}_q\hat{b}_{q-p}^{\dagger}+V^*(\boldsymbol{q},\boldsymbol{q}-\boldsymbol{p})\hat{C}_q^{\dagger}\hat{C}_p b_{q-p}^{+}\}. \tag{E.1}$$

The first two terms are the exciton and the phonon energy, and the third is the exciton–phonon interaction. The functions γ, g, g_s and g_d are presented diagrammatically in Fig. 29(b)–(e). They may be expressed in terms of the bare phonon Green function $K^{(0)}(\omega,\boldsymbol{q})$ defined as

$$\langle b_{n\alpha}(t)\bar{b}_{m\beta}(t')\rangle_{S_{\rm ph}^{(0)}}=\int\frac{d\omega}{2\pi}\,d\boldsymbol{q}\,K^{(0)}_{\alpha\beta}(\omega,\boldsymbol{q})e^{-i\omega(t-t')+i\boldsymbol{q}(\boldsymbol{R}_n-\boldsymbol{R}_m)} \tag{E.2}$$

we thus obtain

$$\gamma(\boldsymbol{p},\boldsymbol{p}')=2\pi|V(\boldsymbol{p}',\boldsymbol{p}'-\boldsymbol{p})|^2(1+N[\Omega(\boldsymbol{p}'-\boldsymbol{p})])\delta[\varepsilon(\boldsymbol{p})-\varepsilon(\boldsymbol{p}')+\Omega(\boldsymbol{p}'-\boldsymbol{p})]$$
$$+2\pi|V(\boldsymbol{p},\boldsymbol{p}-\boldsymbol{p}')|^2N[\Omega(\boldsymbol{p}-\boldsymbol{p}')]\delta[\varepsilon(\boldsymbol{p})-\varepsilon(\boldsymbol{p}')+\Omega(\boldsymbol{p}'-\boldsymbol{p})], \tag{E.3a}$$

$$g(\boldsymbol{p},\boldsymbol{q}_0;\Omega)=2\pi|V(\boldsymbol{q}_0,\boldsymbol{q}_0-\boldsymbol{p})|^2(1+N[\Omega(\boldsymbol{q}_0-\boldsymbol{p})])\delta[\Omega-\varepsilon(\boldsymbol{p})-\Omega(\boldsymbol{q}_0-\boldsymbol{p})]$$
$$+2\pi|V(\boldsymbol{p},\boldsymbol{p}-\boldsymbol{q}_0)|^2N[\Omega(\boldsymbol{p}-\boldsymbol{q}_0)]\delta[\Omega-\varepsilon(\boldsymbol{p})+\Omega(\boldsymbol{p}-\boldsymbol{q}_0)], \tag{E.3b}$$

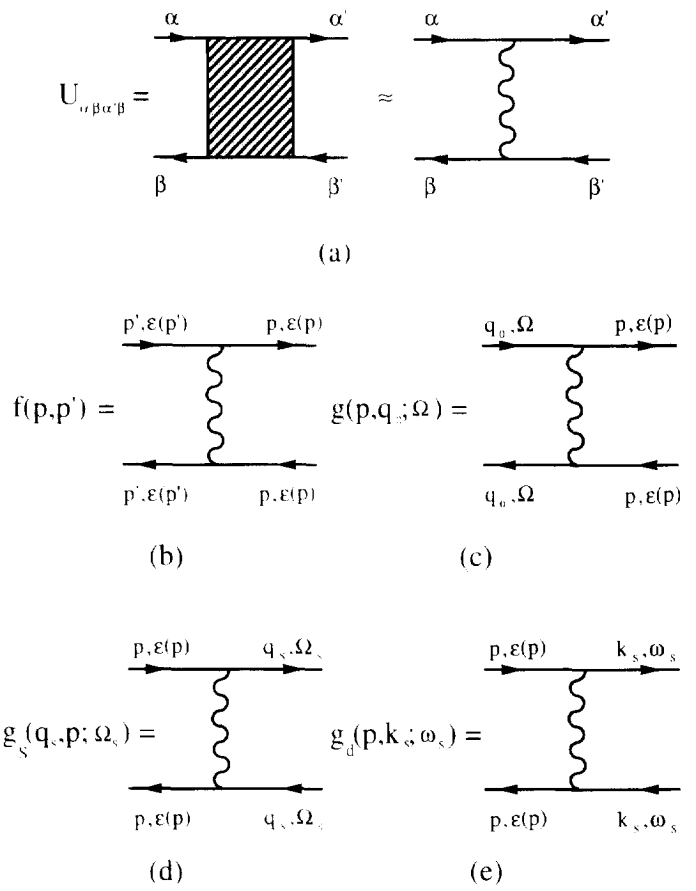

Fig. 29. (a) Diagrammatic representation for the function $U_{\alpha\beta\alpha'\beta'}$ in the first-order perturbation theory (b)–(e). Diagrammatic form of the functions f, g, g_s, g_d respectively.

$$g_s(\boldsymbol{q}_s, \boldsymbol{p}; \Omega_s) = 2\pi |V(\boldsymbol{p}, \boldsymbol{p} - \boldsymbol{q}_s)|^2 (1 + N[\Omega(\boldsymbol{p} - \boldsymbol{q}_s)]) \delta[\Omega_s - \varepsilon(\boldsymbol{p}) + \Omega(\boldsymbol{p} - \boldsymbol{q}_s)] + 2\pi |V(\boldsymbol{q}_s, \boldsymbol{q}_s - \boldsymbol{p})|^2 N[\Omega(\boldsymbol{q}_s - \boldsymbol{p})] \delta[\Omega_s - \varepsilon(\boldsymbol{p}) - \Omega(\boldsymbol{q}_s - \boldsymbol{p})] , \tag{E.3c}$$

$$g_d(\boldsymbol{p}, \boldsymbol{k}_s; \omega_s) = |V(\boldsymbol{p}, \boldsymbol{p} - \boldsymbol{k}_s)|^2 \frac{1}{-\omega_s + \varepsilon(\boldsymbol{p}) - \Omega(\boldsymbol{p} - \boldsymbol{k}_s) + i0} + |V(\boldsymbol{k}_s, \boldsymbol{k}_s - \boldsymbol{p})|^2 \frac{1}{\omega_s - \varepsilon(\boldsymbol{p}) - \Omega(\boldsymbol{k}_s - \boldsymbol{p}) - i0} . \tag{E.3d}$$

$N(\Omega)$ are the Bose occupation numbers at temperature T.

$$N(\Omega) = [\exp(\Omega/kT) - 1]^{-1} \tag{E.4}$$

We will also derive expressions for the functions in the Haken–Stroble model (see [5]) where $f(\boldsymbol{p}, \boldsymbol{p}')$ is independent of $\boldsymbol{p}$ and $\boldsymbol{p}'$, i.e.,

$$f(\boldsymbol{p}, \boldsymbol{p}') = \text{const.} \tag{E.5}$$

To obtain the functions g, g_s and g_d, we need to introduce a physical realization of a model which satisfies the condition of Eq. (E.5). This is the model with uncorrelated on-site baths. The material Hamiltonian has the following form

$$\hat{H}_m = \sum_n \Omega^{(0)} \hat{C}_n^+ C_n \sum_{m \neq n} J_{mn}^{(0)} \hat{C}_m^+ C_n + \sum_n \int_0^\infty d\varepsilon_n \, n(\varepsilon_n) \varepsilon_n \hat{b}_{n\varepsilon_n}^+ \hat{b}_{n\varepsilon_n}$$
$$+ \sum_n \int_0^\infty d\varepsilon_n \, n(\varepsilon_n) a(\varepsilon_n) \hat{C}_n^+ \hat{C}_n (\hat{b}_n + \hat{b}_n^+) \,. \tag{E.6}$$

To satisfy Eq. (E.5) we assume that the exciton band width W is much smaller than the temperature $W \ll T$, so that for $\omega \leqslant W$ we can put

$$N(\omega) \approx N(\omega) + 1 \approx kT/\omega \,. \tag{E.7a}$$

We will also assume that the bath density of states $n(\varepsilon)$ and the exciton–bath coupling $a(\varepsilon)$ satisfy

$$n(\varepsilon)(a(\varepsilon))^2 = u_0 \varepsilon \,. \tag{E.7b}$$

Evaluating the functions $\not{f}$, g, g_s and g_d using the diagrammatic form presented in Fig. 29 and substituting the Green function $K^{(0)}$ from Eq. (E.2) and the bare exciton–bath vertex obtained from the Hamiltonian (E.6) we get:

$$\not{f}(\boldsymbol{p}, \boldsymbol{p}') = u_0 T \,. \tag{E.8a}$$

When the detuning of all frequencies in the function g, g_s and g_d from the exciton band is much smaller than the temperature T we also have

$$g(\boldsymbol{p}, \boldsymbol{q}_0; \Omega) = u_0 T \tag{E.8b}$$

$$g_s(\boldsymbol{q}_s, \boldsymbol{p}; \Omega) = u_0 T \tag{E.8c}$$

$$g_d(\boldsymbol{p}, \boldsymbol{k}_s; \omega_s) = \int_0^\infty d\varepsilon \, [2\varepsilon^2 / ([\omega_s - \varepsilon(\boldsymbol{p})]^2 - \varepsilon^2 + i0)] \tag{E.8d}$$

The integral in the r.h.s. of Eq. (E.8d) is divergent. We, therefore, need to use a more realistic model to obtain g_d, for example we can restrict the possible bath energies by an energy ε_0 and put ε_0 instead of ∞ in the upper limit of the integral.

Appendix F. Green function expressions for optical signals in disordered molecular aggregates; the role of energy transport

In this appendix we derive expressions for the signals in disordered molecular aggregates (Eqs. (10.2)–(10.4) and (10.8)).

To calculate $\bar{\Gamma}^{(b)}$ we need to perform the summation of diagrams presented in Fig. 18a. We are interested in spectral transport which has the time scale of the exciton–phonon dephasing time, which is much longer than the elastic dephasing time. Elastic scattering leads to a homogeneous distribution of exciton populations for a fixed energy on the time scale of the elastic dephasing rate. This means that spectral transport takes place in energy space, and one can end up with an

equation describing the evolution of the exciton population as the function of energy. Formally this equation can be derived making use of a standard approach of eliminating first the fast processes. In our specific case this means that we first make the summation over all diagrams with a fixed number of phonon lines. The result of summation over ladder diagrams with disorder lines between two phonon lines for small ω and $\boldsymbol{q}$ is given by a function $L(\boldsymbol{p}, \boldsymbol{p}', \varepsilon; \boldsymbol{q}\omega)$ which depends on the initial and final exciton momentum in scattering on disorder ($\boldsymbol{p}$ and $\boldsymbol{p}'$) and its energy ε, and has the form

$$L(\boldsymbol{p}, \boldsymbol{p}', \varepsilon; \boldsymbol{q}\omega) = |G(\boldsymbol{p}, \varepsilon)|^2 |G(\boldsymbol{p}', \varepsilon)|^2 \sigma^4 \rho(\varepsilon) \times \frac{1}{i\omega - \Gamma_0(\varepsilon) - \Gamma_{ph}(\varepsilon) - D(\varepsilon)\boldsymbol{q}^2} \tag{F.1}$$

where $\Gamma_{ph}(\varepsilon)$ is due to the exciton–phonon interaction self-energy, and can be written in the form of Eq. (10.6b) with F from Eq. (10.5).

Making use of Eq. (F.1) we can write the result of summation of diagrams in Fig. 18d with all possible number of phonon lines in a form

$$\begin{aligned}
&\bar{\Gamma}^{(b)}(\omega_s \boldsymbol{k}_s; \omega_1 \boldsymbol{k}_1, -\omega_2 - \boldsymbol{k}_2, \omega_3 \boldsymbol{k}_3) \\
&= \sum_{n=0}^{\infty} \int d\boldsymbol{p} \frac{\sigma^4 \rho(\frac{1}{2}(\omega_1 + \omega_2))}{i\omega - \Gamma_0(\frac{1}{2}(\omega_1 + \omega_2)) - \Gamma_{ph}(\frac{1}{2}(\omega_1 + \omega_2)) - D(\frac{1}{2}(\omega_1 + \omega_2))\boldsymbol{q}^2} \\
&\quad \times \prod_{j=1}^{n} \int \frac{d\Omega_j}{2\pi} \frac{\rho(\Omega_j) F(\Omega_j, \Omega_{j-1})}{i\omega - \Gamma_0(\Omega_j) - \Gamma_{ph}(\Omega_j) - D(\Omega_j)\boldsymbol{q}^2} \\
&\quad \times |G(\Omega_n, \boldsymbol{p})|^2 \bar{\Gamma}(\omega_3 + \Omega_n, \boldsymbol{p} + \boldsymbol{k}_3)
\end{aligned} \tag{F.2}$$

with $\Omega_0 \equiv \frac{1}{2}(\omega_1 + \omega_2)$, and $F(\varepsilon, \varepsilon')$ given by Eq. (10.5).

Reducing the summation over n in Eq. (F.2) to solving a linear integral equation we get Eqs. (10.2)–(10.4). Eq. (10.8) can be derived in a similar manner.

Appendix G. The multidimensional spectral density $\kappa(\varepsilon', \varepsilon, \varepsilon'')$

In this appendix we present a scheme for the derivation of the Green function expressions (Eqs. (12.8) and (12.9)) for the multidimensional spectral density function $\kappa(\varepsilon', \varepsilon, \varepsilon'')$ of a molecular nanostructure defined in Section 12 (see Eq. (12.3)).

In Section 12 the spectral density κ was expressed in terms of a four-point correlation function of the polarization operators in a system without external sources (see Eqs. (12.5) and (12.6)). In this correlation function expression for κ, the polarization operators are not ordered with respect to times. To apply the Green function technique for this correlation function we follow [23] and introduce a time loop consisting of four-time axis as it is shown in Fig. 30a; this is a generalization of the Keldysh time loop [81, 82] which consists of two-time axis. We will denote the number of the axis by Greek indices which take the values 1, 2, 3 and 4. For a complete set of system variables Q we introduce the trajectories $Q^{(\alpha)}(t)$ with

$$\begin{aligned}
&Q^{(1)}(t = +\infty) = Q^{(2)}(t = +\infty), \qquad Q^{(2)}(t = -\infty) = Q^{(3)}(t = -\infty), \\
&Q^{(3)}(t = +\infty) = Q^{(4)}(t = +\infty)
\end{aligned} \tag{G.1}$$

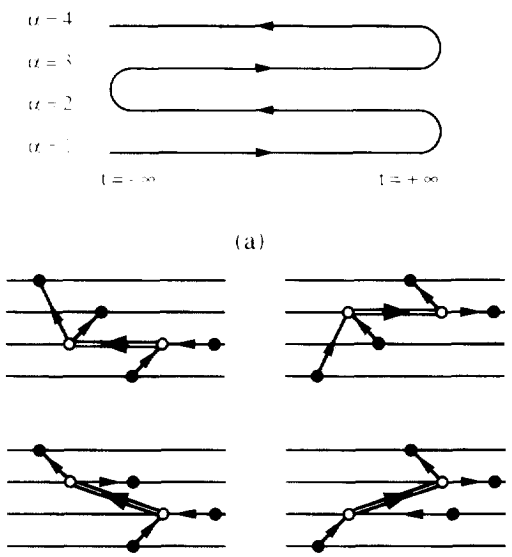

Fig. 30. The multidimensional spectral density of $\kappa(\omega', \omega, \omega')$ in molecular nanostructures. (a) Four-component time loop (b)–(e). All possible skeleton diagrams contributing to $\langle \hat{P}(t_4)\hat{P}(t_3)\hat{P}(t_2)\hat{P}(t_1)\rangle$ with respect to positions of time arguments on the four-component time loop.

according to the structure of the loop in Fig. 30a. The analogue of the Keldysh action $S^{(k)}$ is the action $\hat{S}$ defined as

$$\hat{S} = \sum_{\alpha=1}^{4} (-1)^{\alpha-1} S^{(\alpha)}, \quad S^{(\alpha)} \equiv S[Q^{(\alpha)}(t)] \tag{G.2}$$

where $S[Q(t)]$ is the action of the system.

The path-integral representation for the correlation function (Eq. (12.6)) has the following form

$$\langle \hat{P}(t_4)\hat{P}(t_3)\hat{P}(t_2)\hat{P}(t_1)\rangle = \langle P^{(4)}(t_4)P^{(3)}(t_3)P^{(2)}(t_2)P^{(1)}(t_1)\rangle_{\hat{S}} \tag{G.3a}$$

with

$$P^{(\alpha)}(t) = \mu \sum_{n} [C_n^{(\alpha)}(t) + \bar{C}_n^{(\alpha)}(t)], \tag{G.3b}$$

where C and $\bar{C}$ are the classical variables corresponding to the operators $\hat{C}$ and $\hat{C}^+$ (we work with the system of interacting bosons defined by Eq. (6.1), the same as in Appendix C). At this point, we can make use of the path-integral representation (G.3) and follow the procedure of Appendix C. The only difference between the Green function technique used here and the Green function technique of Appendix C is that the additional index α denoting the number of a time axis in the loop takes four values $\alpha = 1, 2, 3, 4$ instead of two $i = \mathrm{L}, \mathrm{R}$ (or, alternatively $\alpha = +, -$). The calculations become more tedious but they do not differ conceptually from those of Appendix C, and we can make the same choice of diagrams (perturbative contributions) as in Appendix C. The function κ can be presented in the form of Eq. (12.7a), the contributions $\kappa^{(a)}$, $\kappa^{(b)}$, and $\kappa^{(c)}$ depend on exciton–exciton scattering (they are q-dependent), the contributions $\kappa^{(d)}$ and $\kappa^{(0)}$ do not depend on

g and one can set $g = 0$ when calculating these contributions.

$\kappa^{(0)}$ has the form

$$\kappa^{(0)}(\varepsilon', \varepsilon, \varepsilon'') = 4\pi\mu^4 \operatorname{Im} G(\varepsilon') \operatorname{Im} G(\varepsilon'')\delta(\varepsilon) - 4\pi\mu^4 \operatorname{Im} G(\varepsilon') \operatorname{Im} G(\varepsilon'')\delta(\varepsilon'' + \varepsilon' - \varepsilon) - 4\pi\mu^4 \operatorname{Im} G(\varepsilon') \operatorname{Im} G(\varepsilon - \varepsilon')\delta(\varepsilon'' - \varepsilon') , \tag{G.4}$$

where $G(\omega) \equiv G(\omega, \boldsymbol{k} = 0)$ (see Section 12).

When $\kappa^{(0)}$ is substituted into the Kramers–Kronig representation Eq. (12.4) we get zero, i.e., this term does not contribute to the nonlinear response since it is related to a free-boson system. The contribution $\kappa^{(d)}$ is an exciton–phonon interaction induced term in a system without the exciton–exciton interaction (a free-boson system interacting with the phonons in our notation). The skeleton diagrams contributing to the exciton–exciton scattering induced terms are presented in Fig. 30(b)–(e). Applying the procedure of Appendix C we obtain the GFE for κ in terms of G, $\mathscr{G}^{(2)}$, and $\bar{\Gamma}$ (the contributions $\kappa^{(a)}$, $\kappa^{(b)}$, and $\kappa^{(c)}$ are the analogues of the contributions $R^{(a)}$, $R^{(b)}$, and $R^{(c)}$ to the nonlinear response). Expressing $\mathscr{G}^{(2)}$ in terms of $\mathscr{L}$, and $\mathscr{D}$ in terms of the modes φ_α, $\bar{\varphi}_\alpha$ (see Appendix D and Appendix F) we finally obtain Eqs. (12.8) and (12.9).

References

[1] A.S. Davydov, Theory of Molecular Excitons (Plenum, New York, 1971).

[2] E.I. Rashba and M.D. Sturge, eds., Excitons (North-Holland, Amsterdam, 1982); V.B. Broude, E.I. Rashba and E.F. Sheka, Spectroscopy of Molecular Excitons (Springer, Berlin, 1985).

[3] M. Pope and C.E. Swenberg, Electronic Processes in Organic Crystals (Oxford, New York, 1982).

[4] R.S. Knox, Theory of Excitons (Academic, New York, 1963); E.A. Silinsh, Organic Molecular Crystals (Springer, Heidelberg, 1980).

[5] J. Knoester and S. Mukamel, Phys. Rep. 205 (1991) 1.

[6] G. Scheibe, Angew. Chem. 50 (1937) 212; E.E. Jelly, Nature 10 (1937) 631.

[7] A.H. Hertz, Adv. Colloid Interface Sci. 8 (1977) 237.

[8] D. Möbius and H. Kuhn, J. Appl. Phys. 64 (1988) 5138; D. Möbius and H. Kuhn, Isr. J. Chem. 18 (1979) 375.

[9] E.W. Knapp, P.O.J. Scherer and S.F. Fischer, Chem. Phys. Lett. 111 (1984) 481; E.W. Knapp, Chem. Phys. Lett. 85 (1984) 73.

[10] Advanced Materials, Special issue on Laser Spectroscopy and Organic Dyes (1994).

[11] F.C. Spano, J.R. Kuklinski and S. Mukamel, Phys. Rev. Lett. 65 (1990) 211; A.A. Muenter, D.V. Brumbaugh, J. Apolito, L.A. Horn, F.C. Spano and S. Mukamel, J. Phys. Chem. 92 (1992) 2783.

[12] H. Fidder, J. Knoester and D.A. Wiersma, Chem. Phys. Lett. 171 (1990) 529.

[13] T. Tani, T. Suzumoto, K. Kemnitz and K. Yoshihara, J. Phys. Chem. 96 (1992) 2778; A.E. Johnson, S. Kumazaki and K. Yoshihara, Chem. Phys. Lett. 211 (1993) 511.

[14] F.C. Spano and S. Mukamel, Phys. Rev. A 40 (1989) 5783; F.C. Spano and S. Mukamel, Phys. Rev. Lett. 66 (1991) 1197; F.C. Spano and S. Mukamel, J. Chem. Phys. 95 (1991) 7526.

[15] H. Ishihara and K. Cho, Phys. Rev. B 42 (1990) 1724; Z.K. Tang, A. Yanase, T. Yasui, Y. Segawa and K. Cho, Phys. Rev. Lett. 71 (1993) 1431; H. Ishihara and K. Cho, Mol. Cryst. Liq. Cryst. Sci. Technol. B 4 (1993) 81; Int. J. Nonlinear Opt. Phys. 1 (1992) 287.

[16] H. Fidder, J. Knoester and D.A. Wiersma, J. Chem. Phys. 98 (1993) 6564; A.E. Johnson, S. Kumazaki and K. Yoshihara, Chem. Phys. Lett. 211 (1993) 511; K. Minoshima, M. Taiji, K. Misawa and T. Kobayashi, Chem. Phys. Lett. 218 (1994) 67.

[17] Proc. 6th Int. Symp. on Small Particles and Inorganic Clusters [Special Issue Z. Phys. D 26 (1993)]; K.E. Schriver, M.Y. Hahn and R.L. Whetten, Phys. Rev. Lett. 59 (1987) 1906; J. Wörmer, M. Joppien, G. Zimmer and T. Möller, Phys. Rev. Lett. 67 (1991) 2053; Q. Liu, J.-K. Wang and A.H. Zewail, Nature 364 (1993) 427.

[18] S. Chemla and J. Zyss, Nonlinear Optical Properties of Organic Molecules and Crystals, Vols. I and II (Academic, New York, 1987).
[19] G. Roberts, ed., Langmuir-Blodgett Films (Plenum, New York, 1990).
[20] M. Orrit and Ph. Kottis, Adv. Chem. Phys. 74 (1988) 1; M. Orrit, C. Aslangul and Ph. Kottis, Phys. Rev. B 25 (1982) 7263.
[21] E.I. Haskal, Y. Zhang, P.E. Burrows and S.R. Forrest, Chem. Phys. Lett. 219 (1994) 325; F.F. So, S.R. Forrest, Y.Q. Shi and W.H. Steier, Appl. Phys. Lett. 56 (1990) 674; F.F. So and S.R. Forrest, Phys. Rev. Lett. 66 (1991) 2649.
[22] H. Hoshi, K. Kohama, S. Fang and Y. Maruyama, Appl. Phys. Lett. 62 (1993) 3080.
[23] N. Wang, V. Chernyak and S. Mukamel, J. Chem. Phys. 100 (1994) 2465; N. Wang, V. Chernyak and S. Mukamel, Phys. Rev. B 50 (1994) 5609.
[24] C. Flytzanis and J. Hutter, Contemporary Nonlinear Optics (Academic Press, New York, 1992) pp. 297–365.
[25] S. Schmitt-Rink, D.S. Chemla and D.A.B. Miller, Adv. Phys. 38 (1989) 89; A. D'Andrea and R. Del Sole, Phys. Rev. B 25 (1982) 3714; in: *Excitons in Confined Systems*, eds. R. Del Sole, A. D'Andrea and A. Lapiccirella (Springer, New York, 1987); R. Zimmerman, editor, Nonlinear Optics and Excitation Kinetics in Semiconductors, special issue Phys. Stat. Sol. (b) 188(1) (1995).
[26] H. Haug and S.W. Koch, Quantum Theory of the Optical and Electronic Properties of Semiconductors (World Scientific, New Jersey, 1990).
[27] R. Eccleston, B.F. Feuerbacher, J. Kuhl, W.W. Rühle and K. Ploog, Phys. Rev. B. 45 (1992) 11403; D.S. Citrin, Solid State Commun. 84 (1992) 281.
[28] M.L. Steigerwald and L.E. Brus, Acc. Chem. Res. 23 (1990) 183; M. Bawendi, M.L. Steigerwald and L.E. Brus, Ann. Rev. Phys. Chem. 44 (1990) 21.
[29] G.R. Fleming and R. Van Grondelle, Physics Today 47 (1994) 48; J. Breton, J.-L. Martin, J.C. Lambry, S.J. Robles and D.C. Youvan, in: *Reaction Centers of Photosynthetic Bacteria*, ed. M.E. Michel-Byerle (Springer, New York, 1990) p. 293.
[30] M.H. Vos, F. Rappaport, J.-C. Lambry, J. Breton and J.L. Martin, Nature 363 (1993) 320.
[31] R. Van Grondelle, J.P. Dekker, T. Gillbro and V. Sundstrom, Biochimica et Biophysica Acta 1187 (1994) 1.
[32] Th. Förster, Ann. Phys. (Leipzig) 2 (1948) 55; D.L. Dexter, J. Chem. Phys. 21 (1953) 836.
[33] V.L. Colvin, M.C. Schlamp and A.P. Alivisatos, Nature 370 (1994) 354.
[34] N.C. Greenham, S.C. Moratti, D.D.C. Bradley, R.H. Friend and A.B. Holmes, Nature 365 (1993) 628; A.H. Burroughes, D.D.C. Bradley, A.R. Brown, R.N. Marks, K. Mackay, R.H. Friend, P.L. Burns and A.B. Holmes, Nature 347 (1990) 539.
[35] S.A. Jenekhe and J.A. Osaheni, Science 265 (1994) 765.
[36] A. Garito, R.F. Shi and M. Wu, Physics Today 47 (1994) 51; M.G. Kuzyk, J.D. Swalen, eds., Nonlinear Opt. 6 (1993); G.J. Ashwell, D. Bloor, eds., in: Organic Materials for Nonlines Optics III, Proc. Int. Symp. on Organic Materials for Nonlinear Optics, R. Soc. Chem. (Oxford, England, 1993); Z.G. Soos and G.W. Hayden, in: Electroresponsive and Polymeric Systems, ed. T.A. Skothein, Vol. 1 (Marcel Dekker, New York, 1988); S. Etemad and Z.G. Soos, in: Spectroscopy of Advanced Materials, eds. R.J.H. Clark and R.E. Hester (Wiley, New York, 1991); J.L. Bredas, C. Adant, P. Tackx, A. Persoons and B.M. Pierce, Chem. Rev. 94 (1994) 243; S. Mukamel, A. Takahashi and H.X. Wang, Science 266 (1994) 250.
[37] S. Mukamel, Principles of Nonlinear Optical Spectroscopy (Oxford, New York, 1995).
[38] R. Kopelman, in: Topics in Applied Physics, eds. W.M. Yen and P.M. Selzer, 49 (Springer, Berlin, 1981) p. 241; R. Kopelman, in: Spectroscopy and Excitation Dynamics of Condensed Molecular Systems, eds. V.M. Agranovich and R.M. Hochstrasser (North-Holland, Amsterdam, 1983) p. 139.
[39] V.M. Agranovich and M.D. Galanin, Electronic Excitation Energy Transfer in Condensed Matter, eds. V.M. Agranovich and A.A. Maradudin (North-Holland, Amsterdam, 1982).
[40] V.M. Agranovich and O. Dubovsky, Soviet Phys. JETP Lett. 3 (1966) 223.
[41] R.H. Lehmberg, Phys. Rev. A 2 (1970) 883.
[42] J. Feldmann, G. Peter, E.O. Göbel, P. Dawson, K. Moore, C. Foxon and R.J. Elliot, Phys. Rev. Lett. 59 (1987) 2337.
[43] E.T.J. Nibbering, D.A. Wiersma and K. Duppen, Phys. Rev. Lett. 66 (1991) 2464; E.T.J. Nibbering, D.A. Wiersma and K. Duppen, Phys. Rev. Lett. 68 (1992) 514.
[44] R.W. Schoenlein, D.M. Mittleman, J.J. Shiang, A.P. Alivisatos and C.V. Shank, Phys. Rev. Lett. 70 (1993) 1014.

[45] S. Weiss, M.-A. Mycek, J.-Y. Bigot, S. Schmitt-Rink and D.S. Chemla, Phys. Rev. Lett. 69 (1992) 2685; J.-Y. Bigot, M.-A. Mycek, S. Weiss, R.G. Ulbrich and D.S. Chemla, Phys. Rev. Lett. 70 (1993) 3307; S. Schmitt-Rink, S. Mukamel, K. Leo, J. Shah and D.S. Chemla, Phys. Rev. A 44 (1991) 2124.

[46] J. Jenkins and S. Mukamel, J. Chem. Phys. 98 (1993) 7046; V. Cerynyak and S. Mukamel, Phys. Rev. B 48 (1993) 2470; V. Chernyak and S. Mukamel, J. Chem. Phys. 100 (1994) 2953.

[47] J. Knoester, J. Chem. Phys. 99 (1993) 8466; J. Knoester, Phys. Rev. Lett. 68 (1992) 655.

[48] (a) R. Silbey, in: Modern Problems in Condensed Matter Sciences, eds. V.M. Agranovich and A.A. Maradudin, 4 (North-Holland, Amsterdam, 1983); R. Silbey, Ann. Rev. Phys. Chem. 27 (1976) 203. (b) V.M. Kenkre, in: Exciton Dynamics in Molecular Crystals and Aggregates, ed. G. Hohler (Springer, Berlin, 1982); P. Reineker, ibid.

[49] H.J. Eichler, P. Günter and D.W. Pohl, Laser-Induced Dynamic Gratings (Springer, Berlin, 1986).

[50] T.S. Rose, R. Righini and M.D. Fayer, Chem. Phys. Lett. 106 (1984) 13; M.D. Fayer, Ann. Rev. Phys. 33 (1982) 63.

[51] R.F. Loring and S. Mukamel, J. Chem. Phys. 84 (1986) 1228.

[52] N. Bloembergen, H. Lotem and R.T. Lynch, Indian J. Pure Appl. Phys. 16 (1978) 151; A.R. Bogdan, M.W. Downer and N. Bloembergen, Phys. Rev. A 24 (1981) 623; L.J. Rothberg and N. Bloembergen, Phys. Rev. A 30 (1984) 820; L. Rothberg, in: Progress in Optics, Vol. 24, ed. E. Wolf (North-Holland, Amsterdam) (1987) p. 38.

[53] S. Mukamel and R.F. Loring, J. Opt. Soc. Am. B 3 (1986) 595; F.C. Spano and S. Mukamel, J. Lumin 45 (1990) 412.

[54] N. Bloembergen, Nonlinear Optics (Benjamin, New York, 1965); B.J. Orr and J.F. Ward, Mol. Phys. 20 (1971) 513.

[55] D. Bedeaux and N. Bloembergen, Physica 69 (1973) 67.

[56] J.A. Leegwater and S. Mukamel, Phys. Rev. A 46 (1992) 452; N. Wang, J.A. Leegwater and S. Mukamel, J. Chem. Phys. 98 (1993) 5899.

[57] (a) G.J. Small, in: Excited States, ed. E.C. Lim (Academic Press, New York, 1982); (b) S.H. Stevenson, M.A. Connolly and G.J. Small, Chem. Phys. 128 (1988) 157.

[58] V.M. Agranovich and T.A. Leskova, Solid State Commun. 68 (1988) 1029.

[59] J.J. Hopfield and D.G. Thomas, Phys. Rev. 132 (1963) 563; J.J. Hopfield, Phys. Rev. 112 (1958) 1555; 182 (1969) 945; V.M. Agranovich, Zh. Eksp. Teor. Fiz. 37 (1959) 430 [Sov. Phys. - JETP 37 (1960) 307]; L.N. Ovander, Usp. Fiz. Nauk 86 (1965) 3 [Sov. Phys.-Usp. 8 (1965) 337]; V.M. Agranovich and Yu.K. Konobeev, Sov. Phys. Solid State 3 (1961) 260; M. Born and K. Huang, Dynamical Theory of Crystal Lattices (Oxford University Press, London, 1954).

[60] U. Fano, Rev. Mod. Phys. 45 (1974) 553.

[61] M.R. Philpott, Adv. Chem. Phys. 23 (1973) 227; S.I. Pekar, Zh. Eksp. Teor. Fiz. 33 (1957) 1022 [Sov. Phys. JETP 6 (1958) 785]; J.M. Turlet, Ph. Kottis and M.R. Philpott, Adv. Chem. Phys. 54 (1983) 303.

[62] G.M. Gale, F. Vallee and C. Flytzanis, Phys. Rev. Lett. 57 (1986) 1867; L. Claudio Andreani and F. Bassani, Phys. Rev. B 41 (1990) 7536; D. Fröhlich, S. Kirchhoff, P. Köhler and W. Nieswand, Phys. Rev. B 40 (1989) 1976.

[63] J. Knoester and S. Mukamel, J. Chem. Phys. 91 (1989) 989.

[64] A.A. Abrikosov, L.P. Gorkov and I. Ye. Dzyaloshinsky, Quantum Field Theoretical Methods in Statistical Physics (Oxford, New York, 1965).

[65] S. Mukamel, Adv. Chem. Phys. 70 (1988) 165; S. Mukamel, J. Chem. Phys. 82 (1985) 5398.

[66] M. Orrit, J. Bernard and R.I. Personov, J. Phys. Chem. 97 (1993) 10256; U.P. Wild, F. Güttler, M. Pirotta and A. Renn, Chem. Phys. Lett. 193 (1992) 451; W.E. Moerner, Science 265 (1994) 46.

[67] N. Wang, A.A. Muenter and S. Mukamel, J. Chem. Phys. 99 (1993) 3604.

[68] H.P. Van Albada and A. Lagendijk, Phys. Rev. Lett. 55 (1985) 2692; E. Akkermans, P.E. Wolf and R. Maynard, ibid. 56 (1986) 1471; A.A. Golubentzev, Zh. Eskp. Teor. Fiz. 86 (1984) 47 [Sov. Phys. JETP 59 (1984) 26].

[69] E.A. Power and S. Zienau, Phil. Trans. R. Soc. London A251 (1959) 427; E.A. Power, Introductory Quantum Electrodynamics (Longmans, London, 1964); D.P. Craig and T. Thirunamachandran, Molecular Quantum Electrodynamics (Academic Press, London, 1984).

[70] E. Betzig and R.J. Chichester, Science 262 (1993) 1422; R.C. Dunn, G.R. Holtom, L. Mets and X.S. Xie, J. Phys. Chem. 98 (1994) 3094.

[71] M.D. Levenson and S.S. Kano, Introduction to Nonlinear Laser Spectroscopy (Academic Press, New York, 1988).

[72] D.S. Chemla, J.-Y. Bigot, M.-A. Mycek, S. Weiss and W. Schäfer, Phys. Rev. B 50 (1994) 8439.

[73] F.C. Spano and S. Mukamel, J. Chem. Phys. 91 (1989) 683–700; J. Knoester, J. Chem. Phys. 99 (1993) 8466.

[74] M.P. Allen and D.J. Tildesley, Computer Simulations of Liquids (Oxford Science Publications, Oxford, 1987); M.P. Allen and D.J. Tildley, eds., Computer Simulations in Chemical Physics, NATO ASI Series, Vol. 397 (Kluwer, Dordrecht, 1993).
[75] A. Kalvova and B. Velicky, Z. Phys. B 94 (1994) 273; P. Lipavsky, V. Spicka and B. Velicky, Phys. Rev. B 34 (1986) 6933.
[76] K.B. Efetov, Adv. Phys. 32 (1983) 53.
[77] H.A. Lorentz, The Theory of Electrons (Dover, New York, 1952); L. Rosenfeld, Theory of Electrons (North Holland, Amsterdam, 1951).
[78] M.I. Stockman, L.N. Pandey, L.S. Muratov and T.F. George, Phys. Rev. Lett. 72 (1994) 2486; M.I. Stockman, V.M. Shalaev, M. Moskovits, R. Botet and T.F. George, Phys. Rev. B 46 (1992) 2821.
[79] V.N. Popov, Functional Integrals in Quantum Field Theory and Statistical Physics (Dodrecht, Boston; D. Reidel Publ. Co.; Hingham, MA, 1983).
[80] R.P. Feynman and F.L. Vernon, Ann. Phys. 24 (1963) 118.
[81] L.V. Keldysh, Soviet Phys. JETP 20 (1965) 1018.
[82] E.M. Lifshitz and L.P. Pitaevsky, Physical Kinetics (Pergamon, Oxford, New York, 1981).
[83] S. Mukamel, Molecular Nonlinear Optics, ed. J. Zyss (Academic Press, New York, 1994) p. 1; O. Dubovsky and S. Mukamel, J. Chem. Phys. 95 (1991) 7828–7845.
[84] G.S. Morris and M.G. Sceats, Chem. Phys. 3 (1974) 342.
[85] H. Risken, The Fokker-Planck Equation (Springer, Berlin, 1984); Van Kampen
[86] H. Stolz, Time-Resolved Light Scattering from Excitons (Springer, Berlin, 1994).
[87] M. Born and E. Wolf, Principles of Optics (Pergamon, New York, 1980).
[88] J.A. Leegwater and S. Mukamel, J. Chem. Phys., in press.
[89] D. Volkhardt and P. Wolfe, Phys. Rev. Lett. 45 (1980) 842; Phys. Rev. B 22 (1980) 4666.